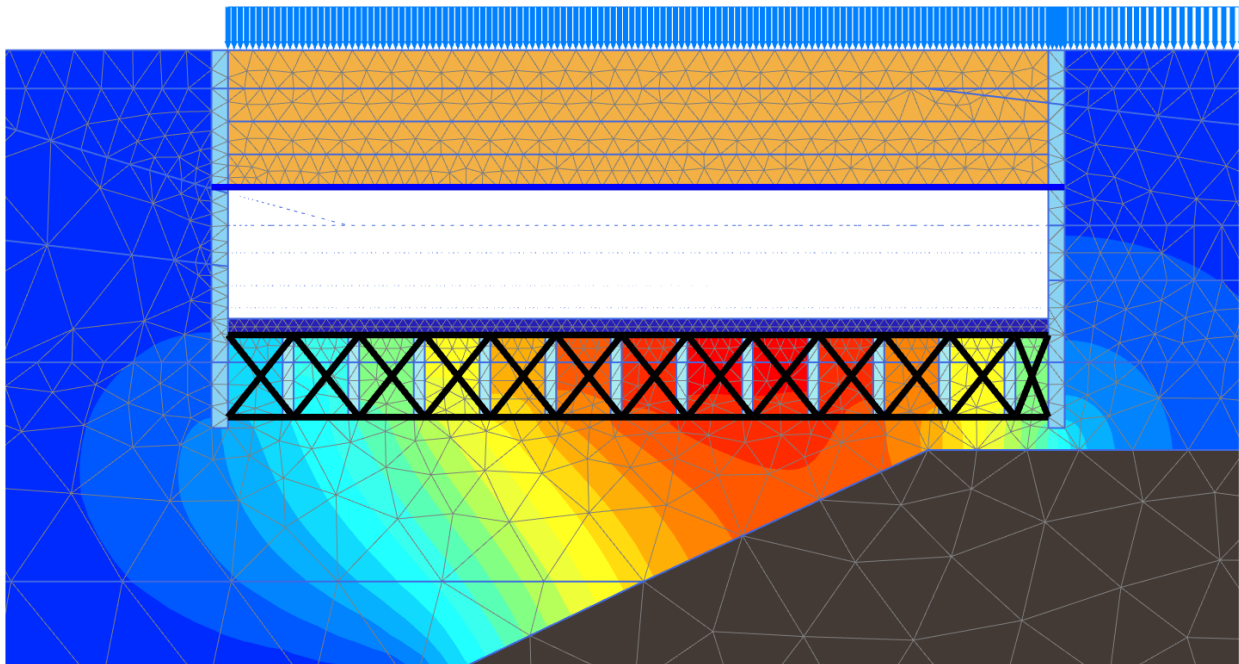




**CHALMERS**  
UNIVERSITY OF TECHNOLOGY

---



# Design of Deep Excavation in Soft Clay

Haga Station in Västlänken Railway Tunnel in Gothenburg

Master's thesis in Infrastructure and Environmental Engineering

NATALIA ORTIZ LÓPEZ  
JUSTYNA WIECZOREK

---

Department of Civil and Environmental Engineering  
*Division of Geology and Geotechnics*  
*Engineering Geology & Geotechnics (EG2)*  
CHALMERS UNIVERSITY OF TECHNOLOGY  
Gothenburg, Sweden 2017  
Master's thesis BOMX02-17-07



MASTER'S THESIS BOMX02-17-07

# Design of Deep Excavation in Soft Clay

Haga Station in Västlänken Railway Tunnel in Gothenburg

*Master's thesis in Civil and Environmental Engineering*

NATALIA ORTIZ LÓPEZ  
JUSTYNA WIECZOREK



Department of Civil and Environmental Engineering  
*Division of Geology and Geotechnics*  
*Engineering Geology & Geotechnics (EG2)*  
CHALMERS UNIVERSITY OF TECHNOLOGY  
Gothenburg, Sweden 2017

Design of Deep Excavation in Soft Clay  
Haga Station in Västlänken Railway Tunnel in Gothenburg  
NATALIA ORTIZ LÓPEZ  
JUSTYNA WIECZOREK

© NATALIA ORTIZ LÓPEZ and JUSTYNA WIECZOREK, 2017

Master's thesis BOMX02-17-07  
Department of Civil and Environmental Engineering  
Division of Geology and Geotechnics  
Engineering Geology & Geotechnics (EG2)  
Chalmers University of Technology  
SE-412 96 Gothenburg  
Sweden  
Telephone +46 (0)31 772 1000

This thesis was created using L<sup>A</sup>T<sub>E</sub>X.

Cover: Pore pressure distribution obtained for the Alternative 1 - Cross-walls with the Soft Soil model in the long-term analysis.

Printed by Chalmers Reproservice  
Gothenburg, Sweden 2017

Design of Deep Excavation in Soft Clay  
Haga Station in Västlänken Railway Tunnel in Gothenburg  
Master's thesis in Infrastructure and Environmental Engineering  
NATALIA ORTIZ LÓPEZ  
JUSTYNA WIECZOREK  
Department of Civil and Environmental Engineering  
Division of Geology and Geotechnics  
Engineering Geology & Geotechnics (EG2)  
Chalmers University of Technology

## Abstract

This thesis attempts to present a numerical analysis of a deep excavation that is planned to take place during Haga railway station erection along the Västlänken tunnel run in Gothenburg, Sweden. The station is to be placed predominantly in hard bedrock. Nevertheless, the final part of the station box is to be found in very soft clay that fills an almost 70 m deep void between two bedrock sections. Such placement creates challenges for foundation design especially against ground heave and differential settlements.

To simulate the behaviour of the excavation, three numerical models have been set up representing cross-walls, piled raft and lime-cement columns as the proposed foundation solutions. All models have been calculated using Soft Soil, and Soft Soil Creep both in short- and long-term scenarios. Additionally, the effect of various lightweight fill materials has been analysed against the long-term settlements.

The most uniform results have been achieved for the cross-walls alternative. The model performs well also in the long-term calculations providing the lowest bottom and total settlements. Large bottom heave values achieved by some models are claimed to be manageable in the service state by use of various preventive measures such as lightweight fill materials and Cordek Cellcore panels.

The performed sensitivity study has explicitly shown the high uncertainty of parameters derived from the poor quality soil investigation and indicated a need for further testing to be done. Calculated high factors of safety suggested overdesign in the service state. As the design was dictated by substantial deformation in the short-term analysis, it is proposed to test underwater excavation as a possible measure to control deformations and deliver more optimised design in the long-term.

Apart from the analysis, various topics describing good practices in numerical modelling in geotechnical engineering have been discussed. The authors trust that such considerations would help a reader to build a proper understanding of setting up numerical models in general.

Keywords: clay, soft clay, soft soil, deep excavation, FEM, railway station, Västlänken, Gothenburg, Haga.



## Acknowledgements

This Master's thesis studies the topic of deep excavations in soft soils such as Gothenburg clay. It is based on a real case study of the deep excavation that is being planned in Haga for Västlänken construction in Gothenburg, Sweden.

It has been realised under the supervision of prof. Minna Karstunen at Chalmers University of Technology, Division of Geology and Geotechnics. Fusion of her considerable theoretical knowledge and Nordic practicality gave us a unique opportunity to combine our research drives with a pragmatic approach. We feel particularly grateful for her time and feedback, but also inspiration as an exceptional role model for us as young female engineers.

We would also like to acknowledge Mats Karlsson who is an Assistant Professor at Chalmers University of Technology. He contributed to this study with his advice about PLAXIS software that proved to be critical for us. His supportive attitude helped us to go through the process of writing and encouraged to further work.

We would also like to mention Stina Berg and Naomi Licudi, who have prepared particularly useful opposition to this thesis. Moreover, Andres Cuarán and Pedro Deus offered their valuable comments and supported us through the writing process.

Last but not least, it is important to us to recognise here our families and friends without whose lifetime support this work would not have been possible.

Natalia Ortiz López and Justyna Wieczorek  
Gothenburg, June 2017



# Contents

|  |              |
|--|--------------|
| <b>Notation</b>  | <b>xvi</b>   |
| <b>List of Figures</b>                                     | <b>xvii</b>  |
| <b>List of Tables</b>                                      | <b>xxiii</b> |
| <b>1 Introduction</b>                                      | <b>1</b>     |
| 1.1 Background . . . . .                                   | 1            |
| 1.2 Aim and objectives . . . . .                           | 2            |
| 1.3 Limitations . . . . .                                  | 2            |
| 1.4 Method . . . . .                                       | 3            |
| 1.5 Outline of the report . . . . .                        | 4            |
| <b>2 Desktop study</b>                                     | <b>5</b>     |
| 2.1 General maps . . . . .                                 | 5            |
| 2.2 Historic maps . . . . .                                | 6            |
| 2.2.1 Roselnundskanalen . . . . .                          | 9            |
| 2.2.2 Rosenlundsbron . . . . .                             | 9            |
| 2.3 Geological maps . . . . .                              | 10           |
| 2.3.1 Quaternary map . . . . .                             | 10           |
| 2.3.2 Depth to bedrock . . . . .                           | 12           |
| 2.3.3 Bedrock quality . . . . .                            | 13           |
| 2.4 Ground water conditions . . . . .                      | 13           |
| 2.5 Surrounding structures . . . . .                       | 15           |
| 2.6 Sustainability . . . . .                               | 16           |
| 2.7 Contamination . . . . .                                | 17           |
| <b>3 Theory</b>  | <b>19</b>    |
| 3.1 Deep excavations . . . . .                             | 19           |
| 3.2 Soft soils . . . . .                                   | 20           |
| 3.3 Soil tests . . . . .                                   | 21           |
| 3.3.1 Undrained triaxial test . . . . .                    | 21           |
| 3.3.2 Direct Shear test . . . . .                          | 22           |
| 3.3.3 Oedometer test . . . . .                             | 22           |
| 3.4 Material models . . . . .                              | 25           |
| 3.4.1 Soil models in PLAXIS . . . . .                      | 25           |
| 3.5 General discussion of material models in FEM . . . . . | 29           |
| 3.6 Loads . . . . .  | 32           |

|          |   |           |
|----------|---|-----------|
| 3.6.1    | Internal loads . . . . .  | 32        |
| 3.6.2    | External loads . . . . .  | 34        |
| 3.7      | Structural elements . . . . .                                       | 36        |
| 3.7.1    | Retaining walls . . . . .   | 36        |
| 3.7.2    | Foundation of the excavation . . . . .                              | 39        |
| 3.7.3    | Supporting elements . . . . .                                       | 43        |
| 3.8      | Soil displacement reduction . . . . .                               | 46        |
| 3.8.1    | Soil replacement . . . . .  | 46        |
| 3.8.2    | Piling and piled raft solutions . . . . .                           | 47        |
| 3.8.3    | Cross-walls . . . . .   | 47        |
| 3.8.4    | Soil mix and compensation grouting for settlement control . . . . . | 48        |
| 3.8.5    | Cordek Cellcore HG . . . . .  | 49        |
| 3.8.6    | Lightweight fill materials . . . . .                                | 50        |
| <b>4</b> | <b>Project requirements</b>   | <b>55</b> |
| <b>5</b> | <b>Input data and soil testing analysis</b>                         | <b>59</b> |
| 5.1      | Boreholes . . . . .   | 59        |
| 5.2      | Soil test results . . . . .   | 60        |
| 5.2.1    | Compressibility and initial stress parameters . . . . .             | 60        |
| 5.2.2    | Strength parameters . . . . .                                       | 63        |
| 5.3      | Conceptual model of soil . . . . .                                  | 63        |
| 5.4      | Model parameters . . . . .  | 65        |
| 5.4.1    | Mohr-Coulomb parameters . . . . .                                   | 65        |
| 5.4.2    | Soft Soil (Creep) parameters . . . . .                              | 66        |
| 5.4.3    | Hoek-Brown parameters . . . . .                                     | 67        |
| 5.4.4    | Interface parameters . . . . .                                      | 68        |
| 5.5      | Loads . . . . .   | 69        |
| 5.5.1    | Internal loads . . . . .  | 69        |
| 5.5.2    | External loads . . . . .  | 70        |
| 5.6      | General discussion of assumptions for input data . . . . .          | 71        |
| <b>6</b> | <b>PLAXIS 2D model</b>  | <b>73</b> |
| 6.1      | Model geometry . . . . .  | 73        |
| 6.2      | Design of calculation features . . . . .                            | 75        |
| 6.2.1    | Model boundaries . . . . .  | 75        |
| 6.2.2    | Mesh design . . . . .   | 75        |
| 6.3      | Developed models . . . . .  | 77        |
| 6.3.1    | Alternative 1 - Cross-walls . . . . .                               | 77        |
| 6.3.2    | Alternative 2 - Piled raft . . . . .                                | 78        |
| 6.3.3    | Alternative 3 - Lime-cement columns . . . . .                       | 79        |
| 6.4      | Consideration about the effect of time . . . . .                    | 80        |
| 6.5      | Construction sequence . . . . .                                     | 82        |
| 6.6      | General discussion of assumptions in PLAXIS 2D model . . . . .      | 83        |
| <b>7</b> | <b>Results</b>  | <b>85</b> |
| 7.1      | Total displacements . . . . .                                       | 85        |

|          |   |            |
|----------|---|------------|
| 7.1.1    | Alternative 1 - Cross-walls . . . . .   | 85         |
| 7.1.2    | Alternative 2 - Piled raft . . . . .  | 87         |
| 7.1.3    | Alternative 3 - Lime-cement columns . . . . .                                       | 89         |
| 7.2      | Displacements in critical areas . . . . .   | 91         |
| 7.2.1    | Surface settlements . . . . .   | 91         |
| 7.2.2    | Bottom heave . . . . .  | 94         |
| 7.3      | Retaining structures . . . . .  | 96         |
| 7.3.1    | Left wall . . . . .   | 96         |
| 7.3.2    | Right wall . . . . .  | 98         |
| 7.4      | Forces . . . . .  | 99         |
| 7.4.1    | Bending moment . . . . .  | 99         |
| 7.4.2    | Strut forces . . . . .  | 101        |
| 7.5      | Factor of safety . . . . .  | 102        |
| 7.6      | Sensitivity analysis . . . . .  | 103        |
| 7.7      | Sustainability assessment . . . . .   | 104        |
| 7.8      | General discussion for results obtained with PLAXIS 2D . . . . .                    | 104        |
| <b>8</b> | <b>Conclusions and recommendations</b>  | <b>109</b> |
| 8.1      | Recommendations . . . . .   | 109        |
| 8.1.1    | Further investigation . . . . .   | 110        |
|          | <b>Bibliography</b>   | <b>111</b> |
|          | <b>Appendix A Quaternary deposits</b>   | <b>119</b> |
|          | <b>Appendix B Depth to bedrock map</b>  | <b>121</b> |
|          | <b>Appendix C Bedrock characterization map</b>                                      | <b>123</b> |
|          | <b>Appendix D Groundwater reservoirs</b>  | <b>125</b> |
|          | <b>Appendix E Comparison of the soil models and their application in<br/>PLAXIS</b> | <b>127</b> |
|          | <b>Appendix F Cordek Cellcore HG data sheet</b>                                     | <b>129</b> |
|          | <b>Appendix G Design drawings of Haga station</b>                                   | <b>133</b> |
|          | <b>Appendix H Soil investigation<br/>summary - boreholes</b>                        | <b>143</b> |
|          | <b>Appendix I Triaxial test results</b>   | <b>145</b> |
|          | <b>Appendix J Oedometer test results</b>  | <b>149</b> |
|          | <b>Appendix K Parameters of clay</b>  | <b>157</b> |
|          | <b>Appendix L Design of cross-walls</b>   | <b>159</b> |

|  |     |
|--|-----|
| Appendix M Design of cohesion piles for piled raft | 161 |
| Appendix N Bending moment<br>results in short-term | 163 |

# Notation

## Greek lower case letters

|               |                   |   |
|---------------|-------------------|---|
| $\gamma_d$    | kN/m <sup>3</sup> | Dry unit weight                             |
| $\gamma_s$    | kN/m <sup>3</sup> | Saturated unit weight                       |
| $\delta_l$    | m                 | Design settlement                           |
| $\delta_m$    | m                 | Initial settlement with retaining structure |
| $\kappa^*$    | -                 | Modified swelling index                     |
| $\lambda^*$   | -                 | Modified compression index                  |
| $\mu^*$       | -                 | Modified creep index                        |
| $\nu$         | -                 | Poisson's ratio                             |
| $\sigma$      | kPa               | Total stress                                |
| $\sigma'$     | kPa               | Effective stress                            |
| $\sigma'_1$   | kPa               | Major effective stress                      |
| $\sigma'_3$   | kPa               | Minor effective stress                      |
| $\sigma_a$    | kPa               | Total axial stress                          |
| $\sigma'_a$   | kPa               | Effective axial stress                      |
| $\sigma'_c$   | kPa               | Preconsolidation pressure                   |
| $\sigma_{ci}$ | kPa               | Uniaxial strength of rock                   |
| $\sigma'_f$   | kPa               | Effective stress at failure                 |
| $\sigma_r$    | kPa               | Total radial stress                         |
| $\sigma'_r$   | kPa               | Effective radial stress                     |
| $\sigma_{v0}$ | kPa               | In-situ vertical effective stress           |
| $\tau$        | kPa               | Shear stress                                |
| $\tau_f$      | kPa               | Shear stress at failure                     |
| $\phi$        | °                 | Friction angle                              |
| $\phi'$       | °                 | Effective friction angle                    |
| $\phi_i$      | °                 | Friction angle of interface                 |
| $\phi_{cv}$   | °                 | Critical friction angle                     |
| $\psi$        | °                 | Dilation angle                              |

## Roman lower case letters

|       |       |  |
|-------|-------|--|
| $c'$  | kPa   | Effective cohesion   |
| $k_x$ | m/day | Permeability in x-direction  |
| $k_y$ | m/day | Permeability in y-direction  |
| $m$   | -     | Reduction factor in Terzaghi and Peck braced excavations envelopes |
| $m_i$ | -     | Intact rock parameter  |
| $p$   | kPa   | Mean total stress  |
| $p'$  | kPa   | Mean effective stress  |
| $q$   | kPa   | Deviatoric stress  |

## Roman upper case letters

|             |                     |  |
|-------------|---------------------|--|
| $B$         | m                   | Width of excavation  |
| $D$         | -                   | Disturbance factor   |
| $E$         | kN/m <sup>2</sup>   | Young's Modulus  |
| $EA$        | kN/m                | Axial Stiffness  |
| $EI$        | kNm <sup>2</sup> /m | Bending Stiffness  |
| $H$         | m                   | Total depth of excavation  |
| $K$         | -                   | System stiffness for deep excavation construction (accounts for retaining walls, anchors and foundation) |
| $K_0$       | -                   | Lateral earth pressure coefficient at rest (in-situ)   |
| $K_0^{NC}$  | -                   | Coefficient of lateral stress in normal consolidation  |
| $L'$        | m                   | Space between cross walls  |
| $L_s$       | m                   | Out of plane spacing   |
| $N$         | -                   | Stability number   |
| $R_{inter}$ | -                   | Strength Reduction Factor  |
| $S_t$       | -                   | Sensitivity  |
| $S_u$       | kPa                 | Undrained shear strength   |

# Abbreviations

|        |   |
|--------|---|
| BREEAM | Building Research Establishment Environmental Assessment Method     |
| CFA    | Continuous Flight Auger   |
| CIRIA  | Construction Industry Research and Information Association          |
| COST   | Cooperation in Science and Technology                               |
| CRS    | Constant Rate of Strain test  |
| CSL    | Critical State Line   |
| CU     | Consolidated-Undrained triaxial test                                |
| CW     | Cross-walls   |
| DSM    | Deep soil mix   |
| EPS    | Expanded Polystyrene  |
| FBA    | Furnace Bottom Ash  |
| FEM    | Finite Element Method   |
| FG     | Foam Glass  |
| GSI    | Geological Strength Index   |
| HB     | Hoek-Brown  |
| LEED   | Leadership in Energy and Environmental Design                       |
| LCC    | Lime-Cement Columns   |
| LECA   | Lightweight Expanded Clay Aggregate                                 |
| MC     | Mohr-Coulomb  |
| OCR    | Over Consolidation Ratio  |
| PFA    | Pulverised Fuel Ash   |
| POP    | Pre-overburden Pressure   |
| PR     | Piled raft  |
| SS     | Soft Soil   |
| SSC    | Soft Soil Creep   |
| SGU    | Sveriges Geologiska Undersökning (eng. Geological Survey of Sweden) |



# List of Figures

|      |   |    |
|------|---|----|
| 2.1  | Aerial photo from 2014 of Rosenlundsbron, Hagakyrka and old houses at the northern part of Haga and Landala [3]. . . . .  | 5  |
| 2.2  | Detailed map of Hagakyrkan and areas around it. Map data copyrighted OpenStreetMap contributors and available from OpenStreetMap [5]. . . . .   | 7  |
| 2.3  | Extract from the 1790 Jubilee Map edition from Göteborgs Stadsbyggnadskontors Archive [6]. First houses can be seen in Haga. . . . .  | 8  |
| 2.4  | Extract from the 1860 Jubilee Map edition from Göteborgs Stadsbyggnadskontors Archive [7]. Hagakyrka got erected. . . . .   | 8  |
| 2.5  | Extract from the 1872 map from Göteborgs Stadsbyggnadskontors Archive [8]. Haga develops to the direction of Heden. . . . .   | 8  |
| 2.6  | Extract from the 1921 Jubilee Map edition from Göteborgs Stadsbyggnadskontors Archive [9]. Canal shapes got simplified, and its' traces can be seen to intersect with proposed Västlänken site plan. . . . .  | 8  |
| 2.7  | Extract from the original Rosenlundskanal drawings from Göteborgs Stadsbyggnadskontors Archive [10]. . . . .  | 9  |
| 2.8  | Drawing of the rebuilt Rosenlundbron from 1999 [11]. . . . .  | 10 |
| 2.9  | Extract from the Quaternary deposits 1:25,000 map from SGU [13]. Blue circle marks Haga area. The whole map can be found in Appendix A. . . . .   | 11 |
| 2.10 | Geological cross-section of Haga area along planned Västlänken route [12]. Each horizontal line marks 10 m difference in elevation, where the bottom of Haga station is at about -20 m depth. From Swedish, there are: Station Centralen - Central Station, Station Haga - Haga Station, Götatunneln - Göta Tunnel. There rest of names mention characteristic points in Gothernburg. . . . . | 11 |
| 2.11 | Depth to bedrock 1:50,000 after SGU [14]. Blue circle marks Haga area. The whole map can be found in Appendix B. . . . .  | 13 |
| 2.12 | Bedrock map 1:50,000 after SGU [15]. Blue circle marks Haga area. The whole map can be found in Appendix C. . . . .   | 14 |
| 2.13 | Groundwater reservoir map 1:50,000 after SGU [16]. The whole map can be found in Appendix D. . . . .  | 14 |
| 2.14 | Foundation type for surrounding buildings to the project area. Based on Trafikverket [17]. . . . .  | 15 |
| 2.15 | The average embodied energy in construction materials [19]. . . . .   | 16 |
| 2.16 | Life-cycle of construction materials based on the example of the UK (sketch reprinted by the courtesy of AKT II). . . . .   | 17 |

|      |  |    |
|------|--|----|
| 3.1  | Deviator vs. mean effective stress. Based on Knappett and Craig [30].  | 22 |
| 3.2  | Failure envelope plot and Mohr-Coulomb shear strength parameters determination. Based on Knappett and Craig [30].  | 23 |
| 3.3  | a) Void ratio ( $e$ ) vs. effective stress ( $\sigma'$ ) relationship, b) Determination of preconsolidation pressure based on Knappett and Craig [30].   | 24 |
| 3.4  | Relationship between a) void ratio ( $e$ ), and logarithm of the effective stress ( $\sigma'$ ), and b) volumetric strain ( $\epsilon_v$ ) and the natural logarithm of effective stress ( $\sigma'$ ). Based on Havel [33]. | 24 |
| 3.5  | Consolidation curve. Based on Olsson [34].   | 25 |
| 3.6  | Logarithmic relation between volumetric strain and effective stress [35].  | 27 |
| 3.7  | Schematic illustration presenting settlements of pile group for plastic and elastic parameters [44].   | 29 |
| 3.8  | Overestimation of the undrained shear strength with Undrained A and Mohr-Coulomb parameters [45].  | 30 |
| 3.9  | Base heave failure mechanism proposed by Terzaghi in 1943 after [30].  | 31 |
| 3.10 | a) Minimum deformation condition to mobilise active state, b) Wall deformation for braced excavation [30].   | 32 |
| 3.11 | Pressure envelopes for braced excavations for a) sands, b) soft to medium clays, and c) stiff fissured clays (Terzaghi and Peck [21] after Puller [25]).   | 33 |
| 3.12 | Pressure envelopes for braced excavations for a) soft and firm clays, and b) stiff and very stiff clay and coarse soils. Based on Twine and Roscoe [49].   | 34 |
| 3.13 | Depth of the Rosenlundskanalen based on the archive information from 1899 [52].  | 35 |
| 3.14 | Examples of retaining walls a) king post (left) and b) sheet pile (right).   | 37 |
| 3.15 | Examples of retaining walls a) contiguous wall (left) and b) secant pile (right).  | 38 |
| 3.16 | Example of a diaphragm wall (left) and the cross-sections through different types of walls (right, [54]).  | 39 |
| 3.17 | Typical arrangement of piles and columns in piled raft solution.   | 40 |
| 3.18 | A 3D representation of cross-walls. Based on Wu et al. [67].   | 41 |
| 3.19 | Procedure of soil-mix columns construction [73].   | 43 |
| 3.20 | The force-displacement diagram displaying the elasto-plastic behaviour of anchors (left) and the anchors with residual strength (right) [43].  | 44 |
| 3.21 | Anchorage types: a) plate anchor, b) ground anchor after [30].   | 45 |
| 3.22 | Detail of rock dowels [82].  | 46 |
| 3.23 | Soil replacement in road construction [83].  | 47 |
| 3.24 | Raft and piled raft solution, where $\Delta$ is the maximum differential settlement [30].  | 48 |
| 3.25 | Principles of compensation grouting design [90].   | 49 |
| 3.26 | Cellcore installation around piles for the raft construction [92].   | 50 |
| 3.27 | Cellcore installation under the raft [93].   | 50 |
| 3.28 | PFA with reinforcement mesh used for the road construction on the soft ground [97].  | 51 |
| 3.29 | Cross-section photo of Lightweight Expanded Clay Aggregate [101].  | 52 |

|      |   |    |
|------|---|----|
| 3.30 | GEOCELL® foam glass gravel [100]. . . . .   | 52 |
| 3.31 | EPS as a light fill material at the Cowgate roundabout construction, Newcastle upon Tyne [104]. . . . .   | 53 |
| 4.1  | Cross-section visualisation of Haga station produced by WSP in 2015 [3]. <i>Uppgång</i> (eng. entrance) mark three proposed entrances to the station - from Pusterviksplatsen, Kungsparken and Handelshögskolan. Besides, there are: <i>övergång mellan berg och lera</i> (eng. transition between bedrock and clay), <i>tekniska utrymmen</i> (eng. technical rooms) and <i>perrong</i> (eng. platform). . . . . | 55 |
| 4.2  | Cross-section just after Haga station, where Jt - area of a new railway track owned by private party. Produced by SWECO and Ramboll for Trafikverket [107]. . . . .   | 56 |
| 4.3  | Critical cross-section of Haga station, where Js6 - underground structures and Js9 - protection zone. Produced by SWECO and Ramboll for Trafikverket [107]. . . . .   | 57 |
| 4.4  | Haga station visualisation by ABAKO Arkitektkontor AB [109]. . . . .  | 57 |
| 5.1  | Analysed boreholes location based on SWECO report [2]. . . . .  | 59 |
| 5.2  | Preconsolidation pressure vs. depth for both oedometer and CRS test results. . . . .  | 61 |
| 5.3  | Over consolidation ratio vs. depth for both oedometer test results. . . . .   | 61 |
| 5.4  | Pre-overburden pressure vs. depth for both oedometer and CRS test results. . . . .  | 62 |
| 5.5  | Modified compression index from oedometer test. . . . .   | 62 |
| 5.6  | Modified swelling index from oedometer test. . . . .  | 62 |
| 5.7  | Modified creep index from step-wise oedometer test. . . . .   | 63 |
| 5.8  | Water content for analysed boreholes vs. depth. . . . .   | 64 |
| 5.9  | Cross section soil layering at km458+990 based on soil tests data and figures from SWECO [2]. . . . .   | 65 |
| 6.1  | General soil geometry in PLAXIS 2D. Graphics present the total size of the numerical model. . . . .   | 73 |
| 6.2  | Fixations of the model boundaries. . . . .  | 75 |
| 6.3  | Inspection of mesh quality in PLAXIS. . . . .   | 76 |
| 6.4  | Model geometry in PLAXIS 2D for Alternative 1 in short term. . . . .  | 77 |
| 6.5  | Model geometry in PLAXIS 2D for Alternative 2 in short term. . . . .  | 78 |
| 6.6  | Model geometry in PLAXIS 2D for Alternative 3 in short term. . . . .  | 79 |
| 6.7  | Model geometry in PLAXIS 2D for Alternative 2 in long term. . . . .   | 82 |
| 7.1  | Total displacements obtained for Alternative 1 using SS model for the short-term. . . . .   | 86 |
| 7.2  | Total displacements obtained for Alternative 1 using SS model for the long-term. . . . .  | 86 |
| 7.3  | Total displacements obtained for Alternative 2 using SS model for the short-term. . . . .   | 87 |

|      |  |     |
|------|--|-----|
| 7.4  | Total displacements obtained for Alternative 2 using SS model for the long-term. . . . .       | 88  |
| 7.5  | Total displacements obtained for Alternative 2 using SSC model for the long-term. . . . .      | 88  |
| 7.6  | Total displacements obtained for Alternative 3 using SS model for the short-term. . . . .      | 89  |
| 7.7  | Total displacements obtained for Alternative 3 using SS model for the long-term. . . . .       | 90  |
| 7.8  | Total displacements obtained for Alternative 3 using SSC model for the long-term. . . . .      | 90  |
| 7.9  | Surface settlements obtained with Soft Soil model for the short-term.                          | 92  |
| 7.10 | Surface settlements obtained with Soft Soil Creep model for the long-term. . . . .             | 92  |
| 7.11 | Surface settlements obtained with the Soft Soil model for the short-term. . . . .              | 93  |
| 7.12 | Surface settlements obtained with the Soft Soil Creep model for the long-term. . . . .         | 93  |
| 7.13 | Bottom heave obtained with the Soft Soil model for the short-term. .                           | 94  |
| 7.14 | Bottom heave obtained with the Soft Soil Creep model for the short-term. . . . .               | 95  |
| 7.15 | Bottom heave obtained with the Soft Soil model for the long-term. . .                          | 95  |
| 7.16 | Bottom heave obtained with the Soft Soil Creep model for the long-term. . . . .                | 96  |
| 7.17 | Horizontal displacements for left wall obtained with the SS model in the short-term. . . . .   | 97  |
| 7.18 | Horizontal displacements for left wall obtained with the SSC model in the short-term. . . . .  | 97  |
| 7.19 | Horizontal displacements for left wall obtained with the SS model in the long-term. . . . .    | 97  |
| 7.20 | Horizontal displacements for left wall obtained with the SSC model in the long-term. . . . .   | 97  |
| 7.21 | Horizontal displacements for right wall obtained with the SS model in the short-term. . . . .  | 98  |
| 7.22 | Horizontal displacements for right wall obtained with the SSC model in the short-term. . . . . | 98  |
| 7.23 | Horizontal displacements for right wall obtained with the SS model in long-term. . . . .       | 98  |
| 7.24 | Horizontal displacements for right wall obtained with the SSC model in long-term. . . . .      | 98  |
| 7.25 | Bending moments on left wall obtained with SS model for the long-term.                         | 99  |
| 7.26 | Bending moments on right wall obtained with SS model for the long-term. . . . .                | 100 |
| 7.27 | Bending moments on left wall obtained with SSC model for the long-term. . . . .                | 100 |
| 7.28 | Bending moments on right wall obtained with SSC model for the long-term. . . . .               | 101 |

|     |   |     |
|-----|---|-----|
| A.1 | Map presenting the type of soil in or near the ground surface in Gothenburg in scale 1:25,000 [13]. . . . .                       | 120 |
| B.1 | Map presenting depth of superficial materials over bedrock in Gothenburg in scale 1:50,000 [14]. . . . .                          | 122 |
| C.1 | Map presents a generalised view of the bedrock distribution in Gothenburg in scale 1:50,000 [15]. . . . .                         | 124 |
| D.1 | Map presenting the groundwater reservoirs in Gothenburg in scale 1:50,000 [16]. . . . .   | 126 |
| E.1 | Comparison of the soil models available in PLAXIS and their suitability of the modelling of various soil types [35]. . . . .      | 127 |
| E.2 | Comparison of the soil models available in PLAXIS and their suitability of the modelling of various design problems [35]. . . . . | 128 |
| E.3 | Comparison of the soil models available in PLAXIS and their suitability of the modelling of various loading types [35]. . . . .   | 128 |
| G.1 | Cross-section at the km458+890 of Västlänken [122]. . . . .   | 134 |
| G.2 | Cross-sections at the km459+120 and km459+165 of Västlänken [123].  | 135 |
| G.3 | Cross-sections at the km459+260 and km459+340 of Västlänken [124].  | 136 |
| G.4 | Cross-sections at the km458+990, km459+100 and km459+060 of Västlänken [107]. . . . .   | 137 |
| G.5 | Temporary arrangements at the km458+500 - 459+000 of Västlänken [125]. . . . .  | 138 |
| G.6 | Permanent arrangements at the km458+500 - 459+000 of Västlänken [126]. . . . .  | 139 |
| G.7 | Temporary arrangements at the km459+000 - 459+500 of Västlänken [127]. . . . .  | 140 |
| G.8 | Permanent arrangements at the km459+000 - 459+500 of Västlänken [128]. . . . .  | 141 |
| H.1 | Figure presents depths of reading from the boreholes presented in SWECO report [2]. . . . .                                       | 143 |
| I.1 | Triaxial results for Clay 2. . . . .  | 145 |
| I.2 | Triaxial results for Clay 3. . . . .  | 146 |
| I.3 | Triaxial results for Clay 4. . . . .  | 147 |
| J.1 | Oedometer test results at 10 m. . . . .   | 149 |
| J.2 | Oedometer test results at 15 m. . . . .   | 150 |
| J.3 | Oedometer test results at 20 m. . . . .   | 150 |
| J.4 | Oedometer test results at 30 m. . . . .   | 151 |
| J.5 | Oedometer test results at 40 m. . . . .   | 151 |
| J.6 | CRS test results at 10 m. . . . .   | 152 |
| J.7 | CRS test results at 15 m. . . . .   | 152 |
| J.8 | CRS test results at 20 m. . . . .   | 153 |
| J.9 | CRS test results at 25 m. . . . .   | 153 |

|      |  |     |
|------|--|-----|
| J.10 | CRS test results at 30 m. . . . .  | 154 |
| J.11 | CRS test results at 40 m. . . . .  | 154 |
| J.12 | Average permeability for CRS tests at all depths. . . . .                        | 155 |
| K.1  | Sensitivity of clay separated by soil layers. . . . .                            | 157 |
| K.2  | Density of clay separated by soil layers. . . . .                                | 157 |
| K.3  | Liquid limit of clay separated by soil layers. . . . .                           | 158 |
| K.4  | Undrained shear strength of clay separated by soil layers. . . . .               | 158 |
| N.1  | Bending moment on left wall obtained with SS model for the short-term. . . . .   | 163 |
| N.2  | Bending moment on right wall obtained with SS model for the short-term. . . . .  | 164 |
| N.3  | Bending moment on left wall obtained with SSC model for the short-term. . . . .  | 164 |
| N.4  | Bending moment on right wall obtained with SSC model for the short-term. . . . . | 165 |

# List of Tables

|     |   |     |
|-----|---|-----|
| 5.1 | Parameters for friction and fill materials in Mohr-Coulomb constitutive model in PLAXIS 2D. . . . .   | 66  |
| 5.2 | Parameters for Clay 1-3 used in Soft Soil and Soft Soil Creep constitutive models in PLAXIS 2D. . . . .   | 66  |
| 5.3 | Parameters for Clay 4-6 used in Soft Soil and Soft Soil Creep constitutive models in PLAXIS 2D. . . . .   | 67  |
| 5.4 | Parameters for bedrock used in Hoek-Brown constitutive model in PLAXIS 2D. . . . .  | 67  |
| 5.5 | Interface strength values for different soils for concrete structures. . .  | 68  |
| 5.6 | Imposed loads from adjacent buildings to the excavation. Based on values provided by Building Department of Hong Kong [117]. . . . .  | 70  |
| 5.7 | Dead load of materials present in adjacent buildings to the excavation. Based on values provided by Building Department of Hong Kong [117].   | 71  |
| 6.1 | Parameters for concrete elements in PLAXIS 2D. . . . .  | 74  |
| 6.2 | Struts parameters applied in PLAXIS 2D models. . . . .  | 74  |
| 6.3 | Example of the mesh design validation based on the three calculations of coarser, designed and finer mesh. The presented example covers the final settlement with Soft Soil model calculated for Alternative 2 - Piled Raft with Foam Glass fill, but similar range of values have been obtained for all of the remaining models. . . . . | 76  |
| 6.4 | Parameters for Alternative 2 - Piled raft. . . . .  | 79  |
| 6.5 | Parameters for LCC soil in Mohr-Coulomb constitutive model in PLAXIS 2D. . . . .  | 80  |
| 6.6 | Parameters for roof slab PLAXIS 2D. . . . .   | 81  |
| 6.7 | Parameters for fill material after excavation in PLAXIS 2D. . . . .   | 81  |
| 6.8 | Construction sequence for Alternatives 1, 2 and 3 in PLAXIS 2D. . .   | 83  |
| 7.1 | Strut loads calculated through FEM and empirical methods. . . . .   | 101 |
| 7.2 | Safety factor for modelled alternatives with Soft Soil model. . . . .   | 102 |
| 7.3 | Safety factor for modelled alternatives with Soft Soil Creep model. . .   | 102 |
| 7.4 | Sensitivity values in % separated by the different alternatives modelled in PLAXIS 2D. The higher the value, the more sensitive the parameter is. . . . .   | 103 |
| 7.5 | Embodied carbon calculated for the three modelled alternatives. . . .   | 104 |
| 7.6 | Comparison of the main parameters for Soft Soil model. . . . .  | 105 |
| 7.7 | Comparison of the main parameters for Soft Soil Creep model. . . . .  | 106 |

|     |  |     |
|-----|--|-----|
| I.1 | Retrieved data for analysis of the effective strength parameters for Clay 2. . . . . | 146 |
| I.2 | Retrieved data for analysis of the effective strength parameters for Clay 3. . . . . | 146 |
| I.3 | Retrieved data for analysis of the effective strength parameters for Clay 4. . . . . | 147 |

# 1

## Introduction

### 1.1 Background

In highly urbanised cities, many properties involve deep underground structures. As cities densify, future investments are being located in areas where development has not been previously considered, mainly due to poor ground conditions. These areas prove to be exceptionally challenging for engineers, specifically for excavation and temporary works design.

One of the soil types that demonstrated to be highly demanding regarding excavation construction is soft clay. An exceptional case of a deep excavation in such soft ground was the construction of Nicoll Highway in Singapore. An about 30-meter-deep excavation failed in April 2004 killing four people and injuring a further three [1]. From that time, multiple hypotheses have been studied, and one of the main theories is being linked to inappropriate Finite Element Modelling (FEM) during the design phase. The incident affected the industry and various engineering publications released after the collapse made engineers much more aware of the fatal consequences linked to the inappropriate design of deep excavations.

Similarly, challenging ground conditions are present in Scandinavia. Gothenburg, on the West Coast of Sweden, is situated on the mixture of deep soft marine clay deposits, crystalline bedrock and man-made fill originating mostly from Dutch times in the 17<sup>th</sup> century. Where present, clay layers can span over 100 m in depth. Such an environment was encountered during Marieholmstunneln (eng. Marieholm Tunnel) excavation where retaining walls reached the depth of about 40 m protecting a 15-meter-deep dry deck used for erecting tunnel sections. Similar works are planned to be repeated in the central part of the city during the excavation of Haga station for the Västlänken (eng. the West Link) project.

Västlänken is the extensive investment planned to boost the railway capacity in the region and support the development of the public transportation sector. As more and more people working in the city commute daily from the nearby areas, the local authorities are trying to create an attractive alternative to commuting by car. Västlänken ground works, similarly to Marieholmstunneln project, are expected to be the most troublesome part of the design. Overcoming them might be costly what triggers the discussion about the viability of the investment on its own.

This Master's thesis continues investigating possible design solutions for Haga station using the geotechnical investigation report made by SWECO AB [2].

## 1.2 Aim and objectives

The principal objective of this paper is to provide various feasible engineering solutions to the stability of the deep excavation problem. This thesis could be used to refine initial consultants design and lead to a more safe and economical scheme.

The aim of the thesis is to check the process of soil parameters derivation and review the existing laboratory testing data. Based on this, the further investigation continues where the numerical model is being set up to provide the base for the analysis of three alternative support systems for the excavation. As the excavation is planned to be exposed for the substantial period, the stability analysis is performed for both short- and long-term conditions. Alternatives are compared based on design performance but also sustainability of the scheme.

As the response to often limited knowledge about soil material models and their consequences in numerical analysis, the study concerning FEM in geotechnical design is simultaneously being conducted. It is aimed to demonstrate what kind of consequences are being linked to them when designing deep excavations in soft soils.

## 1.3 Limitations

Despite a significant amount of laboratory data being surveyed for Haga station, only a small portion of these was available to be analysed in this thesis. Moreover, data was delivered in written format. Consequently, certain values were read from graphs, not calculated numerically using proper formulations.

To simplify the numerical model, the elastic and elasto-plastic behaviour of steel and concrete are being considered instead of the non-linear. It is claimed that such simplification does not affect the quality of this study in a great way but enables computational savings.

The location of the performed analysis comprehends the area of the Västlänken project below Roselundskanalen (eng. Roselund Canal) and Nya Allén (eng. New Avenue), located in the kilometres km458+900 and km459+100 according to the project nomenclature. The mentioned section was chosen given its complexity due to the presence of a deep clay layer which extends to a depth of 70 m and the need of performing deep excavations. Other sections of the Haga station which involves tunnels in rock will account for the different type of design which is not included in the presented document.

Furthermore, no temperature effects are being considered in the study, but where appropriate, the reader's attention is drawn to the potential effect of temperature, especially concerning excavation support elements. The construction of strut system was simplified and no waler was adapted in the numerical model. Finally, disturbances caused by the installation of certain structural elements are not being considered.

## 1.4 Method

Initially, the study focused on the literature study so as to develop a better understanding of the topic. The scientific publications and previous theses have been supplemented with numerous reports conducted mostly for Trafikverket (eng. Swedish Transport Administration) and Göteborgs Stad (eng. the City of Gothenburg).

The literature study was followed by the in-depth analysis of the project requirements and soil parameters. All of the parameters used in the further numerical analysis have been derived using available laboratory data. The most important part was the analysis of triaxial and oedometer tests as these highly influence further results. These values created the base for setting up the model. Firstly, the conceptual model has been set up where appropriate layers and desired excavation geometry were reflected. Further, the numerical model in PLAXIS 2D version 2016.01 software has been established where the FEM analysis has been performed.

The numerical model studies the stability of the excavation in short and long term conditions. It is further expanded to examine various alternatives for excavation base support. The optimisation of the design is being performed together with the sensitivity analysis of certain numerical parameters. Joint results, together with recommendations, are being presented in the final part of this thesis.

## 1.5 Outline of the report

Chapter 2 is a desktop study covering the Haga area. It presents numerous general, geological and hydrological maps that are being used in the further analysis.

Chapter 3 presents the results of the literature study. It contains the explanation of basic definitions, general concepts and theory behind the material models and loads used during calculations. Moreover, the chapter familiarises the reader with loads acting on the structure both internally and externally.

Chapter 4 elaborates about the particular requirements of the Västlänken project as desired geometry of the Haga station and allowable settlements in the area.

Chapter 5 summarises derivation of soil parameters from available ground investigation data. It gives all input parameters that are being utilised in the numerical analysis but also displays the conceptual model of the excavation.

Chapter 6 covers four design options for excavation base design in PLAXIS 2D for short- and long-term conditions. It states all design assumptions and clearly defines which material model was used in the calculations.

Chapter 7 summarises the results of the study. It inspects the quality of data that has been available and underlines the conclusions from the sensitivity study.

Chapter 8 stresses the most important findings and recommends further actions regarding the deep excavation design. Appendices familiarise the reader with supplementary information as detailed maps and additional results.

# 2

## Desktop study

Haga is a small district in the city centre of Gothenburg well-known from its charming wooden houses. It covers a relatively small area that spans from Rosenlundkanalen on the north to Skansen Kronan (eng. Crown Sconce) on the south (see Figure 2.1). Historically, it was located outside the city walls and was inhabited by the working class. A bad reputation of the district did not last long, and nowadays it is one of the most popular tourist destinations in Gothenburg.



Figure 2.1: Aerial photo from 2014 of Rosenlundsbron, Hagakyrka and old houses at the northern part of Haga and Landala [3].

### 2.1 General maps

Figure 2.2 presents a detailed map of northern part of Haga district. Hagakyrkan (eng. Haga Church) is situated around 150 m from Rosenlundskanalen and surrounded with a park. The area spanning between the church and canal is very popular among Gothenburg citizens and used mainly for recreation. Rosenlundsbron (eng. Rosenlund bridge) connects Haga with the city centre and is a busy transportation link also used by trams. At the northern part of Rosenlundsbron,

there is Skatteverket (eng. Swedish Tax Agency) and buildings of Göteborgs universitet Utbildningsvetenskapliga fakulteten (eng. Gothenburg University Faculty of Education). At this side of the canal, there is a small ship pier, numerous car parking spaces and Styr & Ställ city bike station.

The Western area of Haga is occupied by charismatic wooden buildings beloved by both citizens and tourists. The district to the East is called Landala and consists of more modern brick buildings that are taller than Haga houses.

Handelshögskola (eng. Gothenburg University School of Business, Economics and Law) stretches over southern areas from Hagakyrkan. The planned Haga station is to connect Göteborgs universitet campuses and provide a viable transportation link to the bustling district.

## 2.2 Historic maps

Gothenburg was founded in 1621 by King Gustavus Adolphus (eng. Gustaf II Adolf) as the protection town and the only gateway from Sweden to the North Sea and Atlantic. Many Dutch, German and Scottish engineers took part in the city erection as they were experienced in dewatering and construction on the muddy ground. Their engineering influence can still be seen today.

Around the 17<sup>th</sup> century, thick city walls were constructed and, together with the canal, to protect the town from Dutch ships and other invaders. Figure 2.3 presents the final stage of wall construction and the canal with its original shape. At this time, Haga was a peripheral district created for the working class. It was densely populated and had a rather poor reputation [4].

At the beginning of the 19<sup>th</sup> century, the city walls were destroyed to allow spreading the town behind the canal. The area of the previous walls was used as a base of construction for Nya Allén. During the same time, Hagakyrkan construction had been finalised in 1859 at the Eastern part of the district. The church together with the surrounding park can be seen on the Jubilee Map from 1860 (see Figure 2.4).

Through the 19<sup>th</sup> and 20<sup>th</sup> centuries, the area was developing further (see Figures 2.5 and 2.6). The map from 1921 presents the canal shape before and after its reconstruction. It gives valuable information about historical canal location and the possible deposition of gravel and sandy material around it.

At this stage, the map shows also building of Stadsbiblioteket (eng. City Library) that has been later on transformed to Samhällsvetenskapliga biblioteket (eng. Gothenburg University Social Sciences Library).

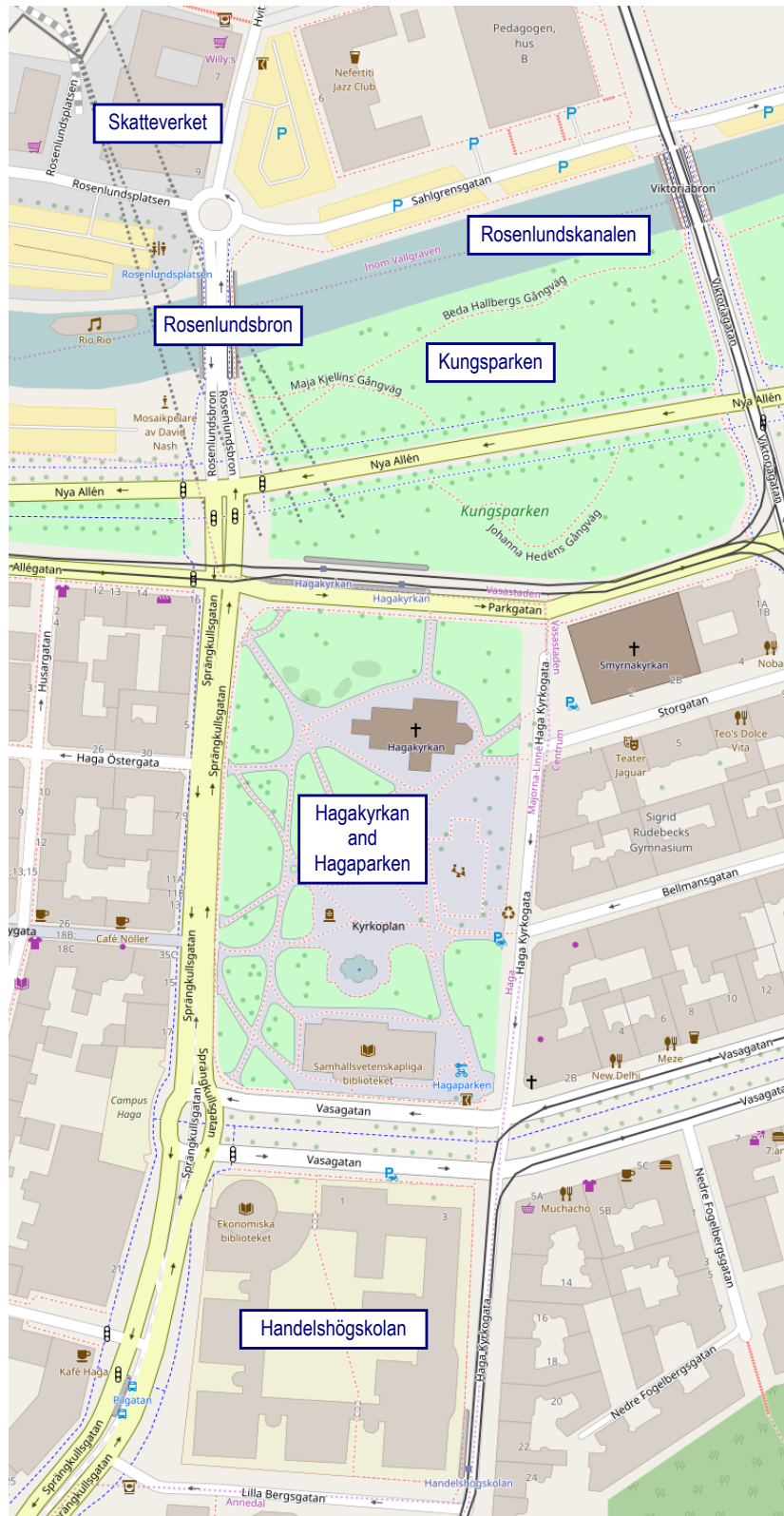


Figure 2.2: Detailed map of Hagakerkan and areas around it. Map data copyrighted OpenStreetMap contributors and available from OpenStreetMap [5].



Figure 2.3: Extract from the 1790 Jubilee Map edition from Göteborgs Stadsbyggnadskontors Archive [6]. First houses can be seen in Haga.

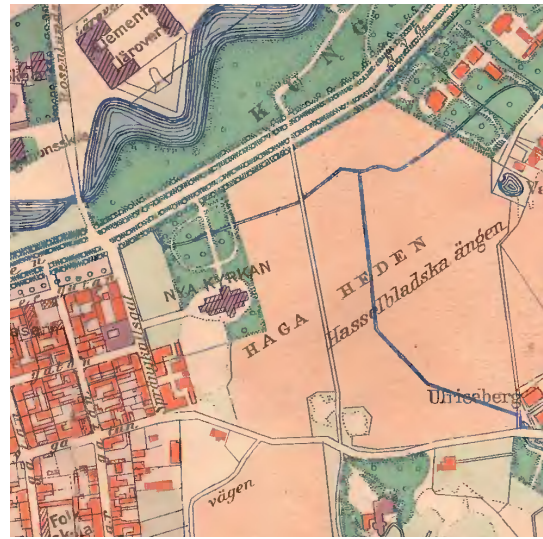


Figure 2.4: Extract from the 1860 Jubilee Map edition from Göteborgs Stadsbyggnadskontors Archive [7]. Hagakyrka got erected.

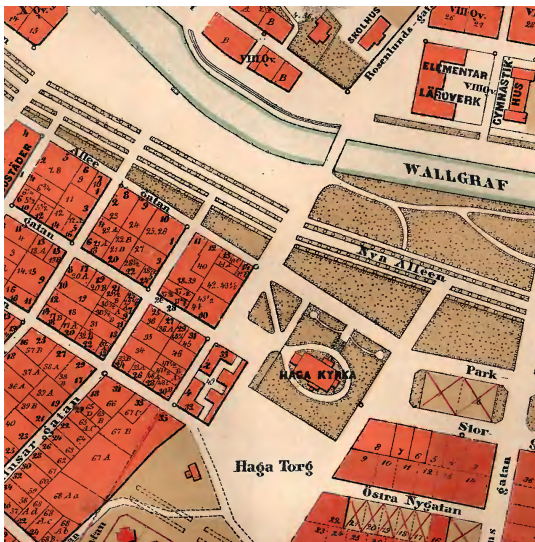


Figure 2.5: Extract from the 1872 map from Göteborgs Stadsbyggnadskontors Archive [8]. Haga develops to the direction of Heden.



Figure 2.6: Extract from the 1921 Jubilee Map edition from Göteborgs Stadsbyggnadskontors Archive [9]. Canal shapes got simplified, and its' traces can be seen to intersect with proposed Västlänken site plan.

## 2.2.1 Roselundskanalen

As Roselundskanalen has flowed through the city centre, it has been regulated and provided with flood protection barriers. Figure 2.7 presents an original drawing of a canal retaining structure. It has been constructed from stones as a massive gravity wall and founded on the wooden grate. Piles in the grate vary in length. The first five under the wall are about 13-15 m long to be reduced in size at the next five to 9-10 m behind it. Such length of the piles might intersect with planned tunnel structure what should be further verified. The whole structure in the plan is claimed to have a width of 6 m [2].

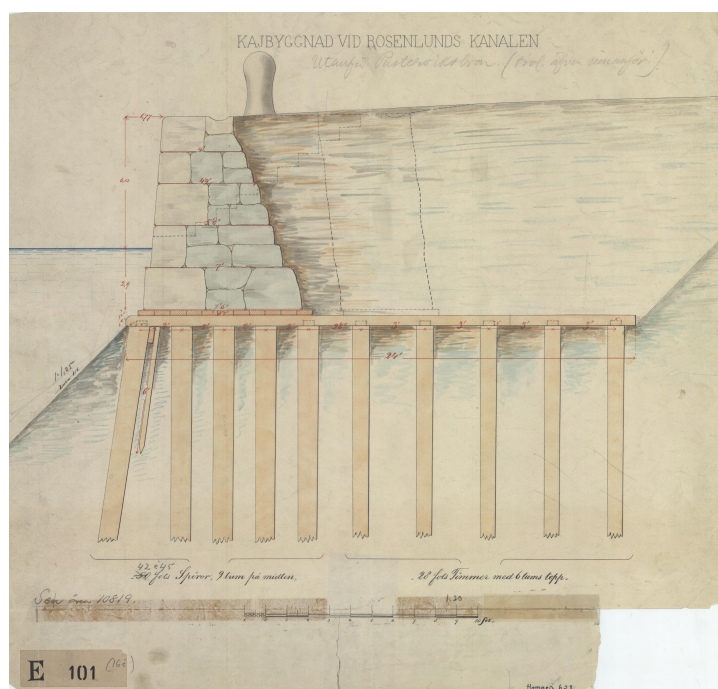


Figure 2.7: Extract from the original Roselundskanal drawings from Göteborgs Stadsbyggnadskontors Archive [10].

## 2.2.2 Roselundsbron

Roselundsbron was erected in 1866. Its further major restorations took place in 1921 and 1999. The bridge is founded in the same location as previous structures and makes use of already existing middle support. It is based on the concrete cohesion piles that depths vary from 34 m under the embankment areas to 39 m under the central support (see Figure 2.8). Some piles are angled from the vertical direction to help spread the load over the wider area [2]. As the depth of piles is substantial, there is a high risk of intersecting them during the tunnel construction.

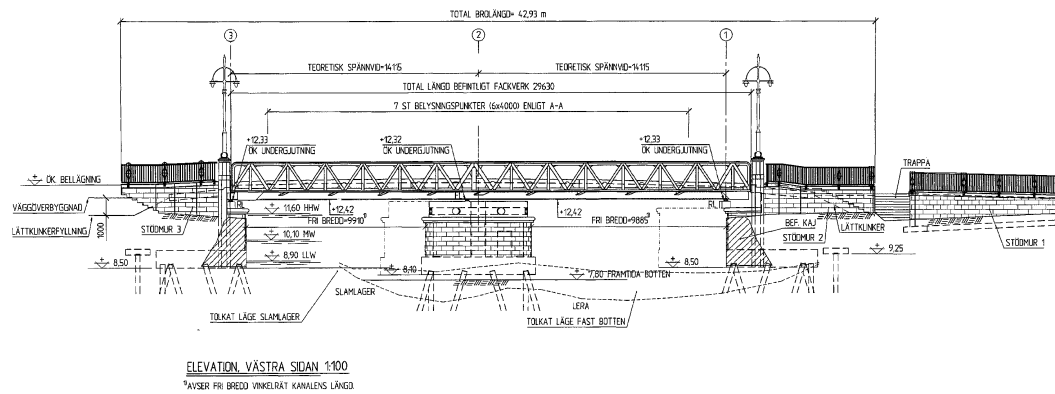


Figure 2.8: Drawing of the rebuilt Rosenlundbron from 1999 [11].

## 2.3 Geological maps

Below Geological maps have been sourced from Sveriges Geologiska Undersökning (SGU, eng. Geological Survey of Sweden). They present quaternary deposits, the depth of surficial materials to the bedrock and, finally, bedrock quality. Information about groundwater reservoirs can be found in the following Section 2.4.

### 2.3.1 Quaternary map

Soil in the central part of Gothenburg vary substantially. The majority of the upper layers is covered with postglacial clay. Figure 2.9 presents quaternary deposits where the vast clay areas (yellow colour) can be seen among crystalline rock formations (red colour). Hagakyrka and Skatteverket buildings are situated in areas where bedrock is close to the surface. According to SGU, Hagaparken (eng. Haga Park) is located predominantly over wave-washed gravel material of higher permeability than clay and can be considered as a natural drainage layer. This can be explained by the historical shape of Rosenlundskanalen that can be seen on maps in Section 2.2. Flowing water deposited part of the material at the side of the canal. With time, sedimentation process occurred and created sandy gravel layers on top of bedrock. The SGU information was not confirmed by the soil investigation, where Hagaparken was identified as being based on about 4 m thick natural soil and silty clay layer over the bedrock foundation [12].

Figure 2.10 presents a geological cross-section along the proposed tunnel route. According to the conceptual model proposed by SWECO, the depth of the filling material varies between 1 to 7 m in depth [2]. Ground investigation information is coherent with the SGU surficial material map. Hagaparken is claimed to have only a thin layer of hummus over the bedrock, while areas towards Samhällsvetenskapliga biblioteken are filled with deeper layers of gravel, sand, clay, brick and wood residues. The areas from Hagakyrkan towards the canal are filled mostly with gravel with some occurrence of brick.

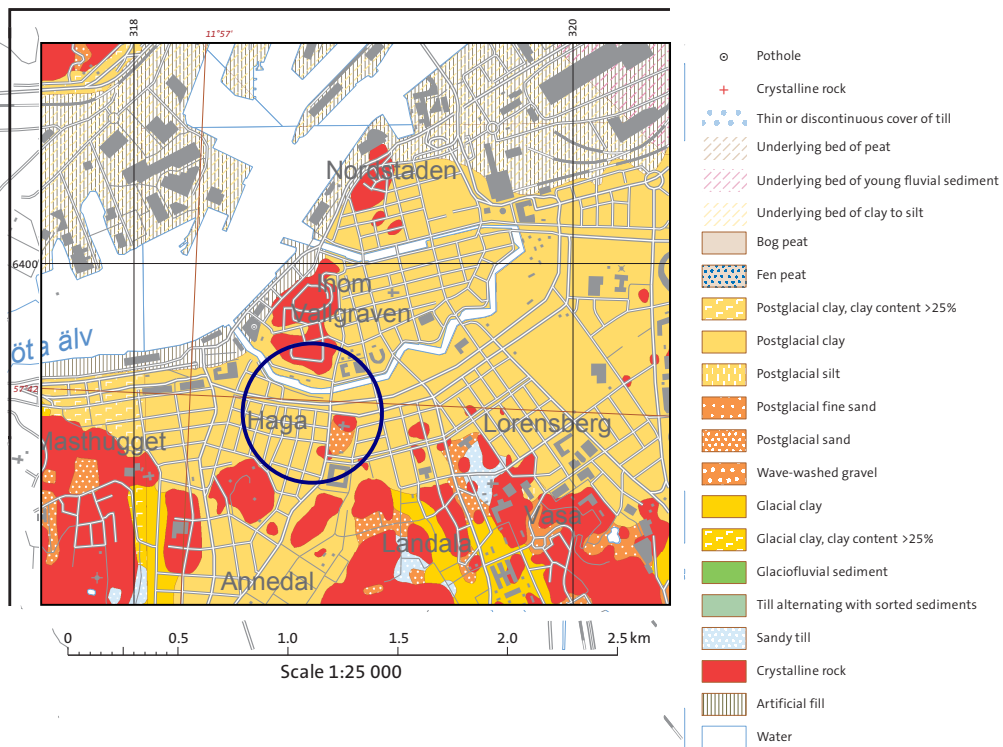


Figure 2.9: Extract from the Quaternary deposits 1:25,000 map from SGU [13]. Blue circle marks Haga area. The whole map can be found in Appendix A.

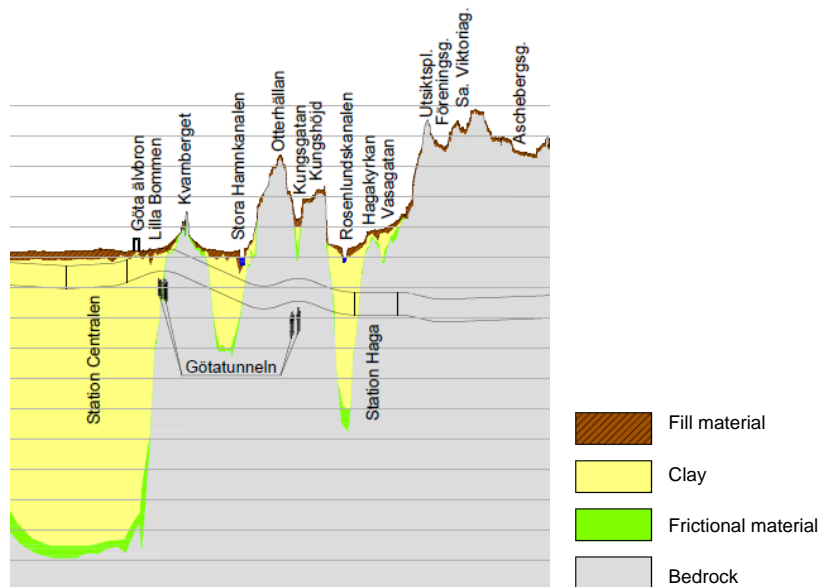


Figure 2.10: Geological cross-section of Haga area along planned Västlänken route [12]. Each horizontal line marks 10 m difference in elevation, where the bottom of Haga station is at about -20 m depth. From Swedish, there are: Station Centralen - Central Station, Station Haga - Haga Station, Götatunneln - Göta Tunnel. There rest of names mention characteristic points in Gothenburg.

Clay in the area is claimed to be soft, normally consolidated to slightly overconsolidated but rather homogeneous. Its depth is the most substantial close to Rosenlundskanalen to decrease to about 2-4 m under the Hagakyrkan area (see Section 2.3.2). The church itself is founded almost solely on the rock formation while the park around consists of a top layer of hummus and 1 to 4 m of silty clay beneath it [2].

Friction material consists mainly of sand and gravel. The deepest layer can be found at the Rosenlundsbron embankment from the side of the Skatteverket building where it has been used as a fill, and its depth is projected to be 8 to 14 m. On the opposite side of the canal, the friction material underlies the thick clay layer and does not exceed 2 m in depth [12].

### 2.3.2 Depth to bedrock

The elevation differences in Gothenburg are substantial and are driven mostly by the depth to bedrock. In the area of Hagakyrka, historical materials mark the location of the previous quarry [12]. This might partly explain the depression between Kungshöjd and Vasagatan. The southern area of Haga towards Annedal is where bedrock is rising. Simultaneously, the area towards the canal is being placed predominantly on the thick clay layer filling very deep cone depression in the bedrock that is claimed to reach levels up to -60 m.

Figure 2.11 presents an overview of the thickness of surficial materials over bedrock. Data correlates well with the quaternary deposits map as the area of deep bedrock (dark brown) covers the same areas as glacial clays in Figure 2.9. From both maps, it can be read that Hagakyrkan is situated mainly on the crystalline bedrock, but the area around the southern part of the building is covered with about 5 m thick layer of soft material.

According to Figure 2.9, the area between two buildings is filled with soft clay up to 30 m in depth underneath which the bedrock layer can be found. Information presented in the SGU map has not found confirmation during the soil investigation process. Consultants noted the depth to bedrock up to 60-65 m at the junction between Haga Nygata and Linnegatan. Information is repeated further in the Trafikverket report from 2016 (see Figure 2.10), where the thick clay layer of undefined depth is presented over the frictional material. Thus, it is claimed that there is a high probability of bedrock being deeper than the SGU materials present. It is probable that interpolation of the information during automatic map generation lead to omitting the lowest point of bedrock in this area what also resulted in the thinner surficial material depth in this place.

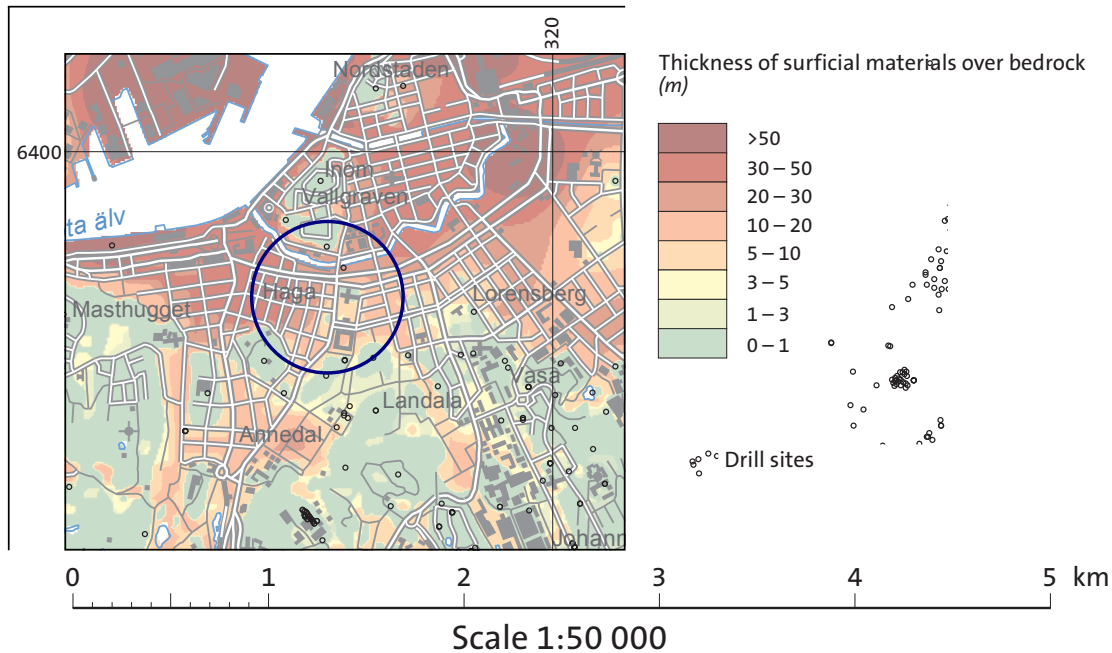


Figure 2.11: Depth to bedrock 1:50,000 after SGU [14]. Blue circle marks Haga area. The whole map can be found in Appendix B.

### 2.3.3 Bedrock quality

The quality of bedrock in the Haga area is claimed to be good, and no major fracture zones cross through the district. Nevertheless, smaller deformation zones can be found to the north from Skatteverket where bedrock is claimed to be fragmented (see Figure 2.12). Similar conditions are to be found to the south of Hagaparken. This means that planned station entrances might be located around fractured zones and a high care should be paid during their erection.

Type of bedrock is uniform over the whole Southern part of the city centre and consists mainly of acidic intrusive rocks like granite, granodiorite and monzonite.

## 2.4 Ground water conditions

SGU map does not present any groundwater aquifers in Haga (see Figure 2.13). The closest ones are located to the north of the canal and to the east around Lorensberg. Information has been confirmed during soil investigation where CPT sounding revealed a rather homogeneous mud without any occurrence of aquifers [12].

The groundwater level is claimed to be very high. Based on the available reports, it is claimed to be located around 1 m below the surface around the tunnel route [2].

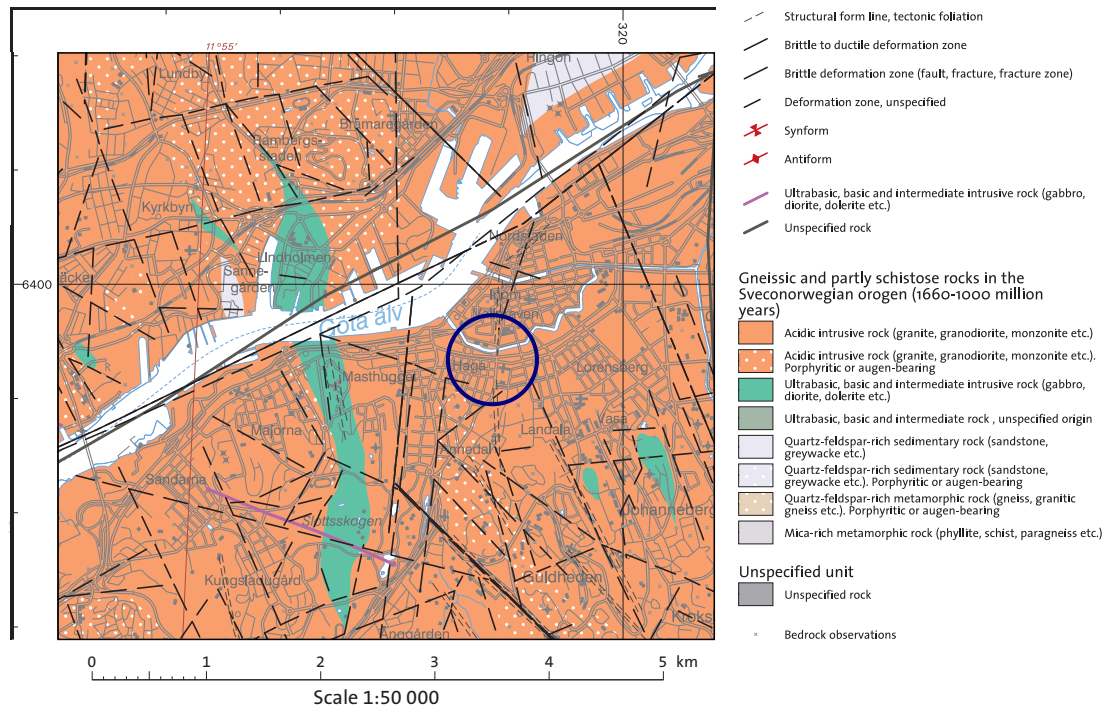


Figure 2.12: Bedrock map 1:50,000 after SGU [15]. Blue circle marks Haga area. The whole map can be found in Appendix C.

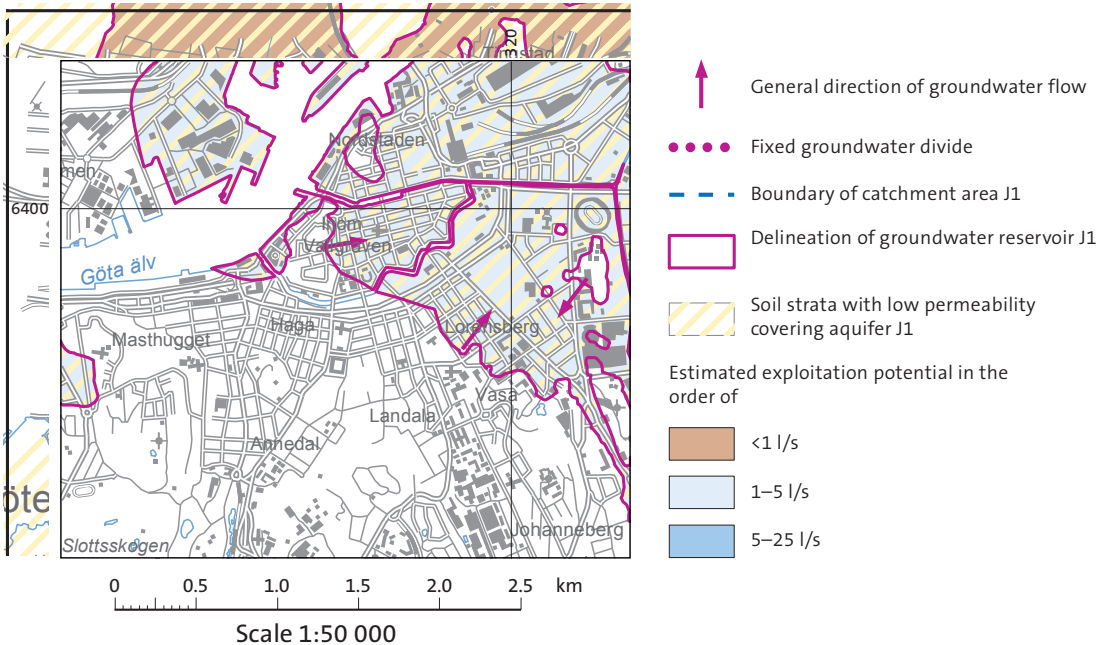


Figure 2.13: Groundwater reservoir map 1:50,000 after SGU [16]. The whole map can be found in Appendix D.

## 2.5 Surrounding structures

A variety of land uses are encountered in the area where the Haga station is planned. Mainly, it is used as commercial, residential and institutional purposes. Additionally, there is a significant diversity related to the age of buildings which implies the application of various construction methods in the same zone. For the case of this study, it is highly important to analyse the type of foundation on which the surrounding buildings are supported. The objective of this is to investigate the disturbance effect from old foundations to the soil structure and to account for the impact of the planned underground construction on the existing buildings.

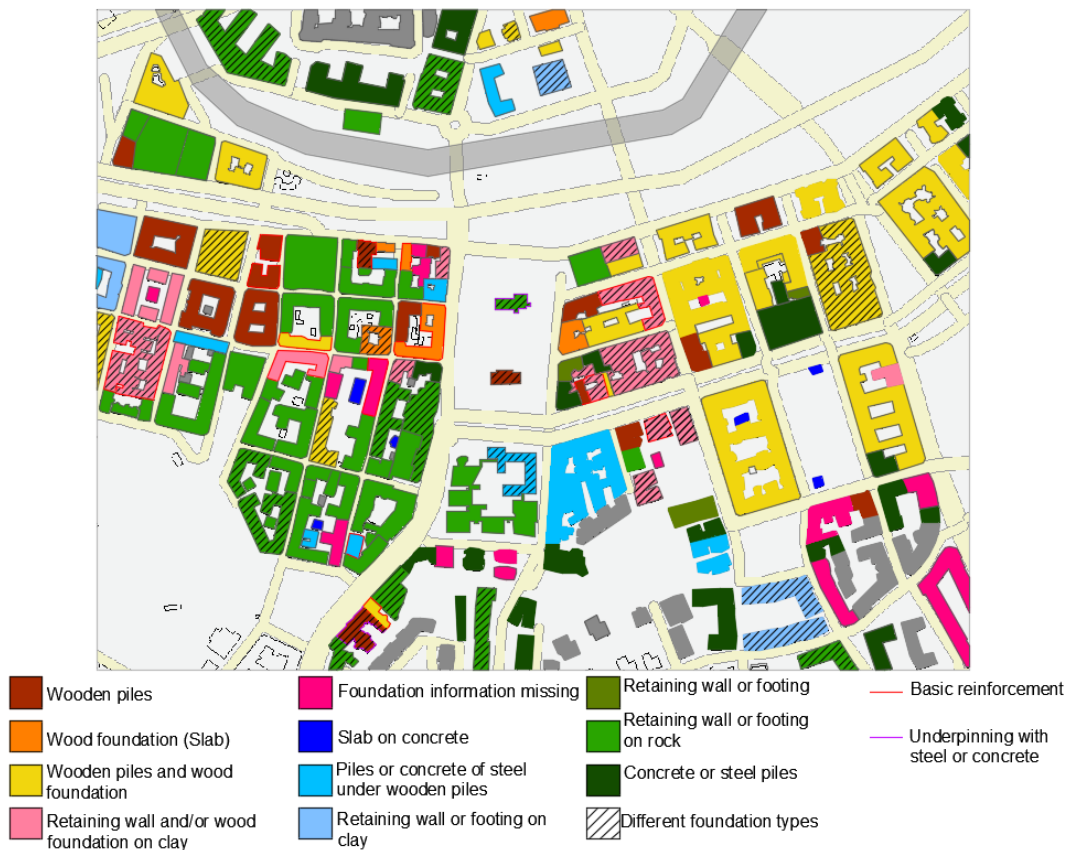


Figure 2.14: Foundation type for surrounding buildings to the project area. Based on Trafikverket [17].

As presented in Figure 2.14, a large variety of foundations structures are found in the area. A significant portion of the foundations are wooden structures which are supported directly on bedrock or in the clay layer. These kind of foundations imply potential serious risks given that considerable changes in the water table will lead to anticipated large settlements of the mentioned structures. Having that in mind, strengthening ground works have been made to reinforce some of the weaker foundations, but there is still a large number of buildings which could be affected during the short- and long-term perspective.

## 2.6 Sustainability

Sustainable development has many definitions, but all can be summarised as a collective effort to ensure the balance between environment protection, social progress and economic growth. The aim is to serve the society without compromising the needs of future generations. United Nations has widely discussed this in their Development Goals [18] which later have been extrapolated to the countries construction legislation by means of i.e. BREEAM assessment in the UK and LEED in the USA.

Construction industry contributes to the overall CO<sub>2</sub> emission by employing materials with high carbon footprint (see Figure 2.15), transporting materials to the site and creating waste that is sometimes difficult to recycle. Thus, it is of common interest to try to tackle these challenges by i.e. re-using existing structures, minimising energy in construction and caring about conserving natural resources. Such principles can be easily employed at the early design stage where the goal is to reduce the construction waste and, consequently, carbon emission and water footprint of the erected structure (see Figure 2.16). These aspects have been taken into account in this study and a short example of such calculations is presented further in Section 7.7.

| ENERGY REQUIREMENT FOR MATERIALS (GJ / TONNE) |                                |
|---|--------------------------------|
| <span style="color: red;">■</span>            | <b>Very high energy</b>        |
| <span style="color: red;">■</span>            | Aluminium 200–500              |
| <span style="color: red;">■</span>            | Stainless steel 50–100         |
| <span style="color: orange;">■</span>         | <b>High energy</b>             |
| <span style="color: orange;">■</span>         | Aluminium 30–60                |
| <span style="color: orange;">■</span>         | Carbon steel 25+               |
| <span style="color: yellow;">■</span>         | <b>Medium energy</b>           |
| <span style="color: yellow;">■</span>         | Reinforcement steel 8.9        |
| <span style="color: yellow;">■</span>         | Clay bricks & tiles 2–7        |
| <span style="color: yellow;">■</span>         | Concrete                       |
| <span style="color: yellow;">■</span>         | Precast 0.8–1.5                |
| <span style="color: yellow;">■</span>         | Blocks 0.8–3.5                 |
| <span style="color: yellow;">■</span>         | In situ 1.5–8                  |
| <span style="color: lightgreen;">■</span>     | <b>Low Energy</b>              |
| <span style="color: lightgreen;">■</span>     | Timber 0.1–5                   |
| <span style="color: lightgreen;">■</span>     | Sand, aggregate <0.5           |
| <span style="color: lightgreen;">■</span>     | Flyash, RHA, Volcanic ash <0.5 |

Figure 2.15: The average embodied energy in construction materials [19].

## END-OF-LIFE SCENARIOS

What happens to a building's structural frame once it is demolished?

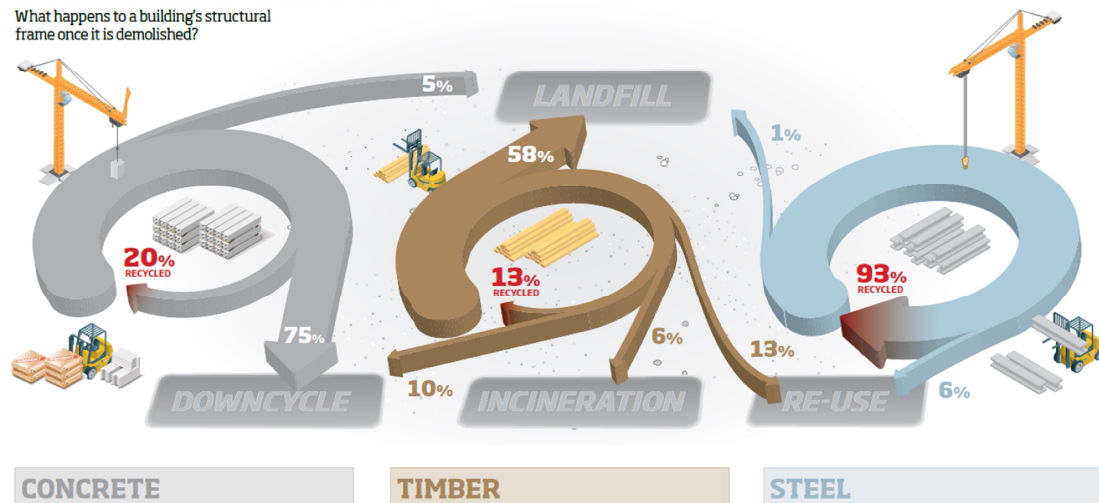


Figure 2.16: Life-cycle of construction materials based on the example of the UK (sketch reprinted by the courtesy of AKT II).

## 2.7 Contamination

SWECO mentions in their report the possibility of soil contamination, especially radon [2]. Having in mind the scope of this thesis, issues related to the possible soil contamination are not considered further but should be appreciated by the reader who is strongly encouraged to review the information available at the source.



# 3

## Theory

The following chapter presents the general concepts and theories that have been utilised during the conceptual model development. They are necessary to understand the problems related to the deep excavation design in soft soils. Bearing in mind the extent of this thesis, it is highly recommended to source the additional details in the bibliography as the scope of this document has been limited to the general information only.

### 3.1 Deep excavations

Historically, a distinction between shallow and deep excavations has been drawn by Terzaghi [20]. In his paper, he stated that excavations which depths exceed their width could be considered as deep excavations. With time, the definition evolved and settled a depth of 6 m as a boundary between shallow and deep excavations [21][22][23].

In the up to date scientific publications, deep excavations being considered are usually much deeper than 6 m. As their depth is substantial, their support system get advanced. Numerous propping levels unable to find a solution to the problem with simple calculation methods. This is a place, where FEM analysis plays an important role.

Nevertheless, in practice, it is sometimes hard to distinguish between shallow and deep excavation. Traditionally, shallow excavations require light temporary structures as the construction process usually proceeded fast from excavation to ground level completion. Nowadays, such structures require much more robust temporary works similar to the ones erected for deep excavations as possible legal problems might stop the construction for a substantial period of time. In such instance, the time might be long enough to allow groundwater dissipation and turn assumed undrained conditions to unsafe zone of drained case.

One more issue to consider is health and safety. Each year, there are numerous examples of health and safety violation when it comes to excavation processes. These figures are still low in comparison to falling from height, but may lead to the conclusion that both shallow, as well as deep excavations, care equally dangerous for people working in the pit [24].

While currently the stability of the excavation as a whole can prove in some places challenging, these are requirements imposed by the existing surrounding structures that drive the design of deep excavations. In one of Puller's works, he summarised pressing problems regarding deep excavations in the urban setting: “(...) *in both the short and long term, the design of the works must be such as to contain deformation of the soil or rock adjacent to the excavation to limits which do not cause distress to existing structures or services* [25].” Consequently, the problem translates to accurate representation of soil-structure interaction that, in majority of cases, drives the whole design process.

## 3.2 Soft soils

Kempfert and Gebreselassie defined soft soils as a geologically young, normally consolidated cohesive deposits [26]. Their publication, as many other authors, extends this definition and includes in the group also normally consolidated, under consolidated or lightly overconsolidated fine grain soils with a very soft consistency. More precise definition was proposed by the EAB of the German Geotechnical Society (ger. Empfehlungen des Arbeitskreis “Baugruben“ der Deutschen Gesellschaft für Geotechnik), where the soft soil can be recognised when it fulfills requirements (not all of them need to be fulfilled simultaneously) [27]:

- very soft to soft consistency with a consistency index  $I_c < 0.75$
- fully or nearly fully saturated
- undrained shear strength  $S_u \leq 40 \text{ kN/m}^2$
- high to medium plasticity
- thixotropic.

Due to their properties, soft soils cause significant problems. They are prone to deformations due to low stiffness. Such movements may lead to (uneven) settlements and consequently damage of neighbouring structures and services [26]. Equally distressing is the prediction of creep in the long-term analysis. One of the famous examples where the soft soil settlements caused major problems is the construction of the Kansai International Airport Islands, which sunk almost twice as much as it was originally predicted [28]. Additionally, where the groundwater level is high, soft soils are sensitive to groundwater level changes and thus might trigger problems with basal heave if the hydrostatic pressure head is high enough.

All of the above arguments makes is particularly challenging to model the soft soils behaviour using FEM. In the recent years, considerable advancements in modelling the strength and deformations have been made. Nevertheless, it still proves to be problematic to predict ground movements around the excavation in soft soils. The leading example of difficulties in applying numerical methods in excavation analysis is the *Benchmarking in Geotechnics* by prof. Schweiger [29]. His publication depicted wide discrepancies in results of numerical analysis provided by numerous professional parties involved in the exercise.

Thus, it is of paramount importance to underline risks and pitfalls related to such analysis. The results are significantly influenced by the choice of the constitutive model and parameters used to describe the stress path and soil deformations. More information about pitfalls in geotechnical engineering analysis using FEM can be found in Section 3.5.

### 3.3 Soil tests

To analyse the soil characteristics Haga, several tests were performed in different locations at the area of interest. Executed tests included undrained triaxial, constant rate strain (CRS) and direct shear and oedometer. A description of the tests and their relation with the required parameters to setup the model is presented in this section.

#### 3.3.1 Undrained triaxial test

The triaxial test is used for measuring the soil behaviour under shear. The method consists in the application of axial ( $\sigma_a$ ) and radial ( $\sigma_r$ ) stress into a cylindrical undisturbed sample in a triaxial apparatus. Its main advantages are the easiness of its execution in all types of soil and the possibility to control drainage conditions during the test. This study utilises only one of the principal types of triaxial tests which is Consolidated-Undrained (CU). In this test, the sample is subjected to a confining pressure, and then the principal stress difference is applied immediately after which does not allow for drainage or consolidation of the specimen [30].

The primary output from the test is the determination of the strength parameters of the soil (friction angle ( $\phi$ ), and effective cohesion ( $c'$ )), which can be examined by the interpretation of different stress invariants graphs. One possibility is to plot the deviatoric stress vs. the mean total or effective stress ( $p$ ,  $p'$ ), which are calculated according to equations 3.1 and 3.2.

$$q = \sigma_a - \sigma_r = \sigma'_a - \sigma'_r \quad (3.1)$$

$$p = \frac{\sigma_a + 2\sigma_r}{3} \quad p' = \frac{\sigma'_a + 2\sigma'_r}{3} \quad (3.2)$$

After plotting the values from different tests made to the same soil material, a linear trend line of the points is visible. This trend line is known as failure envelope (see Figure 3.1) and the strength parameters can be determined from it. The effective cohesion ( $c'$ ) is the value of the intersect of the line with the y-axis (calculated with the expression seen in Figure 3.1), and the friction angle ( $\phi'$ ) is calculated based on the value of the gradient (M) of the envelope (see equation 3.3).

$$M = \frac{q}{p'} = \frac{6\sin\phi'}{3 - \sin\phi'} \quad (3.3)$$

$$\sin\phi' = \frac{3M}{6 + M}$$

For normally or slightly overconsolidated clay (Figure 3.1(b)), the failure envelope should pass through the origin. Therefore, the effective cohesion is equal to zero ( $c'=0$ ) [30].

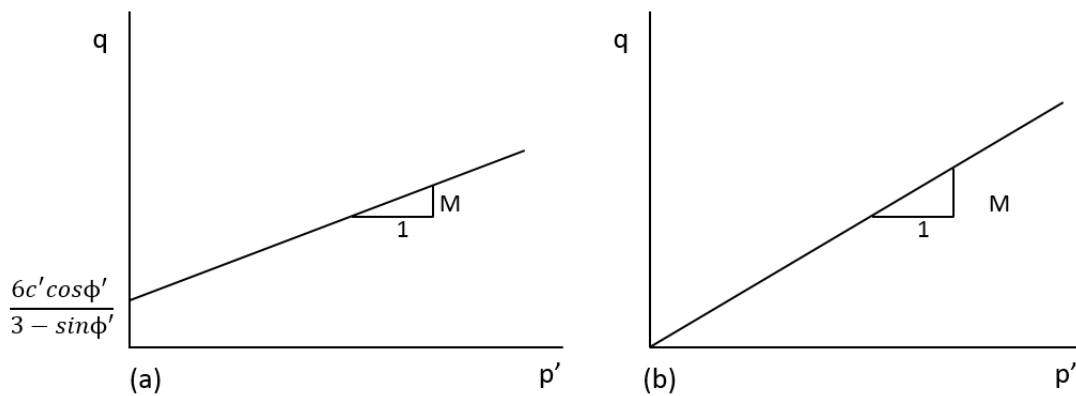


Figure 3.1: Deviator vs. mean effective stress. Based on Knappett and Craig [30].

### 3.3.2 Direct Shear test

The direct shear test similarly to triaxial test is used to measure soil behaviour under shear conditions. Likewise, it can also be used in all types of soils. Similarly to triaxial test, the strength parameters in the direct shear test can be determined by plotting the resultant stress variables. Here, the plotted values correspond to the shear stress at failure ( $\tau_f$ ) against the normal effective stress ( $\sigma'_f$ ).

As seen in Figure 3.2(a), the friction angle is calculated as the inclination angle of the failure envelope, and the effective cohesion as the intercept with the  $y$ -axis. In Figure 3.2(b), the effective cohesion is zero, and the failure envelope is then called the critical state line (CSL). Under this conditions, the critical friction angle ( $\phi_{cv}$ ) is higher than the effective friction angle.

### 3.3.3 Oedometer test

Oedometer test is used to simulate the behaviour of soil under one-dimensional consolidation or swelling. The tested soil is placed inside a metal ring and between two porous stones which support drainage of the sample. The test is carried out in a submerged environment to allow free access to pore water. The type of test

depends on the application of the load. The most common one is the incremental loading test where the application of the load to the sample is cumulative. Another common method is the constant rate of strain test (CRS), where a fixed displacement regulates the applied load.

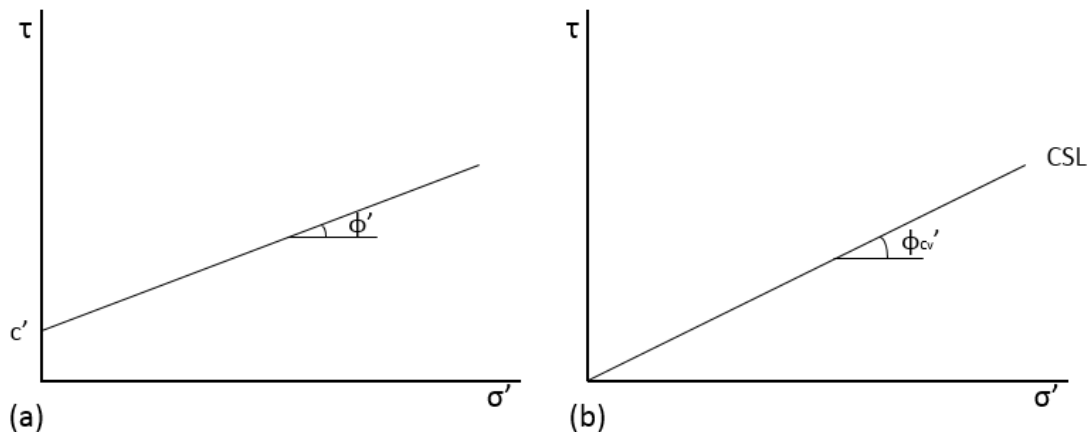


Figure 3.2: Failure envelope plot and Mohr-Coulomb shear strength parameters determination. Based on Knappett and Craig [30].

The results of the test are analysed with the help of the plots presented in Figure 3.3. From the graphical analysis, the assessment of the consolidation history of the soil can be made. Determination of the preconsolidation pressure ( $\sigma_c$ ) can be obtained from geometrical analysis of the void ratio-effective stress relationship. In Figure 3.3(b) the procedure proposed by Casagrande is represented [30][31][32]. The calculation of the overconsolidation ratio (OCR) can be achieved from the performed analysis as the relation between the preconsolidation pressure and the in-situ effective stress ( $\sigma'_{v0}$ ) (see equation 3.4). Another way to represent overconsolidation is the pre-overburden pressure which is calculated as presented in equation 5.1.

$$OCR = \frac{\sigma'_c}{\sigma'_{v0}} \quad POP = \sigma'_c - \sigma'_{v0} \quad (3.4)$$

To determine the parameters used in the Soft Soil (SS) and Soft Soil Creep (SSC) models, a graphical analysis of the different sections of the curve is assessed. The curves from the plot can be divided into compression, swelling and secondary compression (see Figure 3.3(a)). The determination of the regular and modified compression ( $C_c/\lambda^*$ ), swelling ( $C_s/\kappa^*$ ) and creep indexes ( $C_\alpha/\mu^*$ ) is calculated as the slope of the characteristic curve for each parameter (see Figure 3.4). Determination of the regular indexes is made of the logarithm of the effective stress vs. the void ratio. As for the modified indexes, this is calculated for the plot of the natural logarithm of the effective stress vs. the volumetric strain.

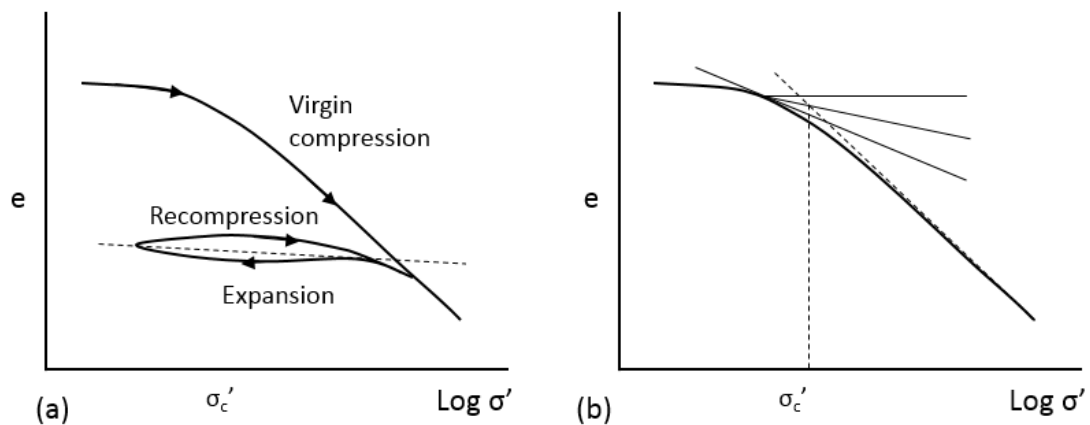


Figure 3.3: a) Void ratio ( $e$ ) vs. effective stress ( $\sigma'$ ) relationship, b) Determination of preconsolidation pressure based on Knappett and Craig [30].

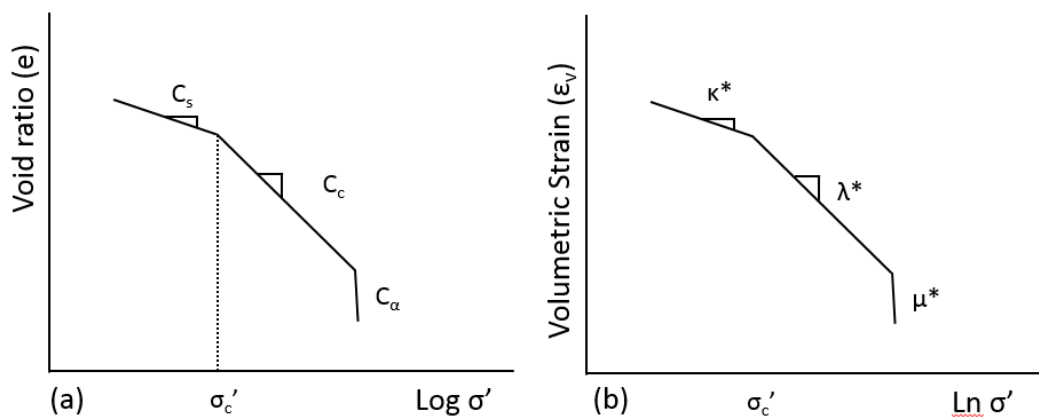


Figure 3.4: Relationship between a) void ratio ( $e$ ), and logarithm of the effective stress ( $\sigma'$ ), and b) volumetric strain ( $\epsilon_v$ ) and the natural logarithm of effective stress ( $\sigma'$ ). Based on Havel [33].

The strain-stress plot does not represent correctly the secondary compression curve. Thus, the creep index is determined as the slope for secondary compression in a strain-time plot. The data for these curves is retrieved from an incremental oedometer test. The slope has to be measured in the section of the curve where the behaviour starts to be more linear, and therefore the primary consolidation has ended (see Figure 3.5).

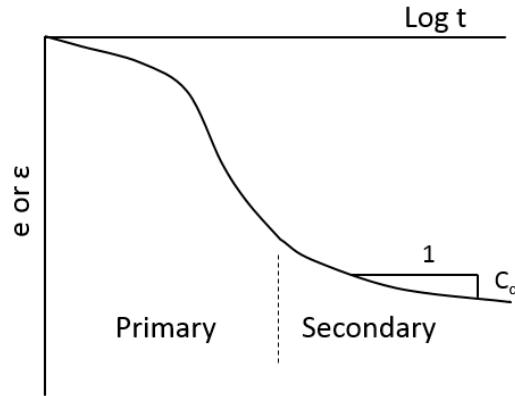


Figure 3.5: Consolidation curve. Based on Olsson [34].

## 3.4 Material models

There are various material models available to represent the behaviour of the soil during the numerical analysis. Through them, the accuracy of the calculations is affected by the application of i.e. diverse stress-strain relationships. Different models give different solutions due to their different assumptions (such as yield surface, elastic law, flow rule and others). The choice of material model is an important part of correct modelling of the soil behaviour, and for retrieving representative results that can be translated into the design.

### 3.4.1 Soil models in PLAXIS

PLAXIS 2D incorporates a variety of material models which can be used to fit the characteristics of the ground on-site. The choice of the model depends on the mentioned features of the analysed soil, but also of the quality and amount of available data. A description of some of the soil models available in PLAXIS 2D is made in this section. The comparison of the available soil models in PLAXIS 2D and their application has been presented in Appendix E.

#### Linear elastic perfectly plastic (Mohr-Coulomb)

The Mohr-Coulomb (MC) model is one of the simplest available models in PLAXIS 2D. It is often used as a first approximation of the soil behaviour, as in reality soils have a non-linear response when changes in stress or strain are being applied to them. The MC model is based on two principles, the linear part based on Hooke's Law of isotropic elasticity, and the plastic behaviour based on the Mohr-Coulomb failure criterion complemented most commonly with a non-associate flow rule [35].

The MC model uses five principle parameters to define the elasticity, plasticity and dilatancy of the soil [35], where:

|               |  |
|---------------|--|
| $E'$          | Young's modulus                                |
| $\nu'$        | Poisson's ratio                                |
| $\phi'$       | Friction angle                                 |
| $c'$ or $S_u$ | Effective Cohesion or Undrained Shear Strength |
| $\psi$        | Dilatancy angle                                |

The choice between  $c'$ , or  $S_u$ , depends on the type of parameters which are being used to characterise the soil. Therefore, if the parameters are in terms of effective strength, the effective cohesion value is used; if the parameters are in terms of undrained shear strength, the  $S_u$  value is used.

### Soft Soil

The Soft Soil (SS) model is a type of Cam-Clay model which were formulated to represent the behaviour of soft soils in three aspects which are the strength, compression and critical state [36]. The SS model in PLAXIS 2D is characterised by a non-linear stress dependency of soil stiffness, failure mechanism according to MC criterion and a distinction between primary loading and unloading-reloading [35].

In the SS model, the strain-stress relation is assumed to be logarithmic as represented in Figure 3.6. From this plot, the two most important parameters to define the model are retrieved, which represents the compressibility of the material during primary loading ( $\lambda^*$ ), and during unloading and reloading ( $\kappa^*$ ).

A list of the parameters used in the SS model are presented below:

|             |   |
|-------------|---|
| $\lambda^*$ | Modified compression index                            |
| $\kappa^*$  | Modified swelling index                               |
| $\nu'$      | Poisson's ratio                                       |
| $\phi'$     | Friction angle  |
| $c'$        | Effective cohesion                                    |
| $\psi$      | Dilatancy angle                                       |
| OCR-POP     | Over consolidation ratio or pre-overburden pressure   |
| $K_0^{NC}$  | Coefficient of lateral stress in normal consolidation |

The value for  $K_0^{NC}$  is determined with Jaky's formula (see equation 3.5) [37].

$$K_0^{NC} = 1 - \sin\phi' \quad (3.5)$$

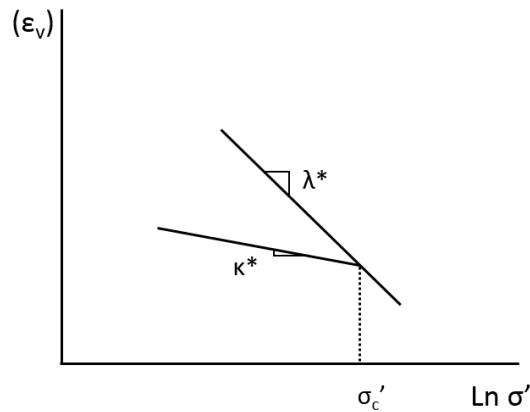


Figure 3.6: Logarithmic relation between volumetric strain and effective stress [35].

### Soft Soil Creep (time dependent behaviour)

The Soft Soil Creep (SSC) model is an advanced model in PLAXIS 2D which allows consideration of creep the soil model [35]. This model is suitable especially for constructions in soft soils where settlements from creep could involve serviceability issues. The SSC has the same characteristics as the SS model plus the consideration of secondary compression, and the ageing of the pre-consolidation stress.

The parameters used in the SSC model are the same as the ones presented in the SS model section, except from the modified creep index ( $\mu^*$ ) which allows for the consideration of creep in the soil model behaviour.

### Hoek-Brown

Hoek-Brown (HB) failure criterion is used as an approximation to estimate the strength of rock masses, based on the assessment of block stability [38][39]. The criterion started as a combination of the properties of intact rock with reduction factors to these properties according to the nature of the joints in the rock mass [40].

Modifications of the HB failure criterion were made to make it usable for application in numerical models [40]. The Hoek-Brown model included in PLAXIS 2D is based on the revision made in 2002 by Hoek, Carranza and Corkum [40]. Revision combines the HB failure criterion, which involves shear and tensile strength, with Hooke's law of isotropic linear elastic behaviour.

The formulation of the HB failure criterion is shown in the equation 3.6.

$$\sigma'_1 = \sigma'_3 + \sigma_{ci} \left( m \frac{\sigma'_3}{\sigma'_{ci}} + s \right)^{0.5} \quad (3.6)$$

where:

|               |  |
|---------------|--|
| $\sigma_{ci}$ | Uniaxial compressive strength of the intact rock material  |
| m and s       | Material constants which are dependent of the disturbance factor of the rock mass (D), and the Geological Strength Index (GSI) |

For more information about the calculation of the mentioned parameters see Hoek, Carranza and Corkum [40]. The input parameters of the Hoek-Brown model in PLAXIS are listed below:

|               |  |
|---------------|--|
| E             | Young's modulus  |
| $\nu$         | Poisson's ratio  |
| $\sigma_{ci}$ | Uni-axial compressive strength of the intact rock                    |
| $m_i$         | Intact rock parameter  |
| GSI           | Geological Strength Index  |
| D             | Disturbance factor   |
| $\psi_{max}$  | Dilatancy angle (at $\sigma'_3 = 0$ )                                |
| $\sigma_\psi$ | Absolute value of confining pressure $\sigma'_3$ at which $\psi = 0$ |

Typical values for the input parameters can be found in the extensive literature from Hoek, E. [40][41][42], and can be determined by evaluating the type of rock, block stability, history of invasive construction methods in the area among others.

### Interface between soil and construction material

To model the behaviour of underground foundation structures accurately, an interface must be included on each face of the structure which is in contact with the soil. PLAXIS 2D introduces two options for the interface behaviour as rigid or manual. The rigid option is used when the interface should not have a reduced strength. In this case, the strength reduction factor ( $R_{inter}$ ) has a value of 1.0. This case is mostly applied for extended interfaces beyond the limit of the structure. The second option to define the interface manually. In this case, it is assumed that the interface between the soil and the structure is weaker than the surrounding soil, and, therefore, the  $R_{inter}$  has to be less than 1 [43]. Calculation of this parameter is made with equation 3.7, where  $\phi_i$  is the skin friction angle of the interface.

$$\tan\phi_i = R_{inter}\tan\phi \leq \tan\phi \quad (3.7)$$

### 3.5 General discussion of material models in FEM

Nowadays, availability of powerful computers made numerical analysis an accessible tool for geotechnical engineers. Its arrival did not change the soil mechanics itself, but rather allowed a more visual representation of the results. Nevertheless, for many practitioners, this was enough to be biased by the easiness of calculations and forgot about the pitfalls in numerical modelling. It also attracted many people with limited knowledge of soil mechanics to attempt geotechnical assessments. Even properly trained engineers tend to forget about limitations of numerical modelling. In this view, knowledge of the engineer performing the analysis is of profound importance.

Similarly, the numerical analysis is directly affected by the soil investigation data. With the poor quality of input data, even the most sophisticated numerical tool is not going to deliver the reliable results. Equally important is the process of setting up the model where the boundary conditions, meshing and model geometry are decided upon. Part of these aspects has been discussed in details in the following Section 6.2. Unfortunately, the numerical programmes manuals offer minimum help in this regard. They are, in many cases, brief, and it is of user interest to seek for additional information at source or test if the programme works as is assumed to be.

One of the most popular is an elastic model. It is particularly easy to define but gives satisfactory results only in limited cases. The more accurate representation can be obtained with elasto-plastic analysis as it can present the non-linear soil behaviour as presented in Figure 3.7 where elastic settlement profile of pile group is misinterpreting the actual soil behaviour.

Equally important is the appropriate representation of groundwater behaviour and its effect on the numerical analysis. One of the most striking examples is previously mentioned Nicol Highway where Undrained A option combined with Mohr-Coulomb parameters led to the overestimation of the undrained share strength and resulted in much higher soil capacities than in reality (see Figure 3.8).

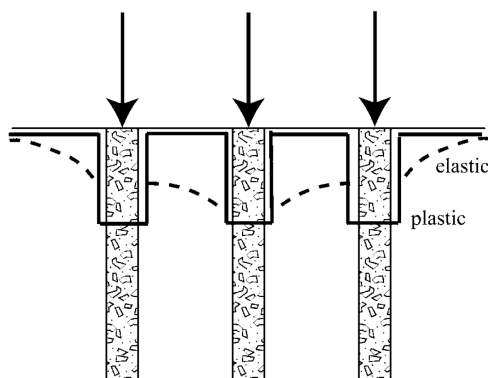


Figure 3.7: Schematic illustration presenting settlements of pile group for plastic and elastic parameters [44].

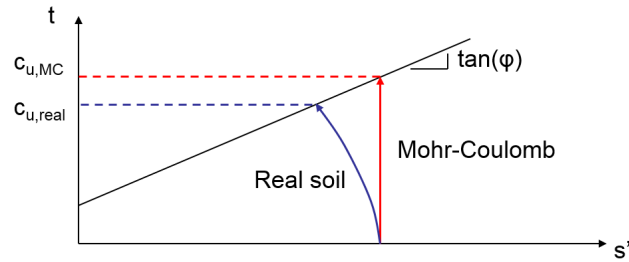


Figure 3.8: Overestimation of the undrained share strength with Undrained A and Mohr-Coulomb parameters [45].

To accurately represent the structural elements, it is advised to use multi-node elements instead of single-node structural elements. The user should remember not to place the middle-node of the element close to the end-node of the other. They are not interchangeable and should not be placed together. Similarly, the user might encounter a problem while using the interface elements. As their thickness is equal to zero, there might be problems with numerical stability of the calculation. Thus, it is recommended to check calculations with and without an interface. The interface value should never drive the design results what must be checked during the sensitivity study. It is also recommended to break down the load into small pieces so further refinement of load steps should not affect calculation results [46].

As mentioned in many numerical analysis guidebooks [44][46][47][48], it is of vital importance to analyse the structure together with soil and vice versa. Soil-structure interaction is driven by stiffness or deformation parameters of the soil, not its strength, and consequently should be treated together as they influence each other.

It is also recommended to create a simple model and refine it with time when more detailed soil investigation data are being available and/or when engineers get more familiar with the numerical software. The confidence of person performing analysis is important as the final results are significantly user-dependant [48].

The numerical results should be validated by the *back-of-the-envelope* calculations and sensitivity study to ensure that these are the main parameters that drive the design, not the mesh quality or interface values [44]. The numerical analysis should be performed only when the problem is fully understood, and the first predictions of the results are made. It is of vital importance to compare these results with practical knowledge. The results very different than expected are rarely true and lead to the misleading judgements.

Prof. Wood recommends answering simple questions as a way of preliminary result check: *Are we getting what we are looking for? Is the program doing what it is supposed to do? Are we getting the answer we need?* As he stated in his book, “A model is an appropriate simplification of the reality. (...) The quality of the numerical modelling result can only be as good as the quality of the numerical approximation” [44].

## Basal heave

Soft soils in undrained conditions are especially prone to the base heave. Particularly in deep excavations where the water table is high, the problem of uplift at the bottom of the pit starts to control the design.

Terzaghi initially explained the issue in 1943 (after [30]; see Figure 3.9), where he explained that failure at the base occurs when there is not enough support to resist the average shear stress from the vertical pressure from the adjacent soil uplifting the bottom of the excavation (see equation 3.8). With time, the theory was complemented with practical experience, and nowadays there is much more understanding of what may trigger the basal heave.

$$p = \gamma \cdot h + \sigma_q - \frac{S_u \cdot h}{0.7 \cdot B} \quad (3.8)$$

where:

|            |                          |
|------------|--------------------------|
| $\sigma_q$ | Surcharge load           |
| $S_u$      | Undrained shear strength |
| $\gamma$   | Soil unit weight         |

The basal heave is particularly dangerous as it may lead to the loss of stability of braced excavation due to the soil movement behind the wall. When part of soil is being pushed upwards, it leaves a void behind the wall and allows the retaining structure to move inwards. In this way, the force in the props is relaxed. The failure of the wall might occur and/or the settlement behind the wall would lead to the failure of the adjacent structure [30].

Nowadays, numerous ways to prevent the base heave are being explored; just to mention a few of them: raft foundation, pile foundation, soil-mix columns and submerged excavation. The following sections present the overview of them.

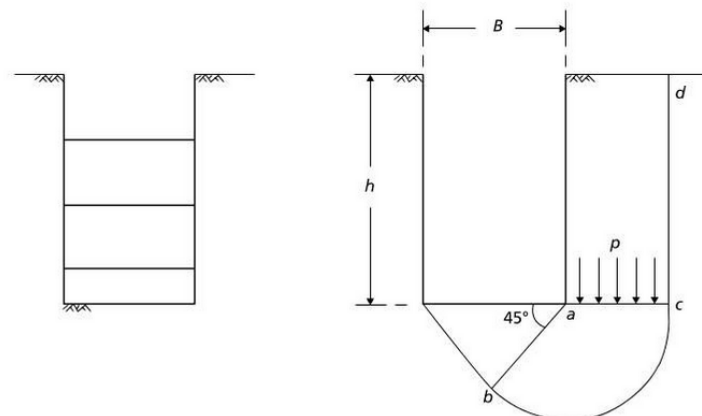


Figure 3.9: Base heave failure mechanism proposed by Terzaghi in 1943 after [30].

## 3.6 Loads

### 3.6.1 Internal loads

The design of a retaining structure is usually made to support a mass of soil [30]. The load from the soil in this study will be referred to as the internal load which accounts for the earth pressures from the soil skeleton and groundwater.

#### Soil load on the wall

The load from the soil in the retaining structure is also referred to as the earth pressure. There are two types of earth pressure to account for in the design of a retaining structure, active and passive. The active condition of the soil is defined as the section behind the wall where the horizontal stresses are decreased due to movement of the wall in the opposite direction of the active side. Reduction of horizontal stresses occurs until a point of plastic equilibrium where the principal total and effective stresses are vertical. The passive condition is located on the other side of the wall, where lateral compression of the soil occurs due to the displacement of the wall. An increase of the horizontal stresses is developed until plastic equilibrium is reached where both total and effective stresses are horizontal [30].

The calculation of earth pressures can be performed by a series of analytic methods such as Rankine's theory and Coulomb's theory for earth pressure. These methods are however limited to cases where the deformation of the wall satisfies the minimum deformation requirements to reach the state of plastic equilibrium required by both passive and active states [30]. Regarding braced excavations, the active state is not applicable for the walls given that the minimum deformation requirement is not fulfilled (see Figure 3.10). Therefore, for this type of excavations, theoretical methods are not adequate to give an accurate prediction of the earth pressures. Braced excavations can be evaluated by empirical and finite element methods. Empirical methods were developed by Terzaghi and Peck [21], and Twine and Roscoe [49] to assess strut loads envelopes. These methods were generated by the analysis of field measurements and are highly recommended as a check for computed strut loads from FEM [25].

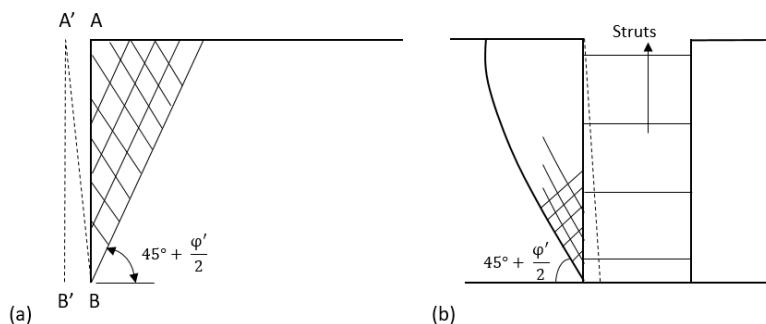


Figure 3.10: a) Minimum deformation condition to mobilise active state, b) Wall deformation for braced excavation [30].

The pressure envelopes developed by Terzaghi and Peck are one of the first empirical procedures for determining strut loads [50]. The envelopes correspond to braced excavations in sand, soft to medium clay and stiff fissured clay (see Figure 3.11). For soft and medium clays (Figure 3.11(b)), a reduction factor ( $m$ ) of approximately 1.0 was found by Terzagui and Peck for most clays [25]. As for stiff fissured clays (Figure 3.11(c)), a reduction factor of 0.4 is usually used, but it can be lowered to 0.2 when movements are minimal and the construction period is short [51].

For deep excavations in clay, Terzagui and Peck found that a variation on the strut loads of approximately 60 % can be obtained. Therefore, the proposition of a stability number ( $N$ ) was made to choose which envelope to use (see equation 3.9). For clays with  $N$  less than 4, the envelope in Figure 3.11(c) must be utilised, as for clay with  $N$  more than 6, the envelope in Figure 3.11(b) is to be used [51].

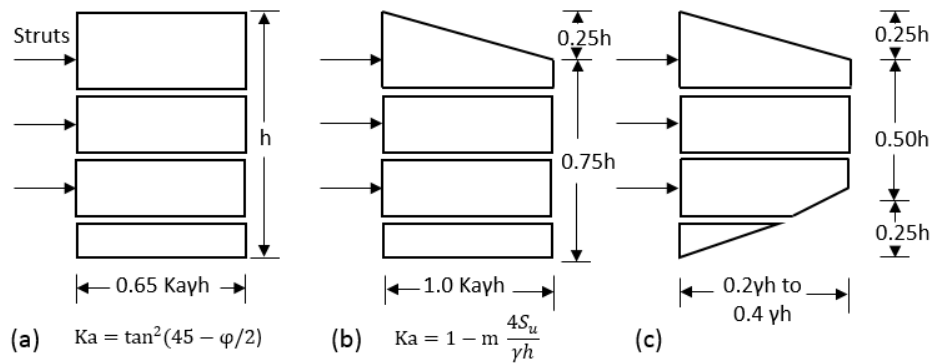


Figure 3.11: Pressure envelopes for braced excavations for a) sands, b) soft to medium clays, and c) stiff fissured clays (Terzaghi and Peck [21] after Puller [25]).

$$N = \frac{\gamma \cdot h}{S_u} \quad (3.9)$$

Pressure envelopes for braced excavations developed by Twine and Roscoe for two types of soils are presented in Figure 3.12. As it can be seen, the upper and lower pressure values are a function of the depth of the excavation ( $h$ ), the unit weight of the soil ( $\gamma$ ). The coefficients  $a$  and  $b$  depend on the configuration of the pit construction. For soft and firm clays, the value of  $a$  and  $b$  are equal to 0.65 and 0.5 respectively for retaining walls constructed until the depth of the excavation. As for retaining walls extended below the bottom of the excavation, the values for  $a$  and  $b$  change to 1.15 and 0.5 [49]. For the envelope presented in Figure 3.12(b), which corresponds to stiff clays and coarse soils, the value of  $b$  depends on the flexibility of the wall. For clays, the value of  $b$  corresponds to 0.3 for flexible, and 0.5 for stiff walls. For coarse soils, the value of  $b$  is 0.2 [49].

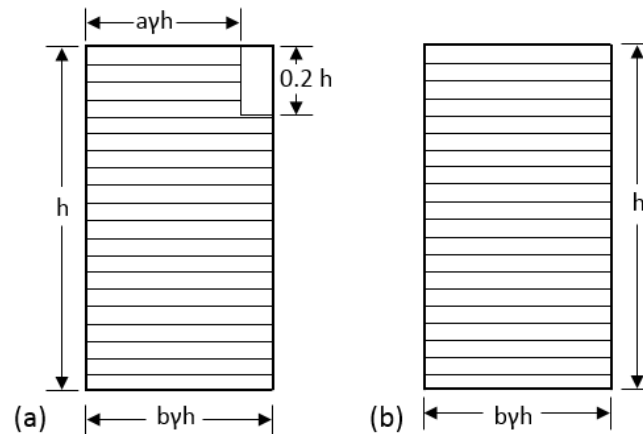


Figure 3.12: Pressure envelopes for braced excavations for a) soft and firm clays, and b) stiff and very stiff clay and coarse soils. Based on Twine and Roscoe [49].

### 3.6.2 External loads

The design of retaining structures must account for additional surcharge loads which will act on the wall. Therefore, loads from traffic on adjacent roads, neighbouring buildings, materials and equipment for construction and other temporary structures must be taken into account [25].

#### Surcharge load around the station

Surcharge load from traffic on nearby roads and from the construction itself, are of great importance in the design of deep excavations in urban areas. The loads from traffic will impose additional stress into the soil. Values from these loads are usually retrieved from manuals written by the transportation administration of the country or region in which the project is going to be developed.

As for the surcharge load from adjacent buildings, these have to be calculated according to the type of structure and materials which were used for its construction. Two types of loads have to be accounted for calculation of total surcharge load from buildings, which are dead and live loads. Dead load refers to the total weight of the materials used for the construction of the building which is irremovable from the site; some examples are façade weight, weight from internal walls and floors and others. As for the live load, this refers to the weight which is not static in the building and could change over time. This applies, for instance, to snow and wind loads. Live load is usually calculated using manuals which have typical values for different types of uses of buildings.



## 3.7 Structural elements

Various structural elements can be utilised to help with soil retention in the urban environment. Solutions vary based on the complexity of the construction to be made, especially the type of soil and depth of the excavation. Majority of elements are treated as permanent solutions, but there are some that can be removed after completion of the work.

### 3.7.1 Retaining walls

Traditionally, simple retaining structures were designed using elementary methods as limit equilibrium and stress field ([55] after [48]). As the complexity of the design builds up, the equilibrium conditions were not satisfied, and alternative methods were explored as the empirical approach for the multi-propped excavations ([56] after [48]). With the advancement of the numerical methods, the analysis of such structures proved to be feasible [54].

Currently, the numerical analysis is used to predict especially soil-structure interaction, and the effect of drainage on the nearby structures as the ground movement behind the wall might cause settlements and potential damage. The list presents a short overview of the types of walls used in the urban environment. While the list is not exhaustive, it suggests the most popular solutions.

#### King post wall

King post wall consists of concrete fill bore hole that form a base for an H-shape pile (see Figure 3.14(a)). Voids between piles can be filled with concrete, timber or steel panels. Structure is considered as a cheap alternative to the sheet pile [57]. It can be utilised as a temporary or permanent solution and retain soil up to 3.5 m, when used as cantilever, and up to 12-15 m, when it is being anchored.

Its application usually limits to sites where the groundwater is below the formation level. It is not suitable for retaining soft or loose soils [54]. Thus, it is not being explored further in this paper.

#### Sheet pile

Sheet pile wall is constructed from the interlocking sheet panels (see Figure 3.14(b)). Traditionally, it was used for dockside or riverside constructions, but currently, it can be seen on a variety of construction sites [58]. It can be used as a permanent solution, but it is especially popular in temporary structures as it can provide major cost savings when sheet piles are to be reused. Maximum single sheet pile length can reach approximately 30 m and retain height up to 8-12 m when it is propped one time, but the design widely depends on the soil type to be retained [54].

Sheet piles can prove to be challenging to install in variable soil conditions where big boulders and rocks can be found. Similarly, it can be difficult to drive the sheet pile into the very stiff clay to the substantial depths. High noise and vibrations during installation can be overcome by more sophisticated construction methodology [58]. Nevertheless, its maximum retaining height is too low to be applied in the Haga station.

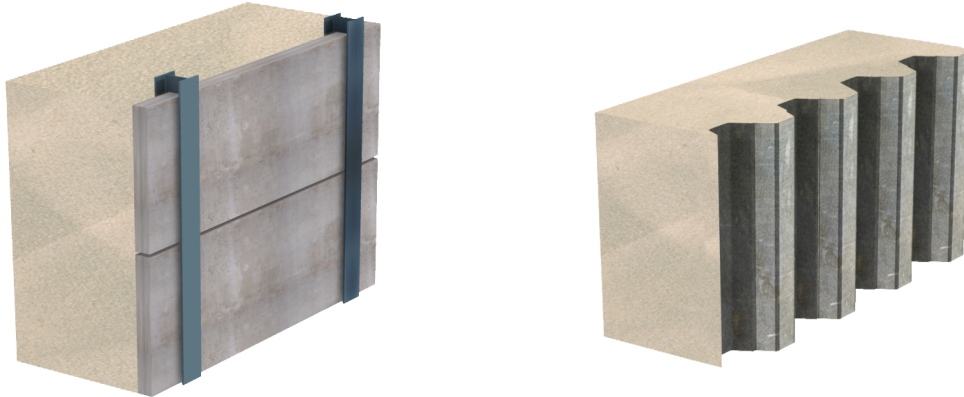


Figure 3.14: Examples of retaining walls a) king post (left) and b) sheet pile (right).

### Contiguous piles

Contiguous piles are single piles installed at a distance from each other (see Figure 3.15(a)). It can be both temporary and permanent structure where the distance between the piles depends on the type of soil to be retained. It is considered as the cheapest piled wall solution when installed by the Continuous Flight Auger (CFA) and is not suitable for retaining water. If this is the case, gaps between piles must be plugged with in-situ concrete or jet-grouting behind the piles in order to prevent water from flowing into the construction pit. This solution is also applied when there is a risk of soil loss through the gaps [54].

The maximum length of contiguous piles is approximately 20 m. It can retain excavations up to 15 m if propped or anchored. Even though it is particularly suitable for soft soils, the Haga station is to be constructed in the ground where the high groundwater level is expected. Thus, this solution proves not to be feasible.

### Secant piles

Secant pile wall consists of female and male piles that partially cover each other as can be seen in the cross-section in Figure 3.16. Female piles go first and later male piles are drilled partially through them. Thus, in typical hard/soft solutions, female piles are constructed from weak concrete, and male piles are being reinforced. Such wall can be considered water resistant only in the short-term conditions. Thus, hard/firm and hard/hard solutions are available where in the strongest solution both types of piles are being reinforced. As both piles must be strengthened and a harder concrete mix is being used, the piling operation is getting more difficult what challenges the cost of the installation [54].

Secant pile wall is particularly suitable for free-draining soil where the CFA rig can be used. It can retain excavations from maximum 15 m for hard/soft to maximum 20 m for hard/hard piles where the penetration depth of piles is maximum 30 m [54]. The more robust the wall, the most possible it is going to be used as a permanent solution. As the excavation depth in Haga area exceeds 20 m, secant pile wall cannot be used.

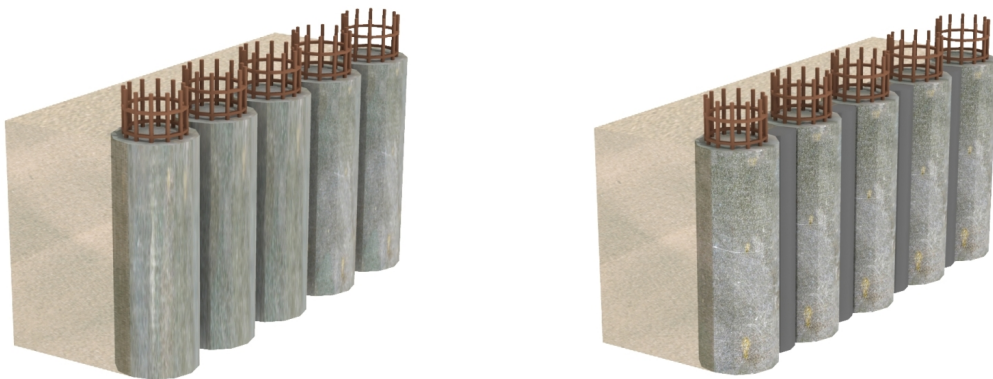


Figure 3.15: Examples of retaining walls a) contiguous wall (left) and b) secant pile (right).

## Diaphragm wall

Diaphragm walls are cast in-situ reinforced concrete walls that are excavated in the presence of the slurry (see Figure 3.16). The slurry, usually bentonite, exerts a hydrostatic pressure on the surrounding ground and, in this way, supports ongoing excavation preventing it from the collapse. Reinforcement cage is placed within the excavated void and concrete is cast from the bottom pushing the bentonite slurry out of the excavated trench. Bentonite slurry can be captured, cleaned and recycled. Such walls can be excavated using a grab or a cutter with the latter one providing a maximum wall depth up to 55 m [59]. This translated to the maximum excavation depth of approximately 35 m [54].

Diaphragm walls are considered the most expensive retaining wall solution, but might prove economical especially on large projects, where the cost of setting up and demobilisation of the plant can be mitigated. They have excellent installation tolerance/verticality up to 1:400 and can be used as the permanent structural elements. If treated as a temporary solution, walls are left in place. Due to less connection points in comparison to the secant pile, they provide better a solution where the groundwater is present [54].

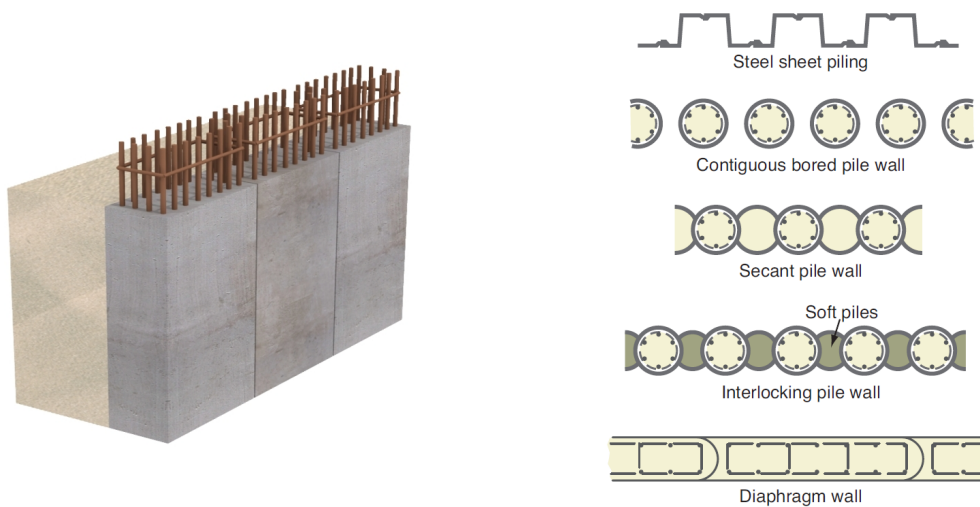


Figure 3.16: Example of a diaphragm wall (left) and the cross-sections through different types of walls (right, [54]).

### 3.7.2 Foundation of the excavation

Deep excavations in soft soils usually require a foundation structure or ground improvement technique below the excavation depth to secure the stability of the construction and to limit deformations of the ground surface. A selection of methods used in similar projects is described in this section.

## Piled raft

Piles are widely used as a foundation for structures placed above low strength soil, due to its ability to transmit the load to more capable load bearing strata [26]. One of the applications of piles foundation is the combination between piles and raft (see Figure 3.17). In this system, both piles and raft act together to support transferring the load from a structure, while simultaneously reducing settlements. As suggested by Fleming et al., it is not the number of piles necessary to carry the load of the structure that drives the foundation design, but the number of piles needed to effectively reduce the differential settlements [60]. Moreover, the piled raft system may be considered as an optimal solution when the fully piled foundations must be applied. Then, this hybrid structure can provide a reduction in number and length of piles. Additionally, application of piled raft foundations reduces heave during the excavation, due to the decrease of ground stresses from the pre-installation of piles [61]. This issue is being discussed in details in Section 3.8.2.



Figure 3.17: Typical arrangement of piles and columns in piled raft solution.

Piles can be divided into two categories depending on the installation method: the first type being displacement piles, and the second called non-displacement piles or bored piles. Both have advantages and disadvantages, but usually bored piles are preferred to be used in urban environments due to lower noise of installation and less disturbance of the surrounding soil. This is also an advantage for sensitive soils, where remoulding could occur due to high installation disturbance. Nevertheless, care has to be taken in dense soil deposits as dilation of the soil could cause heave of surrounding soil affecting nearby structures [30]. As for displacement piles, they usually have a good bearing capacity with low settlements, but their installation generates a significant disturbance in the surrounding soil and high levels of noise and vibration, which could cause the adverse impact on the surrounding foundations and urban environment [26].

## Cross-walls

Cross-walls consists of perpendicular structural elements to the retaining walls which connect them below the excavation level to restrain walls' movement during excavation (see Figure 3.18). Installation of cross-walls as an internal support system have demonstrated to be effective at reducing wall movements, surface settlements and heave effect in deep excavations in soft soils [62][63][64][65]. Construction of cross-walls is performed prior to the excavation; hence techniques such as jet grouting and deep soil mixing can be used for their construction [66]. Development of these type of foundations involves high costs due to the significant amount of concrete and, in some cases, reinforcement needed for its assembly. Previous analysis has shown, however, that a relative reduction of a factor of three in the wall displacement can be achieved with this foundation system which makes it a particularly attractive design option to be considered [64].

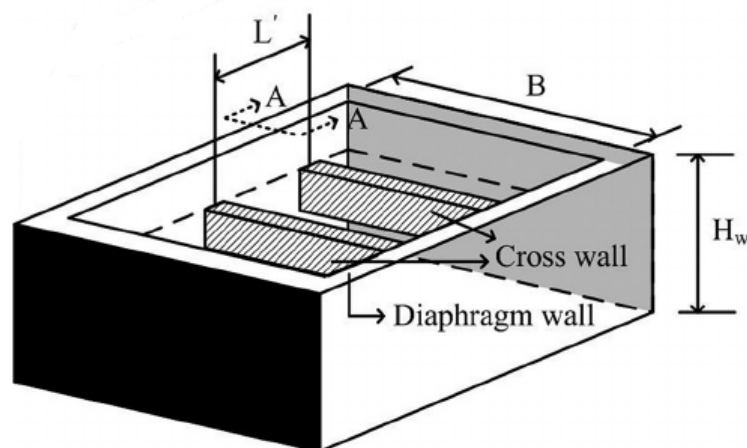


Figure 3.18: A 3D representation of cross-walls. Based on Wu et al. [67].

For the design of cross-walls, determination of adequate space between the walls ( $L'$ ) dictates the stiffness needed for the excavation system to keep the settlements below the design level [68]. Wu et al. proposed a solution for finding the space between the walls for soft clays in Taipei by using regression model where the system stiffness ( $K$ , see equation 3.10) and the limit settlement from design ( $\delta_l$ ) are the main parameters to calculate the required space parameter [67]. The first step consists in the calculation of the expected settlement ( $\delta_m$ ) from the excavation system without the cross-walls with the use of equation 3.11, to evaluate if the settlement is under the design requirements. If not, the value of  $\delta_m$  in equation 3.11 is replaced with the target settlement by design ( $\delta_l$ ) and a regression is made to retrieve the value of  $L'$ .

$$K = \frac{k_2(k_1 + k_3)}{k_1 + k_2 + k_3} \quad (3.10)$$

where:

|       |  |
|-------|--|
| $k_1$ | Axial stiffness of the cross-walls (or retaining wall in case of initial evaluation) |
| $k_2$ | Flexural rigidity of the retaining wall  |
| $k_3$ | Axial stiffness of the lateral support (struts).                                     |

$$\begin{aligned} \delta_m(mm) = &exp(a_0 + a_1B + a_2\ln(H) + a_3\ln(S_u/\sigma'_{vo}) + a_4\ln(L') + a_5\ln(K) \\ &+ a_6[\ln(H)]^2 + a_7[\ln(L')]^2 + a_8[\ln(K)]^2 + a_9\ln(S_u/\sigma'_{vo})\ln(L') \\ &+ a_{10}\ln(L')\ln(K) + E) \end{aligned} \quad (3.11)$$

where:

|       |   |
|-------|---|
| B     | Width of the excavation   |
| H     | Total depth of excavation   |
| E     | Error between the calculated and the actual settlement (usually taken as 0)   |
| $a_x$ | Coefficients equal to: $a_0=11.1908$ , $a_1=-0.0048$ , $a_2=-0.0168$ , $a_3=1.5855$ , $a_4=-0.5071$ , $a_5=-1.1914$ , $a_6=0.2354$ , $a_7=-0.0691$ , $a_8=0.0390$ , $a_9=-0.8365$ , and $a_{10}=0.0196$ . |

Representation of cross-walls in a 2D model is a challenge since there is no particular element in PLAXIS 2D which can simulate their effects in the soil. To validate data for a deep excavation project in Gothenburg, Karsrud et al. replaced the cross-walls with equivalent longitudinal walls to simulate the same resistance against heave. The connection of the cross-walls with the retaining walls was reproduced by employing steel truss with axial and bending stiffness equal to the actual cross-walls [62].

### Soil-mix columns

Deep soil mixing (DSM) is a soil stabilization technique in which the unstable soil is blended with cement type materials to form a soil-mix column with higher strength which will improve the stability of the soil deposit [69]. DSM can be applied to create lime-cement columns (LCC). This technique has been applied in several countries such as Japan and Sweden, in areas where the ground is mainly composed by soft soil deposits [70]. DSM is usually applied as a solution for stability and settlement reduction for embankments, but it has also been used for stability of braced excavations and slopes, for reduction of impact in nearby structures and as a technique for mitigate the risk of liquefaction [71].

Analysis of this type of technique is three-dimensional and is therefore problematic to model in two dimensions. To accomplish this, simplifications of the foundation system has to be made in order to run the numerical model. The volume average technique is one solution which can be implemented in the FEM software to simulate the behaviour of DSM [72]. This technique consists on the simplification of the 3D problem in two dimensions by creating a soil cluster which replace the whole area to be stabilised. The parameters of this soil are to be chosen to represent both the soil and column elements.

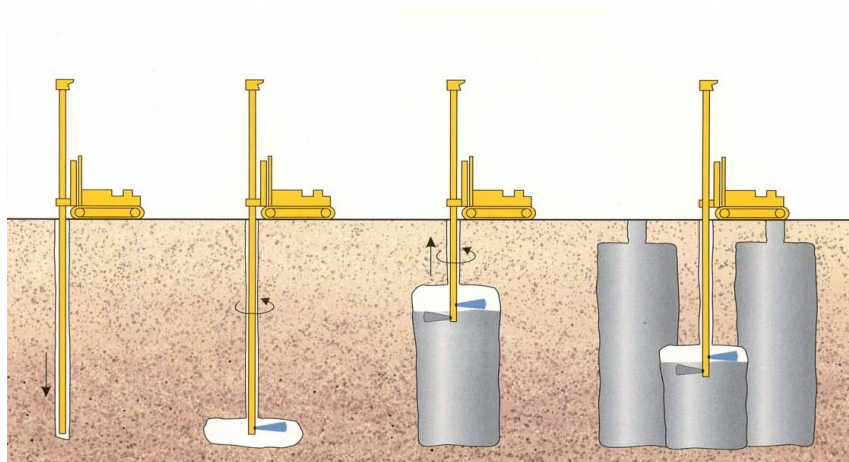


Figure 3.19: Procedure of soil-mix columns construction [73].

### Underwater excavation

The stability of retaining walls has been found to be highly linked to the pore water pressure development on the excavation site [74]. Reduction of the pore water pressure due to the lowered water level on excavations will lead to a decrease of the total stress of the soil.

An alternative to improve the stability of the structural elements is the introduction of an underwater excavation with a base slab construction [75]. In this method, excavation is performed under water until the desired depth, finalising with the construction of a concrete slab. Some cases where this procedure has been applied include the construction of the Marina Bay station for the Singapore metro [76][77] and the construction of the basement for the new Oslo Opera located at the Oslo harbour [75].

### 3.7.3 Supporting elements

There are various types of structural elements used to support the earth retaining structure. Especially for deep excavation, the variety of solution is significant, and its application considerably influences the behaviour of the retaining wall. Thus, it is important to understand not only the advantages but also the limitations of each method. While the below list is not exclusive, it presents the most common solutions.

## Struts

Struts are popular retaining support types. They can be designed as separate, mostly steel, elements or incorporated into the slab design to provide the passive resistance to the displacing wall. Props can cover considerable span and provide a wide open space between the walls for the construction operations. Usually, the maximum distance between the individual props is optimised together with the size of the biggest structural element being installed in the void between them. Depending on the type of connection, a prop can eliminate the differential movement of the walls but cannot stop them from their absolute movement [48].

The main disadvantage is their sensitivity to the temperature effects [78][79]. Depending on the time of installation, props must be monitored and adjusted accordingly to their elongation or shrinkage to ensure their adequate workability. Thus, the thermal properties of the prop should be specified to allow the calculations to be made. PLAXIS 2D allows to model the temperature effects through assigning basic properties to the structural element, such as the specific heat capacity ( $c$ ), and the thermal conductivity ( $\lambda$ ). As mentioned previously, these aspects have not been taken into consideration during the model creation.

PLAXIS models struts as fixed-end anchors. Their properties can be influenced by assigning the axial stiffness ( $EA$ ) and the out-of-plane spacing ( $L_s$ ). Additionally, the strength parameters can be adjusted by maximum tension/compression forces and maximum residual forces used together with the elasto-plastic material type. The visual representation of their effect is presented in Figure 3.20 below.

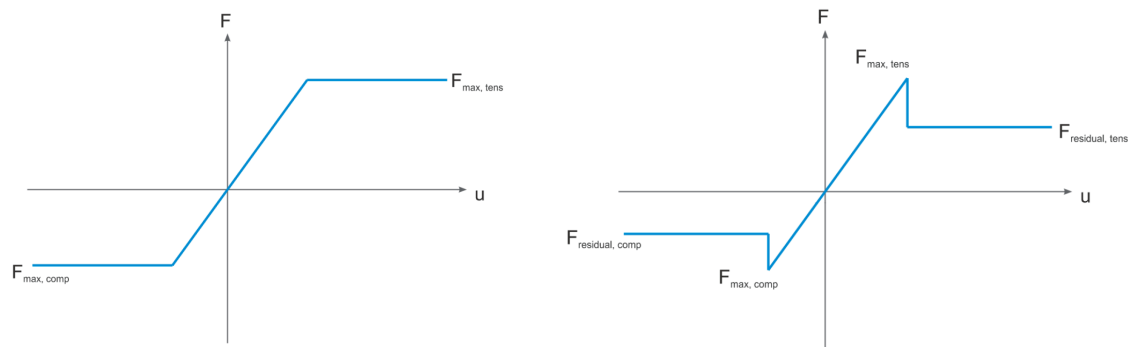


Figure 3.20: The force-displacement diagram displaying the elasto-plastic behaviour of anchors (left) and the anchors with residual strength (right) [43].

## Ground anchors

Ground anchors are passive supports that require development of the stress in the ground. It is achieved by anchoring the rod in a plate or by pre-tensioning the tendon and grouting or by anchoring it in rock (see Figure 3.21). Anchors can be considered as temporary (up to two years) or permanent ground retaining supports.

Anchors are usually installed in non-cohesive soils as sands, gravelly sands and silty sands or stiff cohesive material as stiff clay where the sufficient strength can build up to hold the ground anchor in place [30]. In PLAXIS, anchors can be modelled as the combination of the node-to-node anchor elements with the grout body (embedded beam row element) or rock bolts [43].

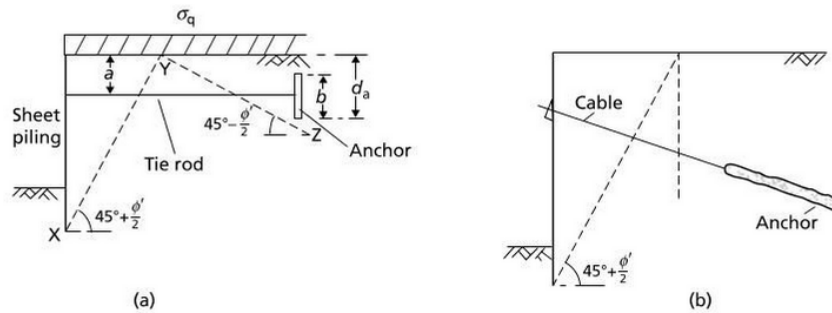


Figure 3.21: Anchorage types: a) plate anchor, b) ground anchor after [30].

Anchors are less sensitive to the temperature variations than props, but much more prone to the groundwater changes [48]. The soil composition plays a vital role in accessing the potential of a corrosive environment to the metal rods as it may affect its strength in the long-term situation.

Interestingly, there is also a legislative point of view to be considered as not in every country it is possible to install the ground anchors under the already existing structure without prior agreement [80]. In this view, struts are considered to be a less administrative laborious choice.

As ground anchors are not suitable support elements for soft clays, they are not being considered further in this study.

### Rock anchoring

Whenever possible, it is beneficial to consider anchoring to the solid rock material. It is usually done by employing rock bolts that are working similarly to anchors in soil. They are used extensively in mining, erection of underground structures and can also be used for retaining wall support.

Alternatively, when bedrock layer is shallow, the wall itself can be driven approximately 2 m deep into bedrock and supported laterally by rock dowels to gain a necessary toe resistance (see Figure 3.22) [81]. Providing that the rock is of good quality, the wall deflection can be minimised, and the number of necessary additional structural supports can be reduced what translates directly to more space for the construction operations.

In PLAXIS, embedded beam row can represent not only a pile behaviour but also a rock bolt. Additionally, the plate element can be driven to bedrock and gain resistance from bedrock layer.

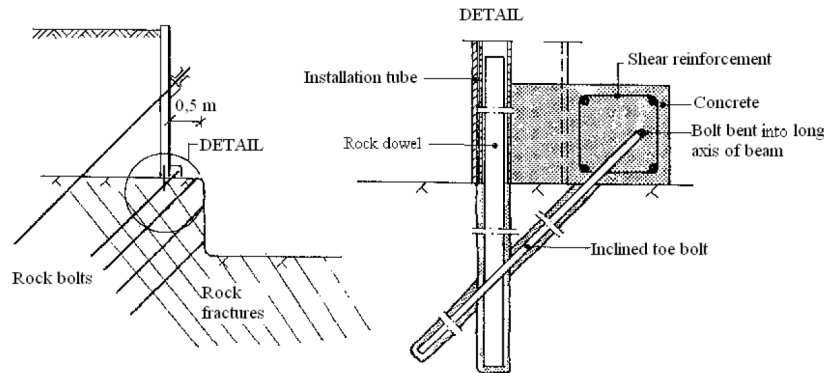


Figure 3.22: Detail of rock dowels [82].

## 3.8 Soil displacement reduction

Ground heave is usually associated with swelling of the soft soils. Commonly, soil can swell due to the excess water present in the ground or as a result of unloading. Consequently, ground heave is a common problem around the excavations and can cause instability, particularly at the bottom of the pit. It is usually accompanied with the soil movement behind the wall.

There are various approaches to providing a stable excavation, especially in the long-term situation. The easy solution is to avoid construction in places with doubtful ground conditions. As this is being increasingly difficult to achieve, the cheapest alternative is to apply the locally available by-products from the industry to minimise the effect of ground heave. As these are not necessarily suitable for all applications, more sophisticated solutions may be considered.

### 3.8.1 Soil replacement

Soil replacement is one of the most invasive actions when it comes to ground heave reduction. It is imposing excavation of soft material and replacing it with a fill of adequate parameters. It is usually used in the Northern Periphery region for rural road construction (see Figure 3.23). It is claimed that the soil replacement depth from 1.5 to about 4.0 m is the maximum that can prove to be economical. As the method is problematic to apply in the urban environment, in places with high water table and where the stability of the excavation sides is crucial, its application limits mostly to provincial areas only [83].



Figure 3.23: Soil replacement in road construction [83].

### 3.8.2 Piling and piled raft solutions

Piles and piled raft solution have been previously discussed as structural elements in Section 3.7.2.

They can also act as heave and settlement relieve components. For large applications, the raft foundation is usually one of the cheapest options, but the structure might suffer due to excessive differential settlements as the raft is rather a flexible solution for structures of substantial size. A hybrid solution of piles and raft acting like a pile cap can reduce differential settlements and prove to be economical in the service state. As can be seen on Figure 3.24, piles are applied in the center of the raft, where they are the most efficient and can contribute to an economic raft design. Additionally, the application of piled raft solution may reduce the overall thickness of the raft and contribute to minimising the rise in the cost [30]. Various perspectives of piled foundation design have been presented in [84][85][86].

### 3.8.3 Cross-walls

Cross-walls have been previously discussed in detail as structural elements in section 3.7.2.

As mentioned, cross-walls proved to be effective at reducing wall movements, surface settlements and heave effect in deep excavations in soft soils [62][63][64][65]. Their erection between the retaining walls, support them and prevent the deformation due to a high transverse stiffness from the cross-walls (see Figure 3.18). In this way, wall movements are restricted and less prone to settlements, especially differential, as the whole structure act as a rigid body.

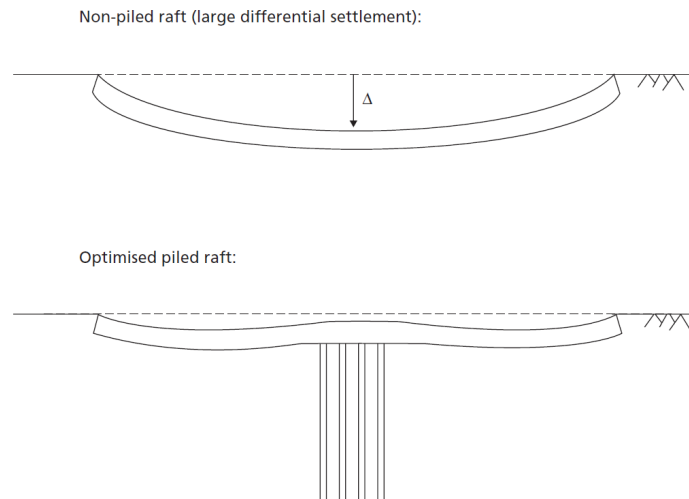


Figure 3.24: Raft and piled raft solution, where  $\Delta$  is the maximum differential settlement [30].

### 3.8.4 Soil mix and compensation grouting for settlement control

Deep soil mix columns (DSM) has been partially discussed as structural element in section 3.7.2.

#### Deep soil mix and grouting technologies

One of the most flexible technologies to support excavation process is grouting. DSM is created using jet grouting and has been applied with success at many projects, especially related to embankment stabilisation. Bergado et al. presented an interesting example of settlement reduction for such structures using DSM columns [87]. For excavation purposes, DSM columns can be applied at the bottom of the excavation pit as a base support system but also as a seal layer for groundwater. Additionally, they may be extended beyond the retaining wall structures to support the weak soil on the active side of the pit.

Besides jet grouting, the excavation can be supported with traditional compaction grouting. Traditionally, in this solution, the cement slurry is being injected at the active side in the area of existing foundations to provide higher bearing capacity and reduction of settlements. This can be a proactive technology but also a remediation action when unpredicted differential settlements have occurred. Grouting is possible from the outside but also in the area of reduced headroom within the existing structure, what makes it particularly attractive and flexible technology to apply. An impressive example of grouting in reduced headroom is the extension of Chicago subway where excavation was performed under the support of grouted wells injected from the existing basement [88].

## Compensation grouting

Compensation grouting, known also as fracture grouting, is a technique used for controlling or reversing the settlement of structures. In this process, grout is being injected between the structure foundation and the process causing settlements (see Figure 3.25). Injected material squeeze in the soil voids and expands stopping or reversing the settlement process by inducing heave by the grout material [89].

Compensation grouting technique can be used in almost any fractured soil where the grout can penetrate. It is a very expensive technique used solely on large-scale projects or in places where the surrounding structures are highly valuable and must be protected during the construction work happening around them. On the contrary to jet grouting, it is not a remedial technique and must be planned together with the construction to be done.

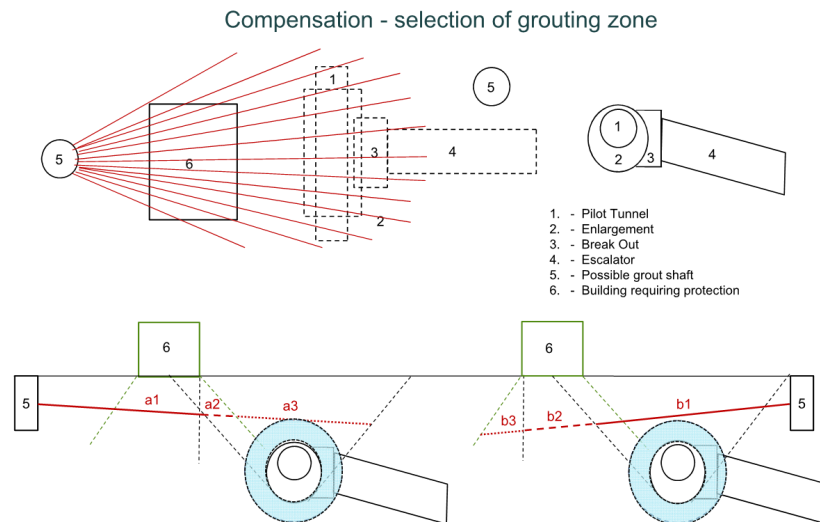


Figure 3.25: Principles of compensation grouting design [90].

One of the most recent and remarkable examples of settlement control induced by tunnelling through compensation grouting have been performed during Cross-rail construction in London. Particularly interesting grouting works have been performed from Finsbury Circus by Bachy Soletanche Ltd, where the surrounding buildings were firstly straightened from past settlements and later protected from further damage caused by tunnelling works [91].

### 3.8.5 Cordek Cellcore HG

Cordec Ltd developed an interesting heave reduction product. The company offers a broad range of collapsible cellular constructions of expanded polystyrene combined with polypropylene boards designed to protect foundations from the effects of ground heave (see Figures 3.26 and 3.27). The polystyrene boards are installed under the raft or piled raft. When the ground heave develops, the panel fails and leaves an empty void for the ground beneath to expand.

For raft thicknesses exceeding 900 mm, it is recommended to use Cellcore HG product range with a rectangular pattern. For a raft of approximate depth of 1500 mm, Cellcore HG grade 40/50 would be suitable. This has a safe working load of 40 kPa and a fail load of 50 kPa. The thickness of the Cellcore panel is dictated by the extent of heave anticipated on site. When heave is expected to be approximately 150 mm, the panel height is designed to be about 300 mm.

Cellcore panels are light weight, easy to install and suitable to use around piles, drainage pipes and capping beams. It is possible to position reinforcement spacers directly on the product. Panels can be incorporated together with Cellvent parts to protect building from hazardous ground gases. More information about the product can be found in Appendix F.



Figure 3.26: Cellcore installation around piles for the raft construction [92].



Figure 3.27: Cellcore installation under the raft [93].

### 3.8.6 Lightweight fill materials

Lightweight fill materials are being used to reduce the permanent loading on the foundation and, consequently, the effect of this loading in the long-term perspective. If the fill material, together with a new structure, provide a lower loading magnitude than the in-situ soil, it is claimed that the structure is to be settlement-free as all settlement has already occurred.

Extraction and replacement of the material found in place are usually very expensive. Thus, it is a good practice to consider locally available by-products to be used as lightweight fill materials. Primarily, their properties must match the desired characteristics, but also fulfil additional requirements. As mentioned in the ROADDEX manual considering roads constructed on peat and soft clay: “*A good lightweight fill material, in addition to being light, should also be durable, resistant to decay, easy to place and compact, have a good compressive strength with low compressibility, and be environmentally friendly* [83]”. Such characteristics of material can also be applied to the excavation.

Besides above mentioned, the buoyancy effect of lightweight fill material should be stressed. The design against it is rather simple and require utilisation of “heavier” light fill materials, simple rods and anchors or adequately thick cover over them. The issue starts to play a role only in places where the groundwater level is expected to reach the fill level. For fills in a dry environment, the risk of buoyancy forces acting on the fill is negligible [94].

### **Pulverised Fuel Ash (PFA)**

Pulverised Fuel Ash and Furnace Bottom Ash (FBA) are by-products of the coal-fired power stations. While FBA falls to the bottom of the furnace, PFA is carried through the combustion chamber as fine-grained particulate material [95]. As almost 80 % of produced ash is PFA, the industry adapted and utilised it in various applications.

On the the most comprehensive studies covering PFA characterisation for geotechnical application has been presented by Pandian [96]. PFA is used as light fill material, especially bridge abutments, but also as a semi-product for concrete mix, concrete blocks and grout production (see Figure 3.28). It has excellent thermal properties and can be easily compacted. Due to the possibility of cross-contamination to the groundwater, it is advised to check the chemical composition of PFA and use it in places with low groundwater level [95][96].



Figure 3.28: PFA with reinforcement mesh used for the road construction on the soft ground [97].

### **Lightweight Expanded Clay Aggregate (LECA)**

Lightweight Expanded Clay Aggregate is created in the rotary kiln where clay material is heated to approximately 1200 °C. During the process, clay expands due to the yielding gases and creates round and almost round-shaped aggregates (see Figure 3.29).

Such aggregate can be produced in various sizes and densities. It has versatile applications ranging from insulation, gardening and drainage, structural backfilling and road construction. As a lightweight fill material, it is characterised by easy storage, transportation and construction process. It might be difficult to compact if not placed in confined areas. One of the recent case studies using lightweight backfill for bridge abutment in Kent was presented in Proceedings of the Institution of Civil Engineers: Bridge Engineering [98].

Due to its properties, LECA is claimed to provide a sharp reduction in earth pressure in comparison to conventional material. Additionally, it contributes to settlement reduction and structural stability [83][99].

### Foamed glass

Foam glass is one of the most sustainable lightweight fill material. It is produced from about 99 % recycled glass bottles that are crushed to the fine powder and mixed with a natural foaming agent. Later, the mixture is baked in a kiln at about 900 °C. During baking process, glass mixture expands and creates the foam-like product. When cooled down to room temperature, foam naturally breaks and creates foamed glass aggregate material (see Figure 3.30) [100].



Figure 3.29: Cross-section photo of Lightweight Expanded Clay Aggregate [101].



Figure 3.30: GEOCELL® foam glass gravel [100].

During baking, pores expand and create individual cells that are not connected with each other. Owing that, the final product has excellent thermal resistance and very high compressive strength. Closed cells guarantee no capillary action and high drainage capacity. Main properties and light weight directly translate into low settlements and low compressibility of the aggregate in the service state. There is no leaching effect and excellent fire resistance. Foam glass properties and its durability convince many governmental authorities to use it during erection of public projects. One example is the construction of the lightweight road embankment along motorway E12 in Hämeenlinna, Finland [102].

Foamed glass can also be produced as panels and used similarly to EPS described in detail in Section 3.8.6.

### Expanded Polystyrene (EPS)

Expanded Polystyrene is relatively cheap lightweight fill material available on the market. It is a form of synthetic aromatic polymer made from the monomer styrene, one of the most widely used plastic. It is an excellent material for filling voids as it can be cut to size on a construction site or bespoke into the most sophisticated forms. Besides, EPS is being used as a thermal insulation material. Light weight and popularity among designers, make it familiar for site workers and rather easy to handle at the construction site (see Figure 3.31) [103].



Figure 3.31: EPS as a light fill material at the Cowgate roundabout construction, Newcastle upon Tyne [104].

On the contrary to foam glass panels, EPS is highly flammable [105]. It is also a rather poor barrier to vapour, what imposes the use of additional mats if use, for example, as an insulation material. EPS stiffness can be adjusted and provided as a very stiff material. Nevertheless, in comparison to foam glass, its compressive strength is usually given at a 1 % strain value what might limit its application where structures are particularly sensitive to long-term deformations. Finally, despite being 100 % recyclable material, EPS causes a substantial risk to the environment as it is not biodegradable [106]. As both materials do not cause leaching, they are considered relatively good solutions for light fill where the groundwater table is in its proximity [83].



# 4

## Project requirements

Västlänken, as a major transportation project in the area, has been restricted with many requirements. During the public consultations, the location of stations has been established. Regarding Haga, it has been decided that three major entrances to the station are being planned - from Pusterviksplatsen, Kungsparken and Handelshögskolan (see Figure 4.1).

Based on the geological study (see Figure 2.10), it can be seen that majority of Haga station is being located in bedrock. This is also reflected in the proposed cross-section through the station presented in Figure 4.2. Haga station will serve four railway tracks that are being connected by two platforms. Three tracks are proposed for passengers trains while the fourth one, located the last to the left, is considered to be a service track. The technical rooms, for access convenience, have been located below the station platforms. The most critical section is located just after the station, where bedrock layer is sharply sloping down (see Figure 4.3). Thus, tracks are proposed to be based on the soft clay layer far above the bedrock. For reference, the most recent in the time of this paper publication technical drawing of the Haga station are presented in Appendix G.

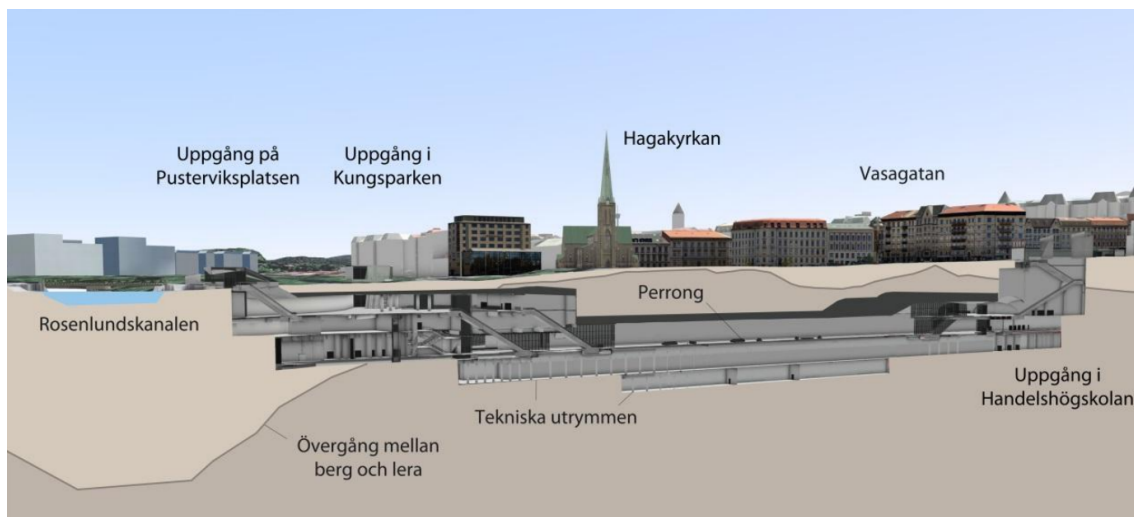


Figure 4.1: Cross-section visualisation of Haga station produced by WSP in 2015 [3]. *Uppgång* (eng. entrance) mark three proposed entrances to the station - from Pusterviksplatsen, Kungsparken and Handelshögskolan. Besides, there are: *övergång mellan berg och lera* (eng. transition between bedrock and clay), *tekniska utrymmen* (eng. technical rooms) and *perrong* (eng. platform).

Desired dimensions of the tunnel after the station are smaller, and this has been reflected in the proposed conceptual model presented in Chapter 5. The intended depth of excavation has been set to 25 m, while the width is to be 78 m. Architect has no intention to have any permanent intermediate support walls and provide an open, undisturbed space in the platform area (see Figure 4.4). Consequently, it is intended to model the excavation as open pit area with no intermediate vertical supports.

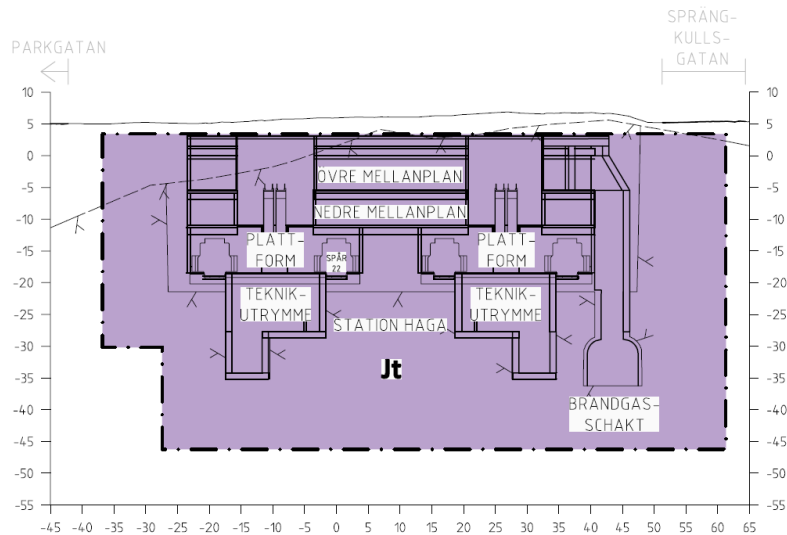


Figure 4.2: Cross-section just after HAGA station, where Jt - area of a new railway track owned by private party. Produced by SWECO and Ramboll for Trafikverket [107].

There is no set level for the maximum allowable settlements in the area. Various documentations from constructions in Gothenburg have been reviewed and as a result a 100 mm settlement limit has been imposed as a maximum value that should not be exceeded by the numerical analysis in the long-term case [62]. HAGA station is a relatively short section of a tunnel placed in the soft clay. Having in mind that the rest of the tunnel is placed in bedrock, the very minimum settlements should be aimed for. Larger settlement of the section placed in soft clay would lead to flexural cracking due to uneven settlements and impose higher stresses on the section placed between bedrock tunnels.

Bearing in mind the purpose of the construction, it is not the total settlements, but the differential settlements that might cause harm in the service state. Railway authorities impose strict limits on the allowable settlement as this has a major impact on the track geometry and later translates to the maximum train speed and disruption in their services. Additionally, the proximity of the station impose an additional requirements for horizontal and vertical track alignments. Based on Swedish regulations the station area shall not be located on track with an average gradient not steeper than 1 in 500 with the absolute minimum of 1 to 300. The vertical slope by the platform should normally not exceed 5‰ [108]. In order to

analyse the differential settlements aspect, a 3D model or multiple cross-section analysis would be necessary. As the scope of this thesis is limited, this aspect is not explored further assuming that the worst settlement is going to occur in the area of the unfavourable cross-section that is being modelled.

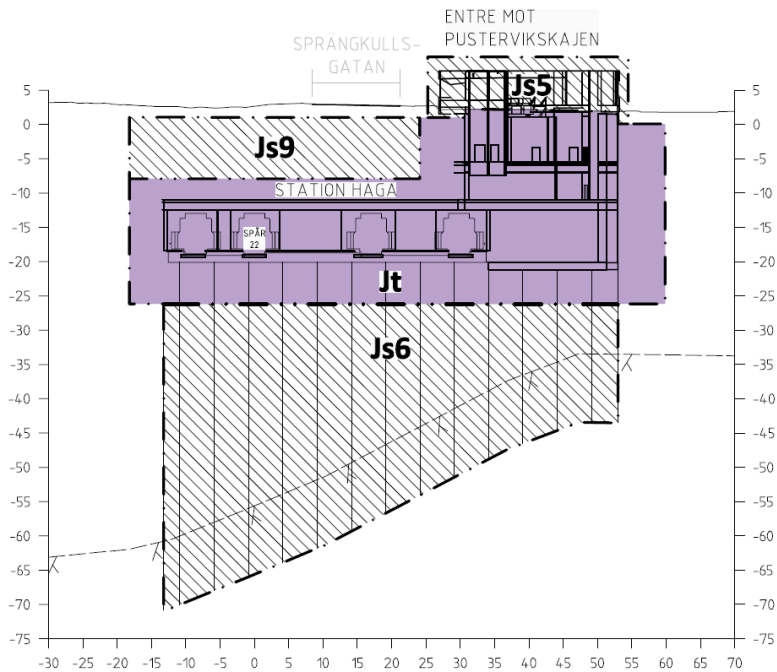


Figure 4.3: Critical cross-section of Haga station, where Js6 - underground structures and Js9 - protection zone. Produced by SWECO and Ramboll for Trafikverket [107].

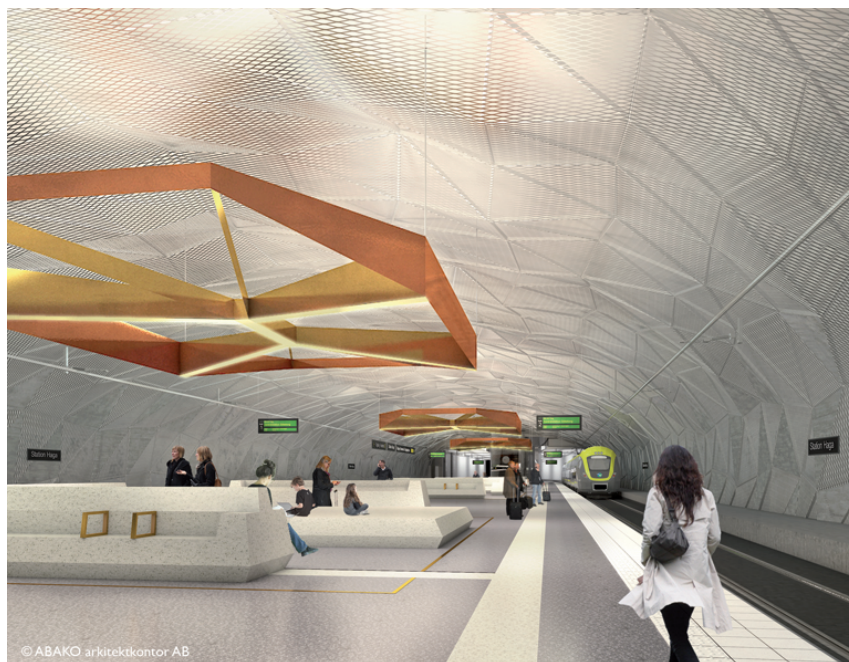


Figure 4.4: Haga station visualisation by ABAKO Arkitektkontor AB [109].



# 5

## Input data and soil testing analysis

This chapter presents the data used for creating the model in PLAXIS 2D. This includes the soil parameters taken from soil tests on site, calculation of the loads influencing the excavation and the general assumptions made to complete the missing data and simplify the problem.

### 5.1 Boreholes

To obtain the soil properties and input parameters for the model, a total of eight boreholes were analysed (see Figure 5.1). According to its location, the boreholes were grouped in pairs so each duo could represent a section of approximately 30 m. Given the available data, four pairs were formed to represent the total 140 m of the chosen cross section.



Figure 5.1: Analysed boreholes location based on SWECO report [2].

The sketch of the drilling depths in each borehole conducted by SWECO has been presented in Appendix H. Unfortunately, no data about z-coordinates of the boreholes has been found in neither of the available reports. Thus, the boreholes have been assumed to be drilled from the same level what can be considered as the approximation.

The direct shear test was performed in all the analysed boreholes, but undrained triaxial test executed for only half of the mentioned drilling (see Appendix I). As for step-wise oedometer and CRS tests, these were performed only in one of the analysed boreholes located in the area of the proposed tunnel (HH5002 in Figure 5.1). Therefore, information from this borehole would have to be extrapolated to complete the soil parameters for the rest of the modelled section.

## 5.2 Soil test results

To analyse the conditions of the clay in the area, soil samples were taken from different drillings in the surrounding of the proposed tunnel. To determine the soil behaviour under both shear and compressibility conditions, a variety of tests were performed. Analysis of all the results was conducted to find the most accurate values to implement in the project. A description of this process is developed in the following sections <sup>1</sup>.

### 5.2.1 Compressibility and initial stress parameters

As mentioned in Chapter 3, the compressibility parameters of soils can be determined with the help of oedometer tests. For this study, two types of oedometer methods were used: incremental oedometer loading test and CRS test. Evaluation of both results was conducted to obtain more accurate soil parameters. The analysed oedometer curves are presented in Appendix J.

To determine the accuracy of each test method, a simple plot of different parameters vs. depth is made to evaluate scattered values. In Figure 5.2, a plot of the effective in situ stress, and the values for preconsolidation pressure ( $\sigma_p$ ) obtained from both oedometer methods is presented. It is visible that the values of  $\sigma_c$  from oedometer test at 20 and 40 m depth could be unreliable given that they are far away from the trendline of the other values of the series. As for the results obtained from CRS test, the values seem to fit the trend line better, and their behaviour is much more similar to the effective in-situ stress plot.

OCR and POP are two parameters of great importance for the soil models selected in PLAXIS 2D. As mentioned in Chapter 2, the clay in the area is slightly overconsolidated which affects the calculation of the initial earth pressures on the soil. For overconsolidated soils, the earth pressure coefficient ( $K_0$ ) is calculated as in equation 5.1 [110]. Therefore, variation in the OCR values could highly affect the calculation of the initial state of the soil.

$$K_0^{OC} = 1 - \sin\phi' \sqrt{OCR} \quad (5.1)$$

---

<sup>1</sup>Test data for other materials in the area were not available for this study.

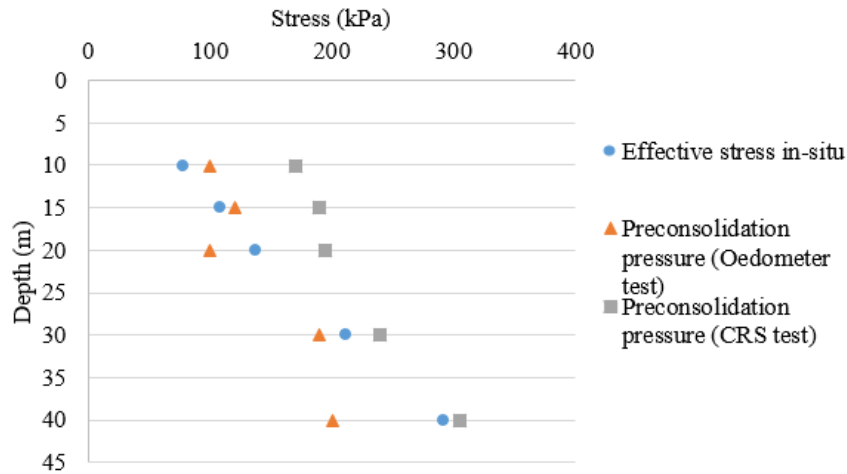


Figure 5.2: Preconsolidation pressure vs. depth for both oedometer and CRS test results.

The over consolidation ratio is calculated as a function of the preconsolidation pressure (see equation 5.1). A graph of the results obtained from both oedometer tests is presented in Figure 5.3. From the graphical point, the OCR values from CRS test seem to have a better fit to what can be expected given that the values start decreasing rapidly with depth until it gets almost stabilised with the lowest samples. Additionally, the curve has less scattered values compared to curve from oedometer test.

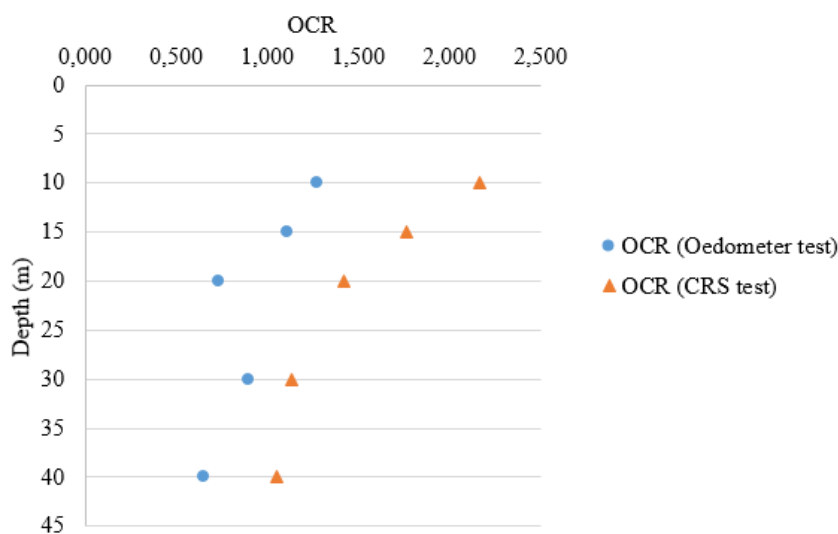


Figure 5.3: Over consolidation ratio vs. depth for both oedometer test results.

Figure 5.4 shows the behaviour of the POP with increased depth. The results from POP for the CRS test shows more linearity than the OCR for the same test. It is visible that more reliable values are obtained from CRS given that results from oedometer show negative pre-overburden pressure from 20 to 40 m depth which is not possible. Therefore, OCR and POP results from CRS test will be considered for use in the model as they seem to be more accurate. However, correction for strain rate has not been applied to this values, which could affect their accuracy. The final selected values selected are presented further in Tables 5.2 and 5.3 in section 5.5.

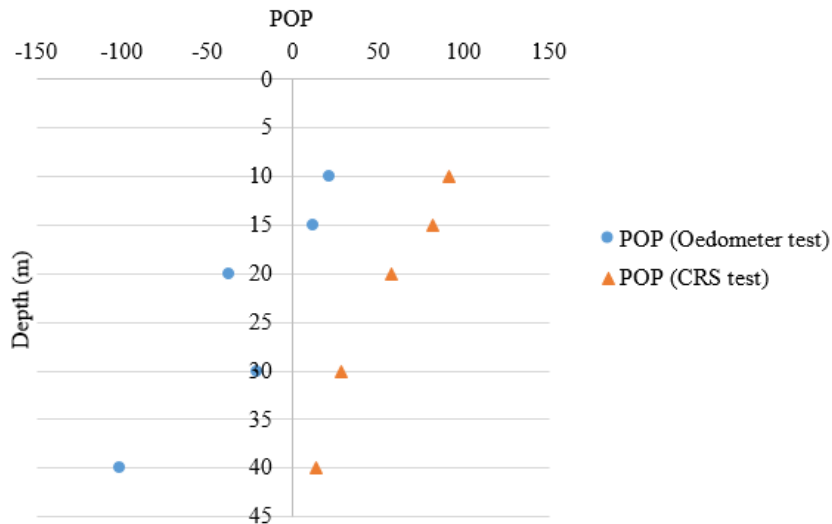


Figure 5.4: Pre-overburden pressure vs. depth for both oedometer and CRS test results.

Having in mind results presented in Figures 5.2 and 5.3, it can also be concluded that the values from both tests at 20 and 40 m depth are unreliable most likely due to sample disturbance and/or oxidation. Figures 5.5, 5.6 and 5.7 present the distribution of the values for  $\lambda^*$ ,  $\kappa^*$  and  $\mu^*$  for the different depths where oedometer test was conducted. As visible, the obtained results for 20 m are the most scattered. A correction of the coefficients at these depths was performed so the model is not affected by the errors linked to the soil investigation process.

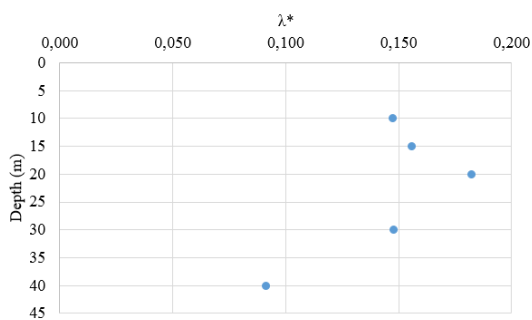


Figure 5.5: Modified compression index from oedometer test.

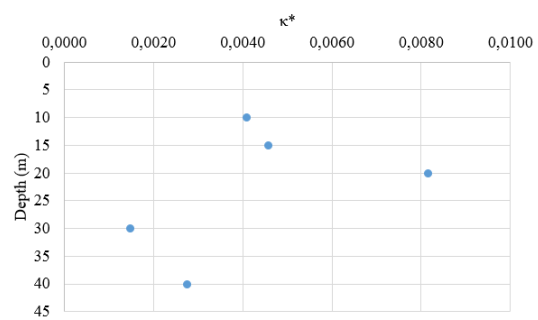


Figure 5.6: Modified swelling index from oedometer test.

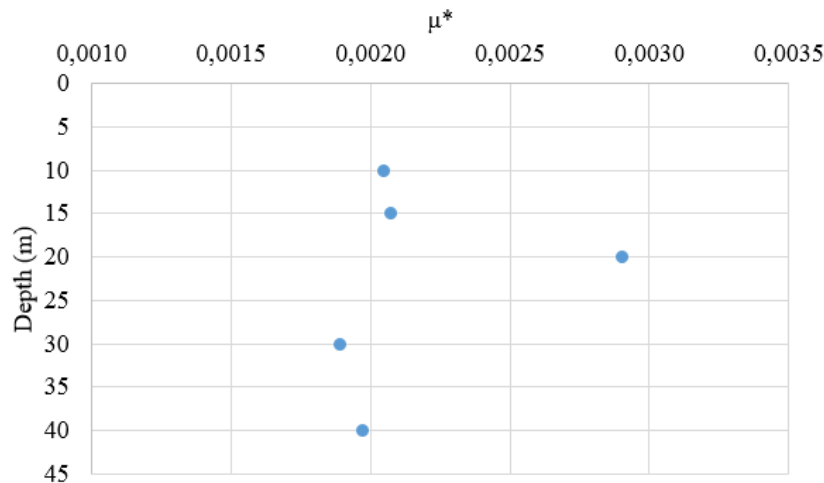


Figure 5.7: Modified creep index from step-wise oedometer test.

## 5.2.2 Strength parameters

For the determination of the strength parameters of the clay, the mean effective stress ( $p'$ ) was plotted against the deviator stress ( $q$ ). The resulting failure envelope was plotted to pass through the origin ( $c'=0$ ), given that, according to the results from OCR, the clay on-site is slightly over consolidated. Due to lack of tests in some of the boreholes, the friction angle was taken from both triaxial test and direct shear test depending on the availability of information. The graphics for the performed analysis are available in Appendix I. The dilation angle for the clay is calculated with an empirical formula given by PLAXIS (see equation 5.2). The effective cohesion, as stated before, it was kept as zero as the analysis is made with critical state.

## 5.3 Conceptual model of soil

As tests information was not available for the entire soil section, the general geometry in PLAXIS was setup in accordance to the one proposed by SWECO from the soil investigations (see Figure 2.10). As for the clay deposit, the conceptual model for its layering was obtained through the analysis of the ground characteristics retrieved from the studied boreholes in the area. The separation of the clay material into different layers was made by comparing the water content measured in the various boreholes at the analysed depths (see Figure 5.8). For values where the differences were not conclusive, analysis of the unit weight of the samples was also compared to decide to which layer the material belongs. With this results, the clay layer was determined to be separated into six different types.

As seen in Figure 5.8, the water content measured along the selected depths presents large variations. This could be caused by middle layers of sand between the clay deposit. Unfortunately, from the available test information, this assumption could have not been confirmed.

The soil profile drawn for the analysis is presented in Figure 5.9. The majority of the excavation in the selected section will be performed in a thick clay deposit composed of six layers with different properties. The clay is widely supported by the bedrock beside the small area which is supported by a thin layer of friction material. Test analysis from the clay material exhibited that the material is slightly overconsolidated with an approximate OCR value of 2.2 in the upper layers and of 1.1 for the deeper layers.

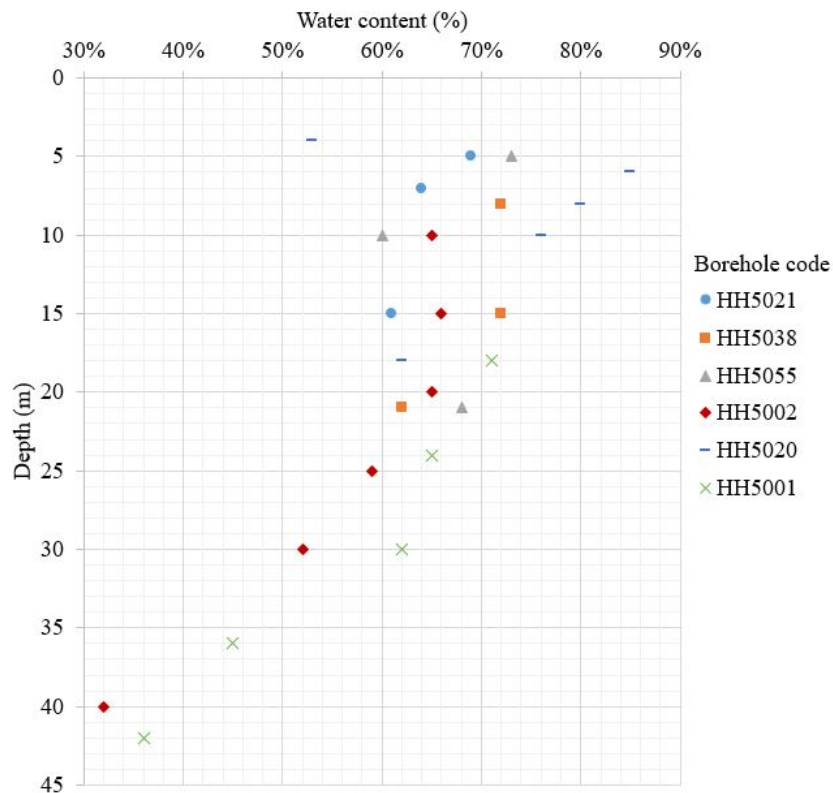


Figure 5.8: Water content for analysed boreholes vs. depth.

Evaluation of the sensitivity ( $S_t$ ) of clays from cone penetration tests performed by SWECO showed that the upper clay layers (1 to 3) have a medium to high sensitivity with  $S_t$  values ranked from 14 to 20 [2]. As for the lower clay layers (4 to 6), the material can be considered to have medium sensitivity with average  $S_t$  values between 7 and 15 [30]. Graphs for additional parameters of the soil layers as sensitivity, unit weight and liquid limit are available in Appendix K.

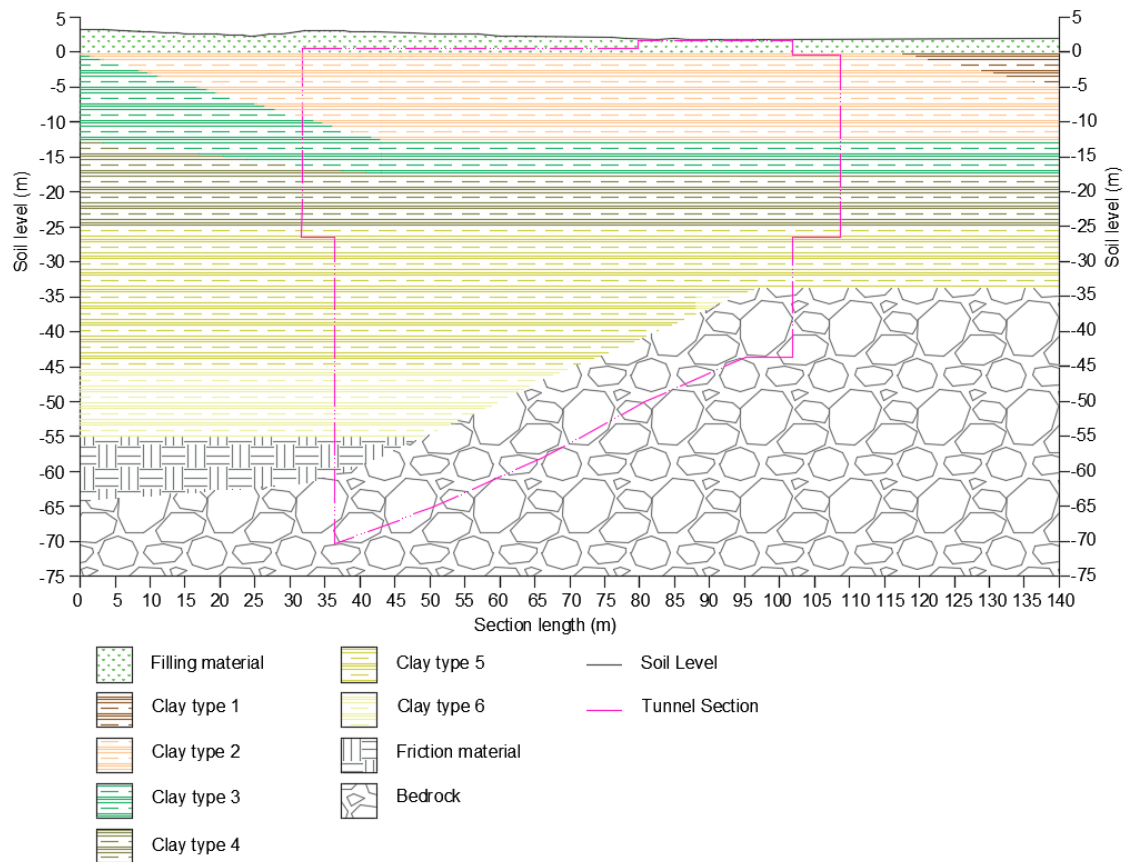


Figure 5.9: Cross section soil layering at km458+990 based on soil tests data and figures from SWECO [2].

## 5.4 Model parameters

To account for the changes in the materials' behaviour, several soil models were used to increase the accuracy of the calculations. Therefore, the parameters were grouped according to the type of soil model that would suit the best the material and available data from the soil investigation.

### 5.4.1 Mohr-Coulomb parameters

Both the fill and the friction materials were modelled using Mohr-Coulomb model. The parameters used in PLAXIS are presented in Table 5.1.

Values for Young's Modulus were retrieved from handbooks and guides about soil modelling for non-cohesive materials of medium cohesion [111][112]. As for strength parameters, these were taken from the geotechnical report about the area performed by SWECO [2].

Table 5.1: Parameters for friction and fill materials in Mohr-Coulomb constitutive model in PLAXIS 2D.

| Parameter                  | Symbol     | Unit              | Fill material | Friction material |
|----------------------------|------------|-------------------|---------------|-------------------|
| Dry Unit Weight            | $\gamma_d$ | kN/m <sup>3</sup> | 18            | 21                |
| Saturated Unit Weight      | $\gamma_s$ | kN/m <sup>3</sup> | 18            | 21                |
| Young's Modulus            | E          | kPa               | 30000         | 35000             |
| Poisson's ratio            | $\nu$      | -                 | 0.35          | 0.35              |
| Effective friction angle   | $\phi'$    | °                 | 30            | 30                |
| Dilation angle             | $\psi$     | °                 | 0             | 0                 |
| Effective cohesion         | $c'$       | kN/m <sup>2</sup> | 1             | 1                 |
| Permeability               | $k_x, k_y$ | m/day             | 1             | 1                 |
| Earth pressure coefficient | $K_0$      | -                 | 0.5           | 0.5               |

#### 5.4.2 Soft Soil (Creep) parameters

All of the clay layers were modelled using two soil models, Soft Soil and Soft Soil Creep. A comparison between the result from both soil models was made to account for changes due to the introduction of creep in the second one. Stiffness and strength parameters were taken from triaxial, direct shear, oedometer and CRS tests. The employed data is presented in Tables 5.2 and 5.3.

Table 5.2: Parameters for Clay 1-3 used in Soft Soil and Soft Soil Creep constitutive models in PLAXIS 2D.

| Parameter                  | Symbol      | Unit              | Clay 1 | Clay 2 | Clay 3 |
|----------------------------|-------------|-------------------|--------|--------|--------|
| Dry Unit Weight            | $\gamma_d$  | kN/m <sup>3</sup> | 11.5   | 9.9    | 9.0    |
| Saturated Unit Weight      | $\gamma_s$  | kN/m <sup>3</sup> | 17.6   | 16.3   | 15.8   |
| Modified compression index | $\lambda^*$ | -                 | 0.147  | 0.156  | 0.147  |
| Modified swelling index    | $\kappa^*$  | -                 | 0.0041 | 0.0046 | 0.0041 |
| Modified creep index       | $\mu^*$     | -                 | 0.0020 | 0.0021 | 0.0020 |
| Effective friction angle   | $\phi'$     | °                 | 23.8   | 23.8   | 26.1   |
| Dilation angle             | $\psi$      | °                 | 0      | 0      | 0      |
| Effective cohesion         | $c'$        | kN/m <sup>2</sup> | 1      | 1      | 1      |
| Poisson's ratio            | $\nu$       | -                 | 0.15   | 0.15   | 0.15   |
| Over consolidation ratio   | OCR         | -                 | 2.165  | 1.760  | 1.760  |
| Permeability               | $k_x, k_y$  | m/day             | 1E(-5) | 1E(-5) | 1E(-5) |
| Earth pressure coefficient | $K_0$       | -                 | 1.086  | 0.9156 | 0.8516 |

For the Clay layers 4 to 6, the friction angle to be used in the model was decreased due to the low values achieved by the upper layers. The value for  $\kappa^*$  for Clay 4 was also modified to keep the value closer to the distribution of the results from other layers.

Table 5.3: Parameters for Clay 4-6 used in Soft Soil and Soft Soil Creep constitutive models in PLAXIS 2D.

| Parameter                  | Symbol      | Unit              | Clay 4 | Clay 5 | Clay 6 |
|----------------------------|-------------|-------------------|--------|--------|--------|
| Dry Unit Weight            | $\gamma_d$  | kN/m <sup>3</sup> | 10.0   | 11.1   | 14.1   |
| Saturated Unit Weight      | $\gamma_s$  | kN/m <sup>3</sup> | 16.3   | 17.5   | 19.0   |
| Modified compression index | $\lambda^*$ | -                 | 0.182  | 0.147  | 0.091  |
| Modified swelling index    | $\kappa^*$  | -                 | 0.0042 | 0.0015 | 0.0027 |
| Modified creep index       | $\mu^*$     | -                 | 0.0029 | 0.0019 | 0.0020 |
| Effective friction angle   | $\phi'$     | °                 | 30.0   | 30.0   | 30.0   |
| Dilation angle             | $\psi$      | °                 | 0      | 0      | 0      |
| Effective cohesion         | $c'$        | kN/m <sup>2</sup> | 1      | 1      | 1      |
| Poisson's ratio            | $\nu$       | -                 | 0.15   | 0.15   | 0.15   |
| Over consolidation ratio   | OCR         | -                 | 1.140  | 1.136  | 1.047  |
| Permeability               | $k_x, k_y$  | m/day             | 1E(-5) | 1E(-5) | 1E(-5) |
| Earth pressure coefficient | $K_0$       | -                 | 0.543  | 0.544  | 0.515  |

### 5.4.3 Hoek-Brown parameters

The bedrock in the area was modelled using Hoek-Brown model to take into account the difference in stiffness of the material compared to the surrounding soil and its different behaviour to the impose loads. The parameters used in PLAXIS to model the bedrock behaviour are presented in Table 5.4.

Table 5.4: Parameters for bedrock used in Hoek-Brown constitutive model in PLAXIS 2D.

| Parameter  | Symbol        | Unit              | Bedrock |
|--|---------------|-------------------|---------|
| Unit Weight  | $\gamma$      | kN/m <sup>3</sup> | 26      |
| Young's Modulus  | E             | kPa               | 53E6    |
| Poisson's ratio  | $\nu$         | -                 | 0.2     |
| Uni-axial compressive strength of the intact rock                        | $\sigma_{ci}$ | kN/m <sup>2</sup> | 150     |
| Intact rock parameter  | $m_i$         | -                 | 32      |
| Geological strength index  | GSI           | -                 | 75      |
| Disturbance factor   | D             | -                 | 0.1     |
| Dilation angle   | $\psi$        | -                 | -       |
| Absolute value of confining pressure ( $\sigma'_3$ ) at which $\psi = 0$ | $\psi_m$      | -                 | -       |

Most of the strength parameters in the model are related to the type of rock, block structure and disturbance history of the rock mass. Therefore, the description of the bedrock on the site will be retrieved from information from the desk study.

As mentioned in Chapter 2, the rock in the area consists of acidic intrusive rock which for the case of Gothenburg could be between granite, granodiorite or monzonite [15]. Parameters such as the intact rock parameters ( $m_i$ ), unit weight ( $\gamma$ ), Poisson's ratio ( $\nu$ ) and Young's modulus (E) will be estimated according to previous research for these rock types [41][42][113].

From the bedrock maps in the area, it was determined that the rock is mostly intact with fewer fractures in dispersed areas [15]. Hence, calculation of the Geological Strength Index (GSI) is made for a rock with good surface quality and blocky structure. As for the disturbance factor from section 4.8, it was analysed that the area presents few disturbances in the bedrock due to the previous foundation of surrounding buildings. Then, a disturbance factor (D) for low impact procedures in the bedrock was accounted for [114].

It is important to mention that the parameters for modelling the bedrock were assumed from information retrieved from maps and typical characteristics of the material in the area. A sensitivity analysis of the parameters must be evaluated to analyse the influence of the soil behaviour to the changes of the chosen values.

#### 5.4.4 Interface parameters

Calculation of the  $R_{inter}$  parameter is made with equation 3.7. To do this, experimental values for skin friction angles between various soils and construction materials are retrieved from the literature [115][119]. For the case of this study, three types of soil materials are found in the area which corresponds to clay, rock and sand (representing filling and friction materials). As for the material of the foundation structures, concrete with the smooth surface will be assumed. The values for  $R_{inter}$  for these types of materials are presented in Table 5.5.

Table 5.5: Interface strength values for different soils for concrete structures.

| Soil           | $R_{inter}$ | Observations                            |
|----------------|-------------|---|
| Clay layer 1-3 | 0.70        | Water content > 30%                     |
| Clay layer 4-6 | 0.75        | Water content > 30%                     |
| Sand           | 0.85        | Filling material, dry conditions        |
| Dense sand     | 0.90        | Friction material, saturated conditions |
| Rock           | 1.00        | Rigid interface                         |

## 5.5 Loads

Besides the calculation of the soil parameters, another main factors to take into consideration in the model are the loads which the tunnel will need to support or resist during its service life. Loads can be divided into internal and external. In this case, the internal loads refer to the forces inside the ground media, such as soil weight and ground water. The external loads refer to the loads produced above the ground level such as traffic, construction works and others. In this chapter, the magnitudes of the loads in the section are presented with a description on how they were derived.

### 5.5.1 Internal loads

The internal loads to be consider in the model are the soil and ground water. These values are automatically calculated from PLAXIS by using the required parameters for soil and groundwater level.

#### Soil loading on the wall

Calculation of earth pressure is performed by means of FE (see Section 2.4.4). In PLAXIS 2D, initial calculation of the stresses on the soil in primary condition is performed with the use of the coefficient of earth pressure at-rest ( $K_0$ ). This parameter can be defined manually or can be automatically calculated by PLAXIS depending on the consolidation state of the soil. For normally consolidated soils,  $K_0$  is computed with Jaky's formula (see equation 3.5), while for overconsolidated soils it is a function of the OCR and POP (see [43]).

#### Ground water

According to SGU maps, the groundwater level is approximately at 2 m below the upper soil level and there are no aquifers in the area. This could be explained by the presence of the thick clay layer in the section. Groundwater load is accounted for the earth pressure calculation in the FEM given that the soil models are expressed in terms of effective stress parameters. In the model, it is assumed that the ground water level is maintained at 2 m below the ground level in the area of the station.

Roselundskanalen has been presented on the model but the variation in the water level in the canal has not been taken into account. Level of water in the canal is assumed to be stable and on the same level as the groundwater level in the surrounding area.

## 5.5.2 External loads

Calculation of external loads in the tunnel will be retrieved from design manuals from Trafikverket and additional researched literature about similar cases.

### Traffic load

Traffic load is a type of live load given that is not permanent on the surface. As no further measurements were made to calculate the exact load from traffic in the area, standard values for Sweden were used for the model. The analysed section accounts for a variety of roads which allow for different types of traffic such as railway (tram), vehicular, pedestrian, and cyclists. Calculation of the surcharge load from traffic is done by reviewing the manual for geotechnical constructions from Trafikverket. For the area of analysis, the standard values for traffic loads are the following [121]:

|                      |                              |
|----------------------|------------------------------|
| 15 kN/m <sup>2</sup> | Vehicular roads              |
| 5 kN/m <sup>2</sup>  | Pedestrian and cyclist roads |

### Structural loads

Structural loads refer to the surcharge load from adjacent buildings. The studied cross section in this study is separated from the nearest building by the distance of approximately 115 m. Still, this load will be considered in the model due to the vast dimensions of the excavation and a high importance of the settlement under the building.

The burden from the adjacent buildings will be calculated for the complex enclosed by the streets Södra Allégatan, Haga Östergata, Skolgatan and Husargatan (see Figure 2.2). For the purposes of a unified imposed load, the following assumptions are made: height of the buildings is unified at four floors; one floor set for commercial use (cafes, restaurants), and the other three for residential use; roof use restricted only for maintenance purposes. These assumptions were based on a visual recognition of the area. In Table 5.6, the values for surcharge loads ( $q$ ) according to the assumed type of building are presented [117].

Table 5.6: Imposed loads from adjacent buildings to the excavation. Based on values provided by Building Department of Hong Kong [117].

| Use   | Quantity | $q$ (kN/m <sup>2</sup> ) | Total $q$ (kN/m <sup>2</sup> ) |
|---|----------|--------------------------|--------------------------------|
| Floor for domestic use and residential activities       | 3        | 2.0                      | 6.0                            |
| Floor for congregation of people (e.g. cafe/restaurant) | 1        | 4.0                      | 4.0                            |
| Inaccessible roofs and flat roofs                       | 1        | 0.75                     | 0.75                           |
|   |          |                          | <b>10.75</b>                   |

For the calculation of the dead load of the buildings, the following assumptions are taken: material of roofs is unified as copper; façade material is be 50 % masonry and 50 % wood; interior wall material will be wood, interior floors is 70 % in wood and 30 % in ceramic tile to account for bathroom and kitchen spaces and concrete plates for foundation. Table 5.7 presents the value of  $q$  for different materials calculated for a type building in the area.

Table 5.7: Dead load of materials present in adjacent buildings to the excavation. Based on values provided by Building Department of Hong Kong [117].

| Material                        | Quantity | $q$ (kN/m <sup>2</sup> ) | Total $q$ (kN/m <sup>2</sup> ) |
|---------------------------------|----------|--------------------------|--------------------------------|
| Roof with metal roofing         | 1        | 0.67                     | 0.67                           |
| Floor with wood flooring        | 2.8      | 0.57                     | 1.61                           |
| Floor with ceramic tile         | 1.2      | 0.72                     | 0.86                           |
| Interior partition wall in wood | 4        | 0.29                     | 1.15                           |
| Facade in wood                  | 4        | 0.38                     | 1.53                           |
| Facade in brick                 | 4        | 2.15                     | 8.62                           |
| Concrete foundation             | 1        | 4.64                     | 4.64                           |
|                                 |          |                          | <b>19.08</b>                   |

By adding both the live and dead load calculated for the building types in the area, a value of 29.83 kN/m<sup>2</sup> is obtained. This value is be used in the model and will be maintained constant.

### Construction loads

The load from construction refers to the surcharge load produce from equipment, workforce and stored materials used for the proposed construction. As stated in Section 3.6.2, the minimum surcharge load from construction is set to be 3.5 kN/m<sup>2</sup> [53]. This value can increased due to the type of machinery used by the contractor, and additional structures or soil filling made as foundations for heavy equipment. Therefore, a conservative assumption of 10 kN/m<sup>2</sup> from construction works will be implemented in the model.

## 5.6 General discussion of assumptions for input data

As discussed in this chapter, the soil investigation data used for this study was scattered, and no planning of numerical modelling was made during the process. Furthermore, soil samples were only taken from a depth of 5 to 40 m below the ground surface which correspond mainly to the clay layer in the. Moreover, the drilling have no z-coordinate value. Consequently, it is not possible to position the borehole data in the correct places and evaluate the continuity of the soil layering accurately.

Due to above mentioned causes, it is claimed that no real in-situ information was analysed for other soil layers as bedrock, filling and friction materials. A description of the principal assumptions made to fill the gaps in the soil investigation is described in this section. Additionally, samples from the boreholes were not taken at the same depth, resulting in deficiencies in the information which made difficult to perform a complete soil profile for each drilling. To solve this, the cross section was divided into four segments which coupled with information from minimum two boreholes. With this, gaps in the information from one drilling were completed by a nearby in order to present a complete soil profile of the clay.

Due to the use of critical state for the calculation of the strength parameters for clay, the effective cohesion for this material was set as zero. Even though, in PLAXIS the value of effective cohesion was set as 1 kN/m<sup>2</sup> for computational reasons.

The value of permeability for the clay deposit was assumed to be the same. Therefore, the permeability parameter set in PLAXIS for all the six clay layers is the same. The permeability parameter was taken from an intermediate value from the CRS results (see Appendix J). For other soil types, the value of permeability was assumed based on the literature study.

Values for dilation angle were assumed as no tests were made from were this data could be retrieved. According to Bolton [118], non-cohesive soils present a linear relation between the friction and dilation angle under extreme stress conditions. Therefore, for the calculation of the parameter, an empirical formula was used (see equation 5.2) [35]. As for clay, the dilation angle was assumed to be zero.

$$\psi = \phi' - 30 \quad (5.2)$$

Additional strength and stiffness parameters for friction and filling materials were collected from the SWECO report [2]. Even though, due to the small presence of these materials in the section, it could be assumed that the reliability of the data would not have a great impact on the final results of the model.

Finally, groundwater level fluctuations were not taken into account as no sound information about this variability could have been found in SGU and SWECO reports. As a result, Rosenlundskanalen water level fluctuation was also ignored. This move allowed to presented groundwater level as a continues profile through the surrounding soil. It is claimed that such approximation of water level in the canal is very close to real situation as elaborated in Section 3.6.2.

# 6

## PLAXIS 2D model

In this chapter, a description of the setup of the PLAXIS model is elaborated. Explanation of the FEM parameters is made as well as a representation of the selected foundation options and a summary of the problems involved in the modelling phase.

### 6.1 Model geometry

The geometry in PLAXIS was created based on the conceptual model of the soil presented in Section 5.3. Due to the gaps in soil investigation information, the borehole location in PLAXIS does not correspond to their real position. The geometry was formed according to the information from the different segments of the cross-section as described in 5.3.

The general geometry used in the model is presented in Figure 6.1. Information to represent the soil conditions was available for a section of about 140 m. All models used in calculations share the same geometry size that has been chosen as three times the size of the excavation in the horizontal direction and almost five times the depth of the excavation in the vertical direction. The location of, especially, a lower boundary can have a great effect on the final results [46]. The depth of the model could have been less extensive and limited to about three times the depth of the planned excavation. Nevertheless, it has been decided to extend it to properly capture the behaviour of the model around the top of bedrock area. Such extensive model allowed also to assure no disturbance at the model boundaries.

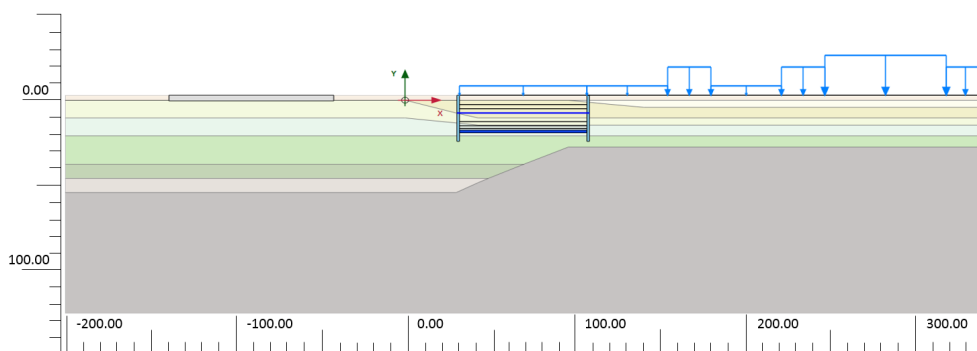


Figure 6.1: General soil geometry in PLAXIS 2D. Graphics present the total size of the numerical model.

The load visible at the far right side represents the only building in the close proximity of the section. The rest of the loads represent pedestrian and traffic loads. They are set only at right side of the excavation to represent the most conservative option, where the loads contribute to the sliding of the whole excavation and there are no supporting loads on the opposite part of the pit.

In Figure 6.1, the excavation is delimited by two vertical soil elements which represent the retaining walls, and a horizontal soil element which represents the base slab. The retaining walls are assumed to be 1.5 m thick diaphragm walls with reinforced concrete and a total length of 33.5 m, which corresponds to an extension of 8 m below the excavation level. The raft was also modelled with reinforced concrete and set to an initial thickness of 0.5 m. The concrete elements in PLAXIS were modelled with the linear elastic material model using the parameters presented in Table 6.1. All of the mentioned dimensions are assumed as a starting point for the design and may change to satisfy the project requirements. The final values are presented along with description of design alternatives.

Table 6.1: Parameters for concrete elements in PLAXIS 2D.

| Parameter       | Symbol     | Unit              | Retaining Wall | Raft       |
|-----------------|------------|-------------------|----------------|------------|
| Drainage type   | -          | -                 | Non porous     | Non porous |
| Dry Unit Weight | $\gamma_d$ | kN/m <sup>3</sup> | 25.0           | 25.0       |
| Young's Modulus | E          | kPa               | 31E(6)         | 31E(6)     |
| Poisson's ratio | $\nu$      | -                 | 0.2            | 0.2        |

The lateral support of the retaining walls is satisfied by means of applying steel struts. The number of levels, vertical position and out-of-plane spacing will be kept constant for all the design alternatives. In PLAXIS 2D, the parameters to simulate the force from the anchor is given by the value of the axial stiffness (EA) of the element and the out-of-plane spacing ( $L_s$ ). For this case, the struts were modelled as hydraulic steel struts with diameter of 1220 mm due to the large width of the excavation. The parameters of the struts are presented in Table 6.2.

Table 6.2: Struts parameters applied in PLAXIS 2D models.

| Parameter            | Symbol | Unit | Struts   |
|----------------------|--------|------|----------|
| Axial stiffness      | EA     | kN   | 2.45E(8) |
| Out of plane spacing | $L_s$  | m    | 10       |

## 6.2 Design of calculation features

Many numerical models, despite the correct assumptions and geometry input, suffer from deficiencies due to inappropriate mesh design and boundary condition influence. This is especially visible when the strain-softening material is used [46]. Thus, special attention has been given to these aspects of the modelling as described in sections below.

### 6.2.1 Model boundaries

The boundary conditions have been assigned as fixed in both directions at the bottom horizontal boundary while the vertical side boundaries restricted lateral movements (see Figure 6.2).

As stated in previous sections, the size of the model may influence the results. A good indicator is the presence of plastic points. If they occur at the model boundary, it might indicate that the model is too small and results affected by the boundary locations. No plastic points have been found at the proximity of the vertical boundaries in neither of the studied models. Thus, it is claimed that the model size has been chosen adequately and no disturbance due to size of the model is expected.

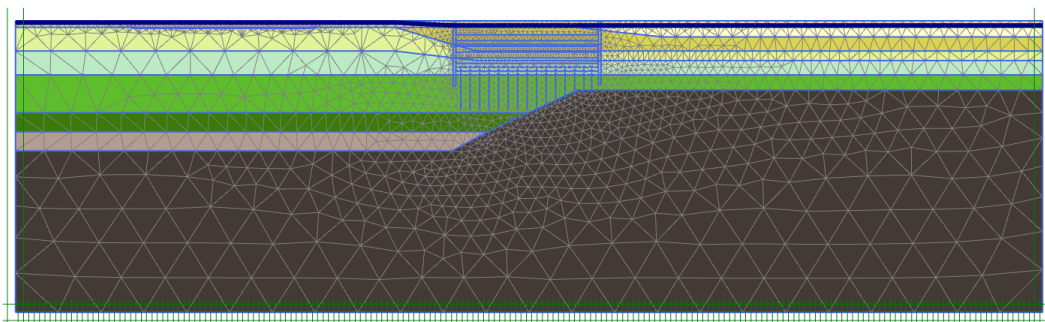


Figure 6.2: Fixations of the model boundaries.

### 6.2.2 Mesh design

Mesh of all presented numerical models have been set up using 15-nodal triangular elements. As mentioned in the COST handbook for numerical analysis in geotechnical engineering, the exact solution can be obtained only if the largest elements size would tend to zero [46]. Since it is not possible, FEM model delivers only an approximation of the reality, not the exact solution, what should be stressed here once again.

To assure results as close to the real values as possible, the models have been set up using fine mesh as a default option. It has been further refined in places of high stress and strain concentrations and coarsens away from the points of interest. This

design movement delivers the most computationally efficient solution and simultaneously allows to focus on the most important parts of the model where a rapid change of boundary loads and stiffness may occur.

The same philosophy is reflected by the meshing of structural elements (when modelled using soil clusters, not beam elements). A good example is a diaphragm wall which thickness is usually small in comparison to length. Thus, a high care has been taken not to create bad quality elements.

Similarly, there are some default structural elements that might be particularly sensitive to mesh quality. In PLAXIS, these are especially embedded beam rows that give variable results if meshing around them is not properly designed. Consequently, the meshing around these elements has been refined to adequately capture their behaviour.

In order to assure the quality of mesh design, it is recommended to inspect the mesh quality output. Figure 6.3 presents the final mesh quality plot. As no elements are rated with values below zero, it is claimed that the quality of all elements is satisfactory. Alternatively, it is a good practice to run calculations with mesh finer and coarser than the designed one. If obtained results are similar (usually within a range of 10 % difference), it is claimed that the mesh has been adequately designed. In this paper, all numerical models have been validated based on this approach. The exemplar results are presented below in Table 6.3.

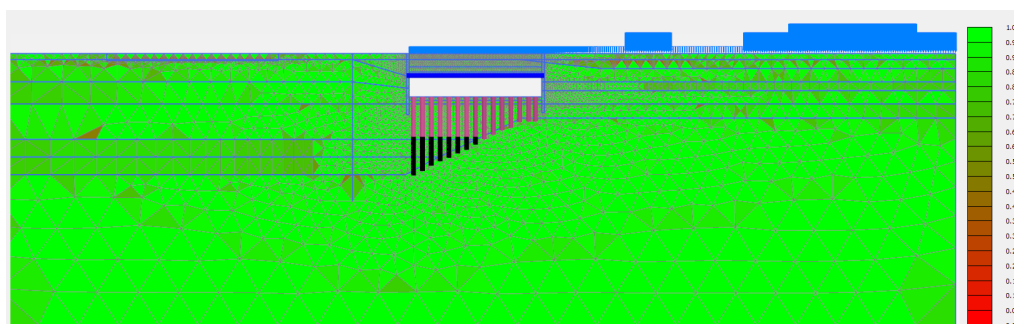


Figure 6.3: Inspection of mesh quality in PLAXIS.

Table 6.3: Example of the mesh design validation based on the three calculations of coarser, designed and finer mesh. The presented example covers the final settlement with Soft Soil model calculated for Alternative 2 - Piled Raft with Foam Glass fill, but similar range of values have been obtained for all of the remaining models.

|  | Unit | Coarser mesh | Designed mesh | Finer mesh |
|--|------|--------------|---------------|------------|
| Maximum settlement of the raft ( $ u $ ) | m    | 0.1323       | 0.1323        | 0.1324     |
| Difference from the designed mesh        | %    | $\pm 0$      | 100           | + 0.076    |

## 6.3 Developed models

Description of the modelled alternatives in PLAXIS 2D is presented in this section. The clay deposits in all the proposed alternatives were modelled both with the SS and SSC soil models, to review the impact of creep. The analysed alternatives include the design of the excavation with base support of soil-mix columns, piled raft, and cross walls.

### 6.3.1 Alternative 1 - Cross-walls

The Alternative 1 includes the cross-walls as a foundation system for the excavation (see Figure 6.4). The initial supporting system was setup as described in Section 6.1. The cross walls were modelled as soil clusters which have the strength parameters of concrete. The thickness and height of the clusters are the same as the actual walls to simulate the stiffness and resistance against heave. The connection between the walls was made by means of steel struts which are represented as black lines connecting the soil clusters in Figure 6.4. The steel elements are placed to simulate the axial and bending stiffness of the walls as described in Section 3.7.2.

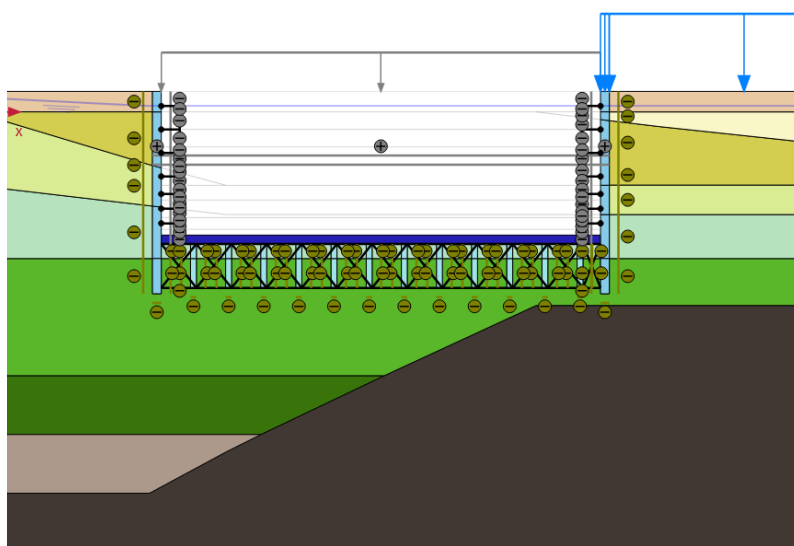


Figure 6.4: Model geometry in PLAXIS 2D for Alternative 1 in short term.

The final thickness of the raft for this alternative was set at 1.5 m after an iterative process where different values were tested to review its impact on the model. The thickness for the cross-walls was set at 1 m and their height at 7.5 m. The dimensions of the retaining walls were maintained to the specifications presented in Section 6.1.

The iterative design process lead to the choice of seven strut levels as a support of the excavation.

The spacing of the cross-walls was determined according to the method proposed by Wu et al. [68], described in Section 3.7.2. With the initial support system of the excavations (two external diaphragm walls and seven levels of struts), the expected settlement is of the order of 226 mm (see Appendix L for calculations). Based on Chapter 4, it was defined that the maximum allowable settlement in the soil should be as minimum as possible; therefore the project requirements are not fulfilled. By using equation 3.11, with a target settlement of 10 mm, the spacing of the cross walls needed for the designed system is 10 m. This spacing was used in PLAXIS 2D as a starting point. The actual separation of the cross-walls was reduce to 5 m after verification with the numerical model that 10 m spacing was not enough to counteract the uplift problem at the bottom of the excavation.

### 6.3.2 Alternative 2 - Piled raft

The second alternative in PLAXIS 2D is modelled with piled raft as foundation system. Its general geometry is presented in Figure 6.5. The structural elements such as diaphragm walls and raft are modelled as soil clusters. The retaining elements have the same dimensions as described in Section 6.1 except from the left wall which was shortened by 1 m. As for the raft, the final thickness was setup to 2 m. The roof slab is set as a plate element and the piles as embedded beam rows.

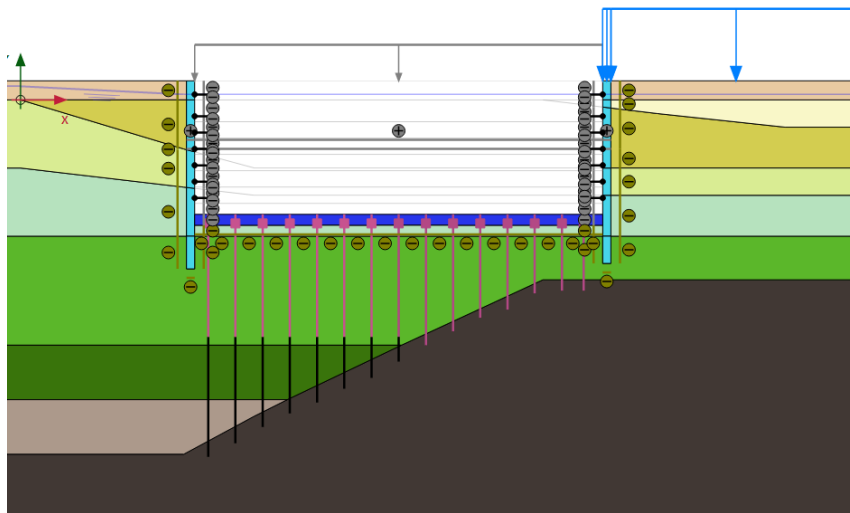


Figure 6.5: Model geometry in PLAXIS 2D for Alternative 2 in short term.

To fulfil the settlement requirements, it is decided to use the stiffness of the bedrock to give support to the piling system. Due to the soil profile in the area, two types of piles were considered. The first group correspond to end bearing piles which will be supported by the bedrock in the area where the distance to the rock strata is close to the bottom of the excavation. The second group of piles is modelled as cohesion piles, and will be located in the area where the bedrock is deeper than 45 m from the

surface level. These elements are driven until a depth of 22 m below the excavation level, and then are anchored to the bedrock in order to prevent the occurrence of uneven settlements. Parameters used for their calculations are presented in Appendix M. Both types of piles are anchor two meters inside the bedrock each. The input parameters for the structural elements are presented in Table 6.4.

Table 6.4: Parameters for Alternative 2 - Piled raft.

| Parameter            | Symbol   | Unit              | Cohesion Piles      | End Bearing Piles |
|----------------------|----------|-------------------|---------------------|-------------------|
| Young's modulus      | E        | kPa               | 31E(6)              | 20E(6)            |
| Unit weight          | $\gamma$ | kN/m <sup>3</sup> | 24.0                | 17.8              |
| Pile type            | -        | -                 | Massive square pile | Circular tube     |
| Diameter             | d        | m                 | 0.275               | 0.5               |
| Thickness            | t        | m                 | -                   | 0.015             |
| Out of plane spacing | $L_s$    | m                 | 5                   | 5                 |

### 6.3.3 Alternative 3 - Lime-cement columns

Alternative 3 includes lime-cement columns (LCC). The general geometry for this option is presented in Figure 6.6. The retaining walls have the same dimensions as described in Section 6.1, and the thickness of the raft was set to 2 m. Due to the strict restrictions for soil movements, the columns are overlapping creating a transverse wall between the retaining walls. As a simplification, the columns will be represented in the model as a block of soil with stiffness characteristics calculated as an average between the columns and the surrounding soil parameters. The total depth for the LCC was set to 10 m.

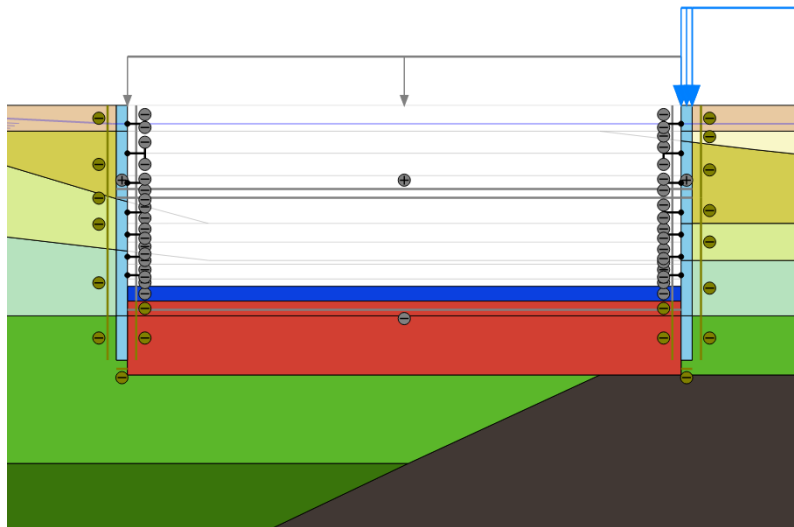


Figure 6.6: Model geometry in PLAXIS 2D for Alternative 3 in short term.

The properties for the soil block, which represents the LCC, were chosen to be average between the surrounding soil and the strengthening material. The soil is model with Mohr-Coulomb model. As no data regarding the improved soil parameters were available, all of the properties for the material are assumptions. The chosen parameters are presented in Table 6.5

Table 6.5: Parameters for LCC soil in Mohr-Coulomb constitutive model in PLAXIS 2D.

| Parameter                  | Symbol     | Unit              | LCC soil block |
|----------------------------|------------|-------------------|----------------|
| Dry unit weight            | $\gamma_d$ | kN/m <sup>3</sup> | 17             |
| Saturated unit weight      | $\gamma_s$ | kN/m <sup>3</sup> | 17             |
| Young's modulus            | E          | kPa               | 333E(3)        |
| Poisson's ratio            | $\nu$      | -                 | 0.2            |
| Effective friction angle   | $\phi'$    | °                 | 32             |
| Dilation angle             | $\psi$     | °                 | 0              |
| Effective cohesion         | $c'$       | kN/m <sup>2</sup> | 100            |
| Permeability               | $k_x, k_y$ | m/day             | 0.5E(-3)       |
| Earth pressure coefficient | $K_0$      | -                 | 0.47           |

Strength parameters such as friction angle and effective cohesion were retrieved for the TK-GEO publication from Trafikverket [121]. The unit weight for the material was assumed to be slightly higher than the unit weight of the surrounding material which in this case was Clay 4. As for the Young's Modulus, this was calculated as the modulus of elasticity of the surrounding clay during unloading. The coefficient of permeability for the LCC soil block was assumed to be a thousand times higher than the coefficient of the surrounding soil.

## 6.4 Consideration about the effect of time

The three design alternatives in Section 6.3 are modelled both in short and long term to analyse the stability of the excavation during the construction stage as well as during the operation of the tunnel. Figures 6.4, 6.5 and 6.6 represent the short term condition of the three alternatives which correspond to the final construction of the excavation where the foundations and the total depth of the pit are reached.

For the long term analysis, additional stages are evaluated where a roof plate is installed, and a fill material is set above the roof of the tunnel. The long term displacements are analysed after a consolidation period of 10 years when the construction is in operation. The roof slab is model as a plate element in PLAXIS 2D; its properties are presented in Table 6.6.

Table 6.6: Parameters for roof slab PLAXIS 2D.

| Parameter         | Symbol | Unit                | Roof Slab |
|-------------------|--------|---------------------|-----------|
| Bending stiffness | EI     | kNm <sup>2</sup> /m | 1.09E(12) |
| Axial stiffness   | EA     | kN/m                | 2.33E(9)  |
| Poisson's ratio   | $\nu$  | -                   | 0.2       |
| Weight            | w      | kN/m/m              | 0         |

As for the fill material, two types are modelled to review their impact on the long term settlements. The chosen materials are foam glass and lightweight expanded clay aggregate (LECA). Their properties are presented in Table 6.7.

Table 6.7: Parameters for fill material after excavation in PLAXIS 2D.

| Parameter             | Symbol            | Unit       | Foam glass     | LECA         |
|-----------------------|-------------------|------------|----------------|--------------|
| Soil model            | -                 | -          | Linear-elastic | Mohr-Coulomb |
| Unit Weight           | kN/m <sup>3</sup> | $\gamma_d$ | 2.25           | 4.8          |
| Saturated Unit Weight | kN/m <sup>3</sup> | $\gamma_s$ | -              | 7.2          |
| Drainage type         | -                 | -          | Non-porous     | Undrained A  |
| Young's Modulus       | kPa               | E          | 1100E(3)       | 70E(3)       |
| Poisson's ratio       | $\nu$             | -          | 0.25           | 0.20         |
| Friction angle        | $\phi$            | °          | -              | 30           |
| Effective cohesion    | $c'$              | -          | -              | 1            |
| Dilation angle        | $\psi$            | °          | -              | 0            |

The principal difference between the two materials concerns their drainage type. Foam glass is modelled as a non-porous material, therefore no pore pressure will be developed in the fill. As for the LECA that is a porous material, pore pressure can be developed in this area resulting in changes in the effective stresses of the fill. This might not be the case as it is dependant on the grading of the LECA fill. Here, a conservative assumption is taken into account.

As the example, Figure 6.7 presents the setting of the model for the piled raft alternative in long term. For this final stage, the roof slab is installed and supports the fill material. The loads of construction are removed leaving just the load from traffic in the area.

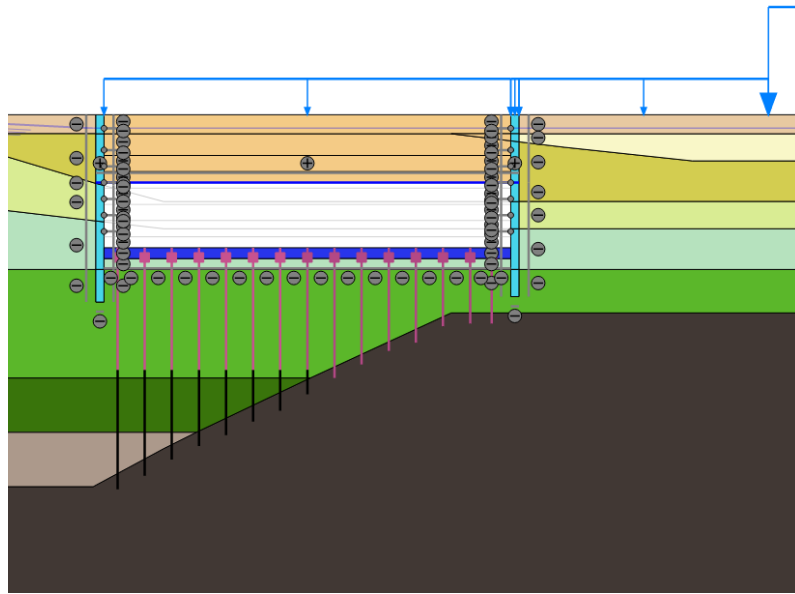


Figure 6.7: Model geometry in PLAXIS 2D for Alternative 2 in long term.

## 6.5 Construction sequence

Similar sequence for the construction was maintained for the three alternatives to enable the comparison among the options. In Table 6.8, description of the sequence for each of the alternatives is presented. For all the different types of calculations used for the constructions stages, the selected loading type was staged construction. For the SS model, no time was set for the construction stages besides the consolidation calculations. For the SSC, as required by PLAXIS, a total period of 3 years was distributed between the first 15 stages. The consolidation period was the same for both constitutive models.

The performed analysis was considered as dry excavation. Therefore, each soil cluster to be removed was set to dry in the model, and the pit was maintained dry during the process. All the structural elements were set with global water level given that they are impermeable and water should not affect their performance. For the fill material, both FG and LECA were set with global water conditions.

Table 6.8: Construction sequence for Alternatives 1, 2 and 3 in PLAXIS 2D.

| Stage  | Description  | Type of calculations |
|--------|--|----------------------|
| 0      | Calculation of initial stresses in the soil with $K_0$ values presented in Chapter 5.  | $K_0$ procedure      |
| 1      | Activation of superficial loads.   | Plastic              |
| 2      | Activation of diaphragm walls and interfaces. For alternatives 1 and 2, activation of piles and cross walls is also performed in this phase.               | Plastic              |
| 3 to 9 | Excavation of 19 m of excavation by sections of 3m. Activation of seven levels of struts starting from 1 m below the surface level and separated each 3 m. | Plastic              |
| 10     | Excavation of final 3 m. For phase 3 activation of layer of soil representing LCC.   | Plastic              |
| 11     | Construction of base slab for all the alternatives   | Plastic              |
| 12     | Safety analysis for short-term condition   | Safety               |
| 13     | Deactivation of the lowest sixth levels of struts. Activation of roof slab.  | Plastic              |
| 14     | Activation of first 5 m of fill material above the roof slab.  | Plastic              |
| 15     | Activation of final 7 m of fill material.  | Plastic              |
| 16     | Consolidation analysis for 10 years. Deactivation of interfaces. Removal of construction loads.  | Consolidation        |
| 17     | Safety analysis for long-term conditions   | Safety               |

## 6.6 General discussion of assumptions in PLAXIS 2D model

Given the problem geometry and the plane strain case, it can be assumed that the state of any x-y section would be maintained through all its parallel plains along the z-dimension. Therefore, any displacement found in the x-y section will be independent of the z dimension, and the model can be simplified to only two dimensions [46]. Given that the present study is the assessment of the most critical section in the Haga station, this assumption can be used as the conservative simplification of the problem. If an evaluation of the whole project is to be done, a model in three dimensions would have to be performed due to changes in the x-y cross-sections along the railway tunnel.

Assembly of two dimensional LCC and cross-walls alternatives required the combination of different elements in PLAXIS which may not resemble the actual behaviour of the elements in the reality. Results from these two alternatives are not fully reliable due to the limitations of the utilised software. Further analysis in 3D for the selected area would be ideal to facilitate more accurate predictions if one of the mentioned alternatives is selected in order.



# 7

## Results

In this section, the results from the numerical model are presented. They include a comparison among different alternatives, time frame and constitutive model assessment. The scale of all graphs has been uniformed in order to enable correlation among various figures.

### 7.1 Total displacements

The total displacements are the first results to be evaluated as they show where the soil is deforming the most and indicate potential problem areas. In this section, the graphs for each of the alternatives are presented for both short- and long-term. Along with this, the graphs of Soft Soil and Soft Soil Creep models are presented to compare whether the location of the major settlements and its magnitude are similar.

#### 7.1.1 Alternative 1 - Cross-walls

Figure 7.1 presents the distribution of total displacements for Alternative 1 in the short-term using the SS model for clay layers. It suggests the majority of the displacements occur in the bottom of the excavation where the raft is located. Displacements get higher values in locations closer to the retaining walls. It can also be seen that the soil on the left side presents larger movements compared to the right side. This is caused by the deeper clay layer in this section increasing the displacement of the retaining structure.

Displacement distribution obtained with the SSC model was almost the same as with the SS model. The difference was mainly that the magnitude of the displacements obtained with the SSC model was nearly double that of the SS model.

Figure 7.2, shows the distribution of total displacements for Alternative 1 in the long-term using the SS model. The major portion of the displacements occurs in the bottom of the excavation, along with the raft, and the cross-walls located on the side of the excavation where the clay deposit is deeper. The distribution of displacements obtained with the SSC model is almost the same as the one presented for the SS model, but the maximum value of displacements reached was 16.4 cm instead of 15.4 cm.

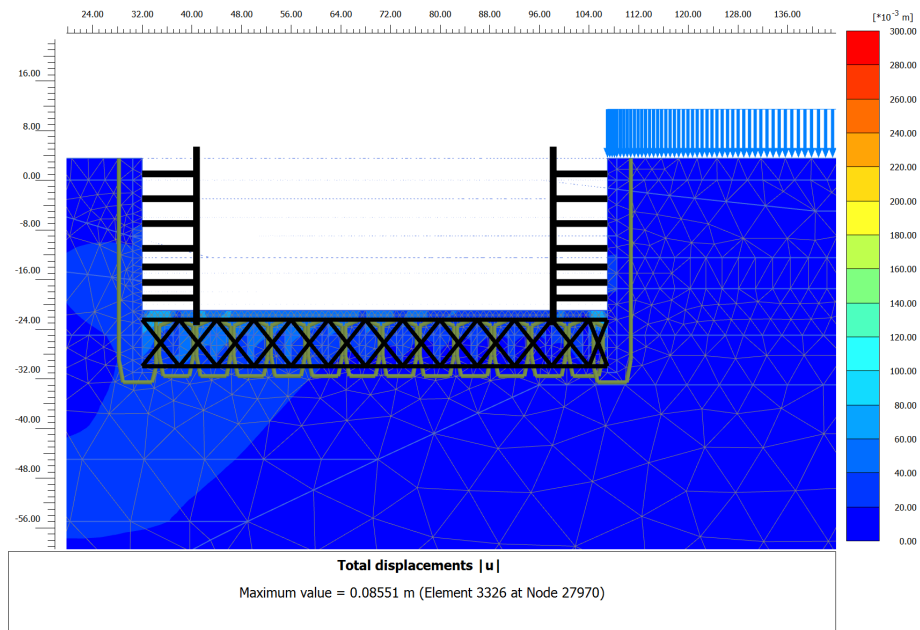


Figure 7.1: Total displacements obtained for Alternative 1 using SS model for the short-term.

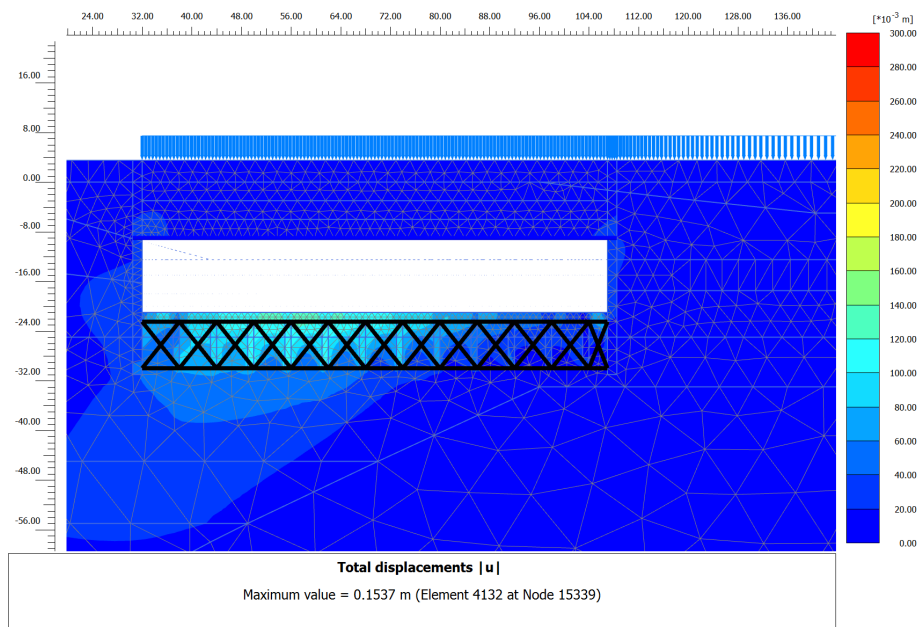


Figure 7.2: Total displacements obtained for Alternative 1 using SS model for the long-term.

## 7.1.2 Alternative 2 - Piled raft

Figure 7.3 shows the displacements distribution for Alternative 2 obtained with the SS model for the short-term. As demonstrated, the highest values of displacements are being generated below the bottom of the excavation beside both retaining structures. The peak is located close to the retaining wall to the left side of the excavation. With the SSC model, the obtained displacements follow the same distribution as presented for the SS model, but the maximum reached 24.9 cm instead of 9.97 cm.

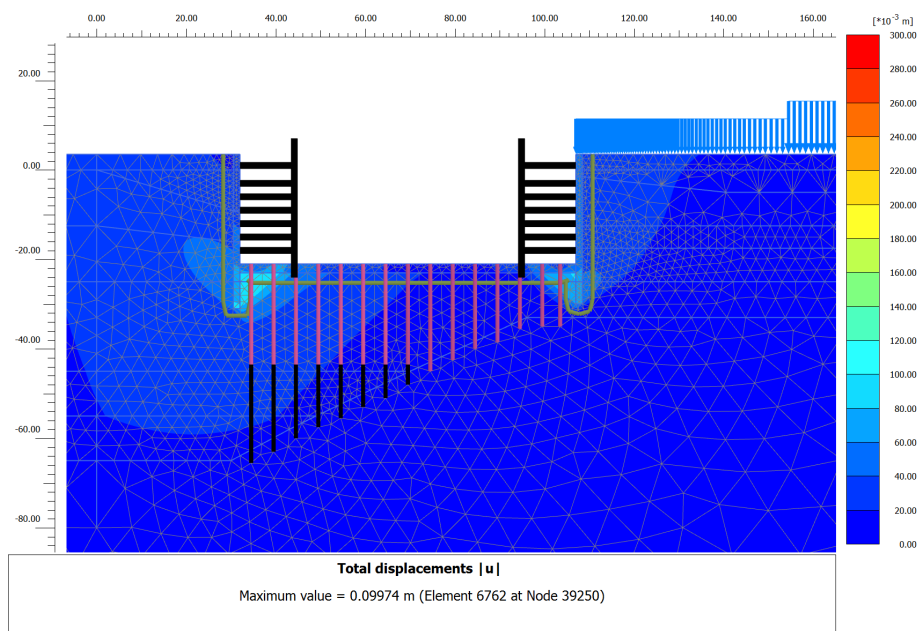


Figure 7.3: Total displacements obtained for Alternative 2 using SS model for the short-term.

For the long-term, the distribution of total displacements obtained for both the SS and the SSC models are quite different. Figure 7.4 shows the displacements obtained with the SS model. As observed, the highest values are obtained below the raft in the area where the clay deposit is thicker. High values are also generated beside the right retaining wall but on a lower scale compared to the left side.

Figure 7.5 presents the long-term displacement distribution obtained with the SSC model for the long-term. As shown, the highest values for displacements are generated closer to the retaining walls below the raft. However, with the SSC high values for deformation are also obtained behind the retaining walls on both sides of the excavation. The magnitude of the maximum displacement with this option is almost doubled compared to the result from the SS model.

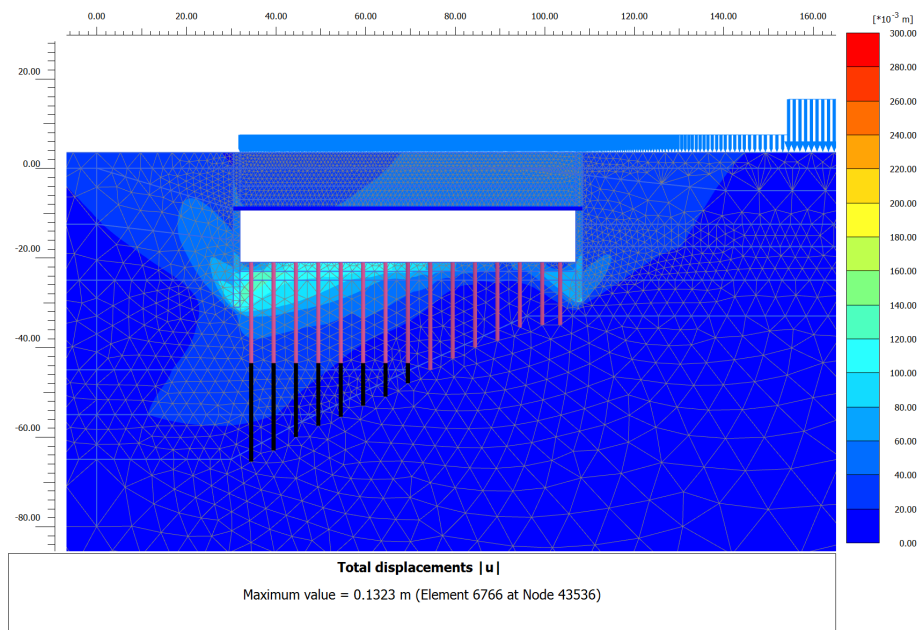


Figure 7.4: Total displacements obtained for Alternative 2 using SS model for the long-term.

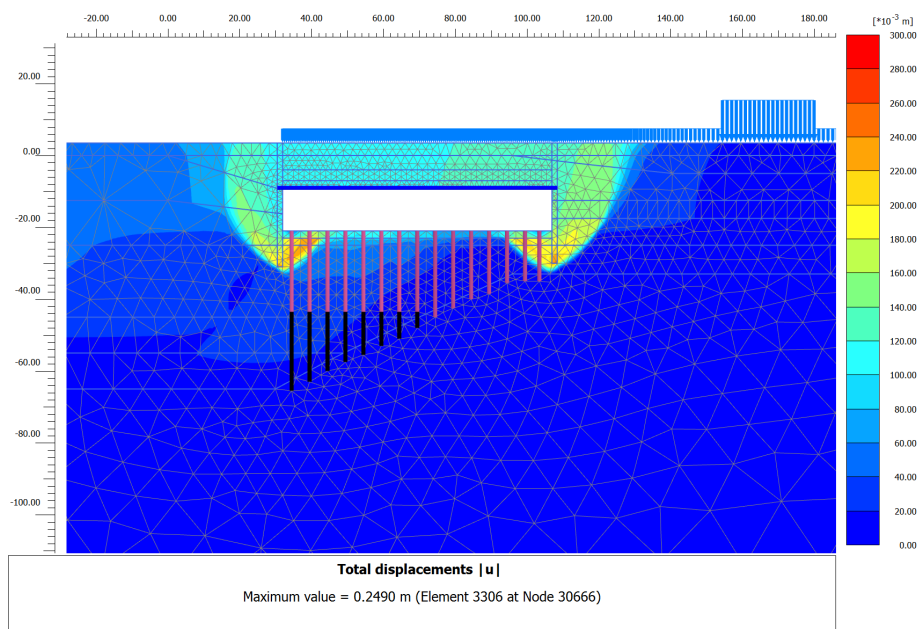


Figure 7.5: Total displacements obtained for Alternative 2 using SSC model for the long-term.

### 7.1.3 Alternative 3 - Lime-cement columns

Figure 7.6 shows the displacements distribution obtained with the SS model for the short-term. As can be seen, the highest values of displacements are being generated below the bottom of the excavation beside the retaining structures. The peak is located close to the retaining wall on the right. Additionally, large values are also obtained in the soil behind both retaining structures. With the SSC model, the obtained displacements follow the same distribution as achieved with the SS model, but the maximum value is 33.05 cm in comparison to 10.94 cm for the SS model.

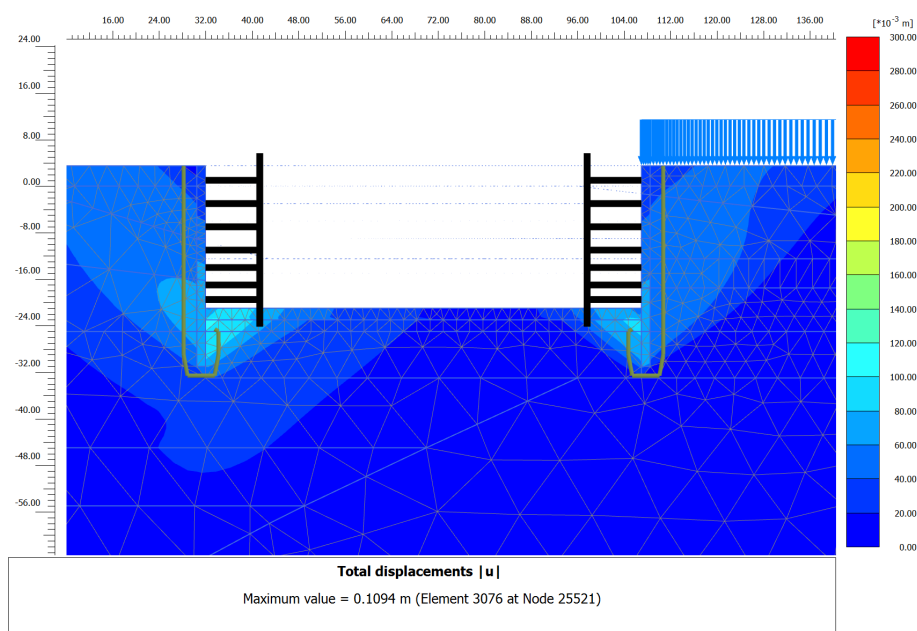


Figure 7.6: Total displacements obtained for Alternative 3 using SS model for the short-term.

For the long-term behaviour, different distributions of displacement are generated for the SS and SSC models. Figure 7.7, presents the distribution obtained with the SS model. As can be seen, the peak value is obtained close to the central area of the raft. This indicates that pore pressure below the bottom of the excavation generates heave of the soil.

Figure 7.8 presents the displacements for long-term obtained with the SSC model. In this option, the larger displacements are obtained beside the retaining structures in both of their faces. It seems that the whole retaining system is being settled and the uplift is less than the one obtained with the SS model. However, the maximum value of displacement is more than double than the obtained with the SS model (13.97 cm vs. 29.82 cm).

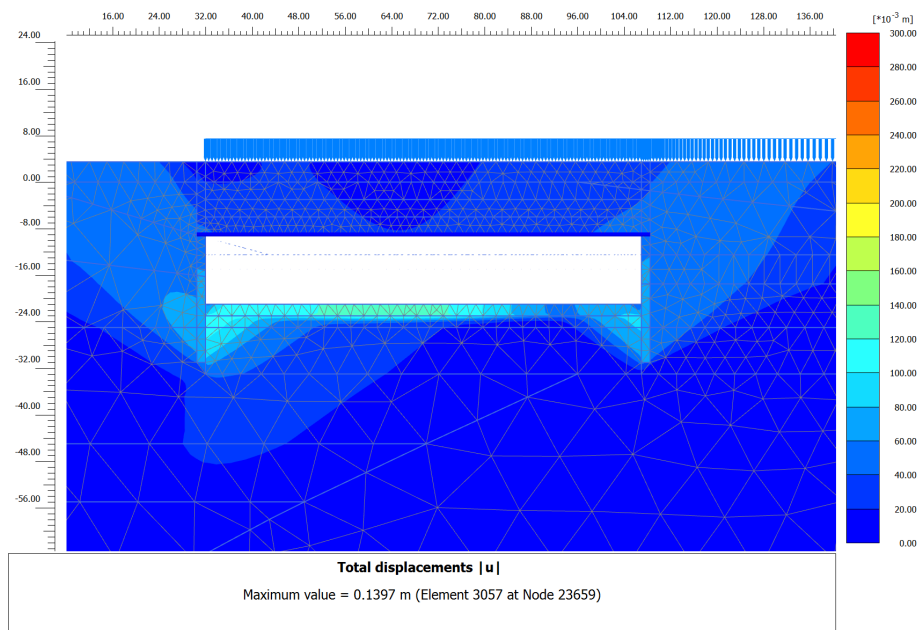


Figure 7.7: Total displacements obtained for Alternative 3 using SS model for the long-term.

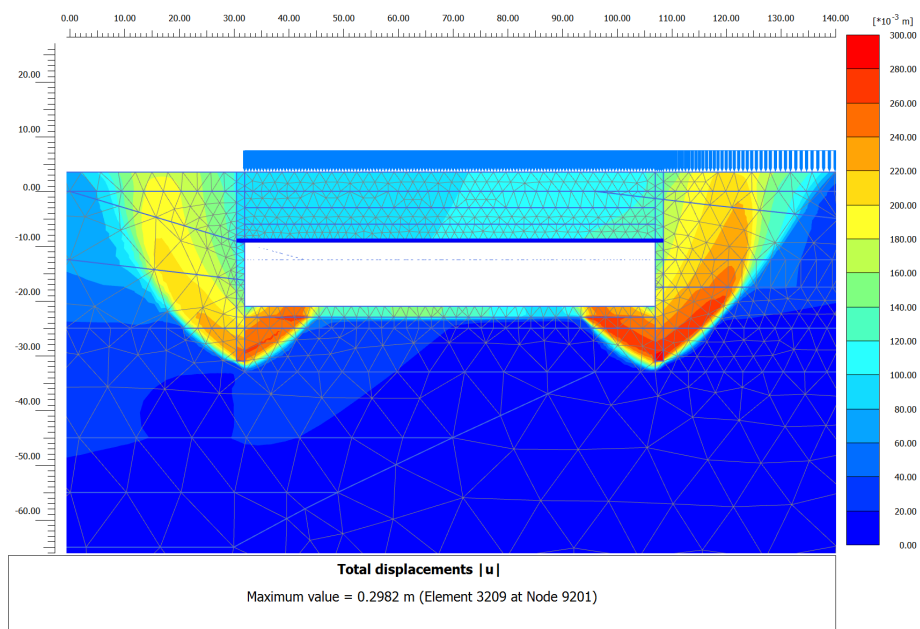


Figure 7.8: Total displacements obtained for Alternative 3 using SSC model for the long-term.

## 7.2 Displacements in critical areas

According to the analysis performed in Section 7.1, the areas where the highest displacements are presented correspond to the bottom of the excavation, the surface level around the excavation and the retaining structures in their whole length. Therefore, in this section the analysis of these three aspects will be presented. Besides, the comparison between the different alternatives is performed.

In this section, the short-term analysis corresponds to the stage where the raft is completed which corresponds to Phase 11 in the model according to Table 6.8. In this case, no comparison is made between the two studied fill materials as they are still not placed during this calculation phase.

For the long-term analysis, the introduction of the two fill materials mentioned in Chapter 6 (FG and LECA) is made in order to compare their impact on the soil displacements. The long-term analysis is performed after a consolidation period of 10 years which corresponds to Phase 16 in the model.

### 7.2.1 Surface settlements

Figures 7.9 - 7.12 display the lines representing the soil settlements. The vertical lines represent the position of the retaining walls. Furthermore, the structural elements corresponding to the location of the crucial elements of the analysed section were placed on the graphs. The rectangle located in the negative area of the x-axis represents the location of Rosenlundskanalen in the section while the rectangle located on the positive side of the x-axis symbolise the only building block which was considered in the model.

#### Short-term

Figure 7.9 presents the surface settlements obtained by using the SS model for the clay deposit. Likewise, Figure 7.10 presents the obtained settlements using the SSC model for the clay deposit.

As demonstrated, the settlements obtained with the SS model are maintained between 0 to 60 mm. Regarding the SSC, the settlements are above this level except for the cross-walls alternative. As evident for both the SS and the SSC models, the foundation alternative which seems to have the best behaviour for surface settlements is cross-walls.

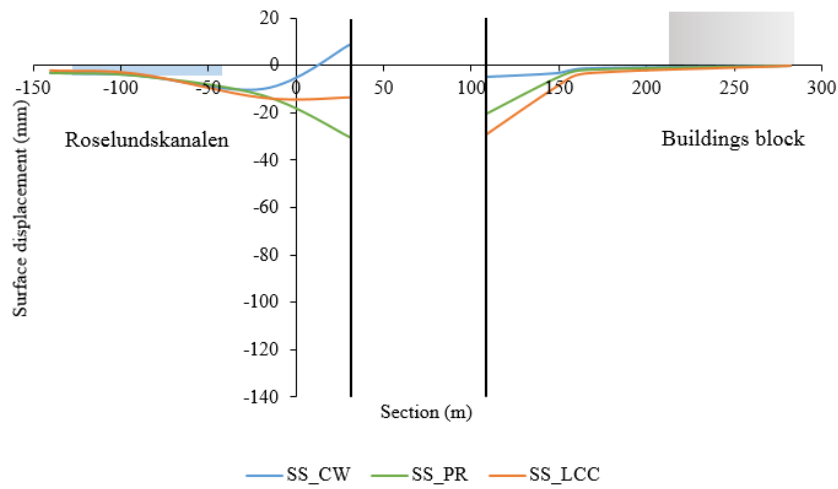


Figure 7.9: Surface settlements obtained with Soft Soil model for the short-term.

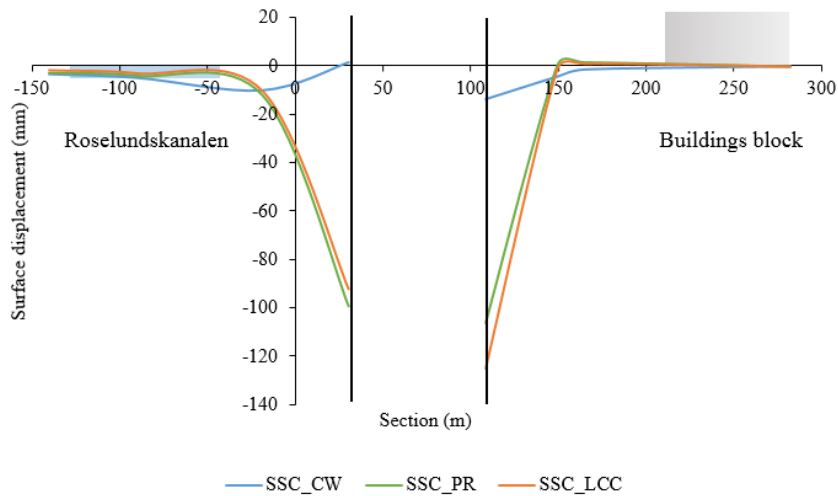


Figure 7.10: Surface settlements obtained with Soft Soil Creep model for the long-term.

### Long-Term

Figures 7.11 and 7.12 present the surface displacement behaviour for the long-term for respectively SS and SSC models. As demonstrated, the cross-walls alternative combined with foam glass is the option which gives the least surface settlements.

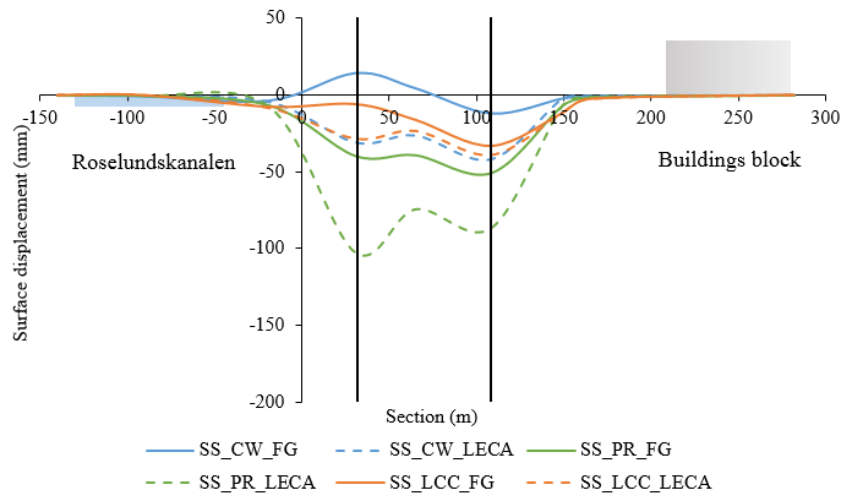


Figure 7.11: Surface settlements obtained with the Soft Soil model for the short-term.

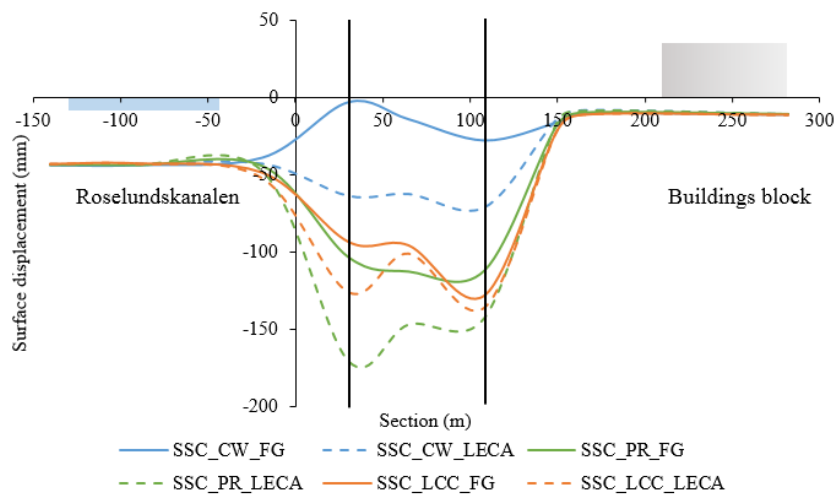


Figure 7.12: Surface settlements obtained with the Soft Soil Creep model for the long-term.

The difference in magnitude between the results from SS and SSC are less apparent in the long- than short-term. However, it is visible that by modelling the clay deposit with SSC, the displacements in the soil obtained for piled-raft and LCC are almost double than the SS results. For the cross-walls option, the magnitude of displacements with both models is almost the same, which could be due to the high stiffness of the modelled system.

## 7.2.2 Bottom heave

The analysis of the bottom heave was performed for both the short- and long-term for the different tested alternatives. Again, the comparison between the two fill materials was executed to analyse their impact on the displacements of the system in the long-term.

### Short-term

Figures 7.13 and 7.14 present the bottom heave behaviour for short-term for both the SS and the SSC models respectively.

As presented in Figure 7.13, the bottom heave for the analysed alternatives varies between 15 to 50 mm. On average, for the SS model, it is the piled-raft option that has the lowest heave and the cross-walls have the largest one. However, the cross-walls present a more even distribution along the section which could be more beneficial for the structure in the service state. For the SSC model, the displacements fluctuate in different areas, but still, the cross-walls alternative is the one which maintains a more linear distribution (see Figure 7.14).

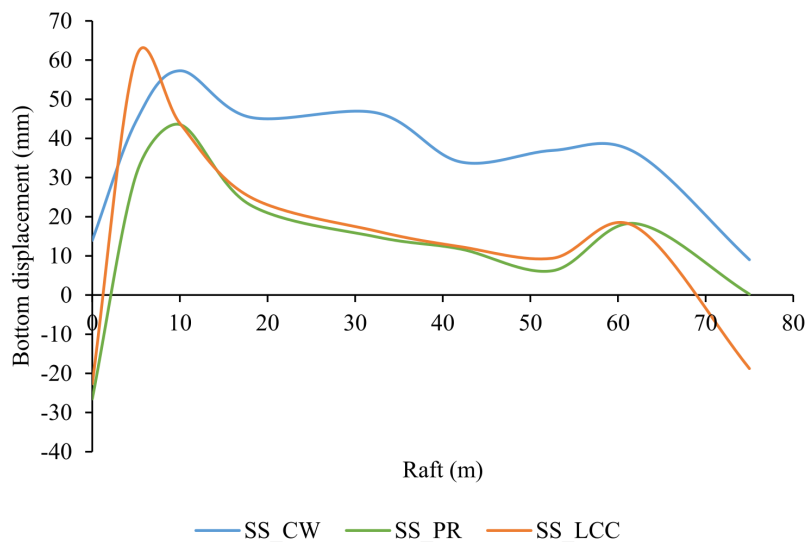


Figure 7.13: Bottom heave obtained with the Soft Soil model for the short-term.

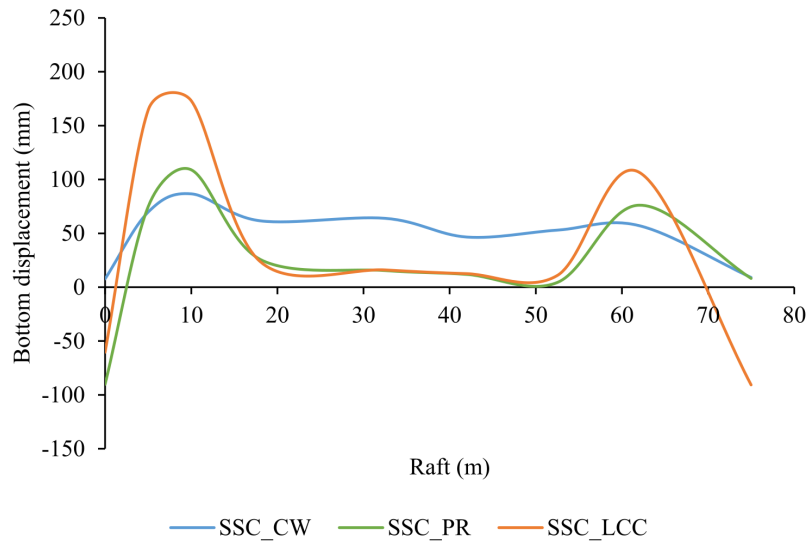


Figure 7.14: Bottom heave obtained with the Soft Soil Creep model for the short-term.

### Long-Term

For the long-term analysis of the bottom heave, the two fill materials are taken into consideration. Figure 7.15 shows the distribution obtained with the SS model. As demonstrated, all of the alternatives obtain the maximum values between 100 and 150 mm close to the central section of the raft. The results reached with foam glass for all the alternatives are lower than the ones obtained with LECA.

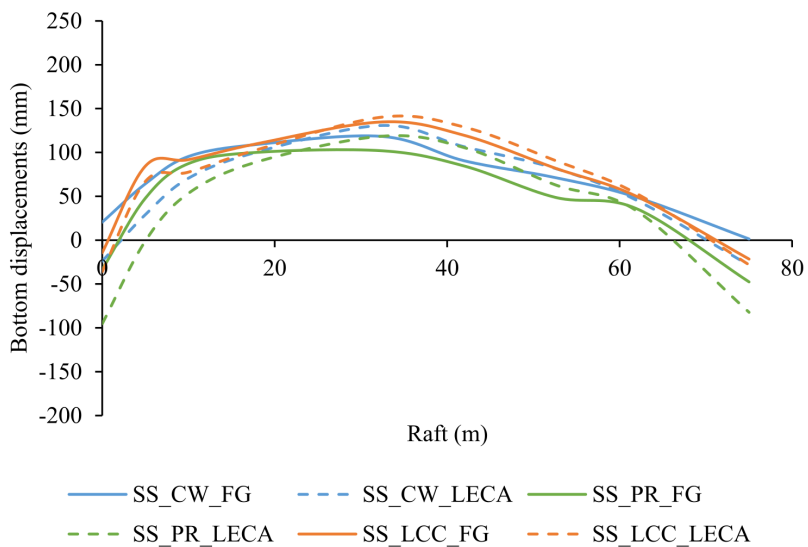


Figure 7.15: Bottom heave obtained with the Soft Soil model for the long-term.

With the SSC, the distribution of bottom heave is higher than the one obtained with the SS model. As pointed out in Figure 7.16, the maximum values are between 100 and 200 mm. Compared to the SS results, in the SSC model, the largest values are obtained mostly close to the retaining structures rather than in the centre of the raft. Additionally, the bottom heave achieved with the foam glass is still lower in almost all the raft area than the one obtained using LECA. With the SSC model, it is the cross-wall alternative that maintains a more constant bottom heave distribution.

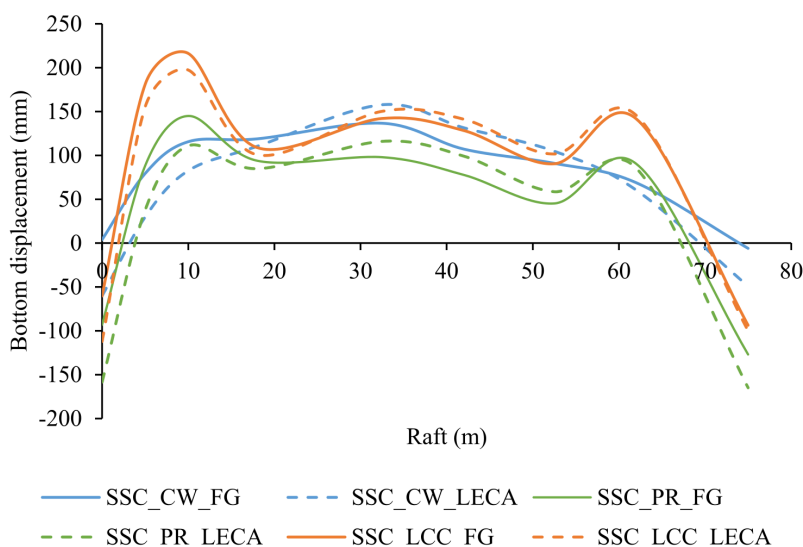


Figure 7.16: Bottom heave obtained with the Soft Soil Creep model for the long-term.

## 7.3 Retaining structures

In this section, the horizontal movement of the retaining structures were analysed, as the vertical movements were described in Sections 7.2.1 and 7.2.2. The analysis is divided into two parts for the left and right wall. A horizontal line was set on the level of the raft to have a reference point on the graphs where the results are presented.

### 7.3.1 Left wall

Figures 7.17 and 7.18 present the behaviour of the left wall in the short-term for both the the SS and the the SSC models respectively. The displacements obtained with the SSC are higher than the results from the SS model. This is true especially for piled raft and lime-cement columns. For the cross-walls, the displacements achieved with the two models are almost the same.

Figures 7.19 and 7.20 present the horizontal displacements of the left wall in the long-term. The generated displacements with both fill materials are similar. Nevertheless, results with LECA showed slightly lower displacements for all the alternatives in the area above the bottom of the excavation. Deformation of the wall follows an incremental distribution for all the alternatives to the level of the raft. At this level, the distribution starts to change. For the cross-walls, the displacements keep increasing in a lower scale due to the stiffness obtained from the foundation system. For the piled raft, the displacements start to increment at a higher rate due to the lack of additional support for the walls. Finally, for the lime-cement columns, in the SS model, the displacements get to a pick point below the base raft and then start to decrease. In the SSC model, the displacements for the LCC continue increasing at a high pace until reaching its maximum point at the foot of the wall.

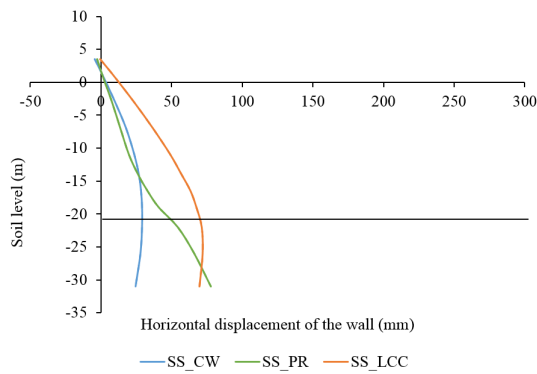


Figure 7.17: Horizontal displacements for left wall obtained with the SS model in the short-term.

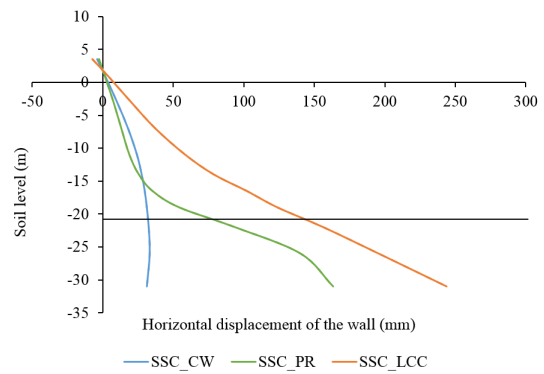


Figure 7.18: Horizontal displacements for left wall obtained with the SSC model in the short-term.

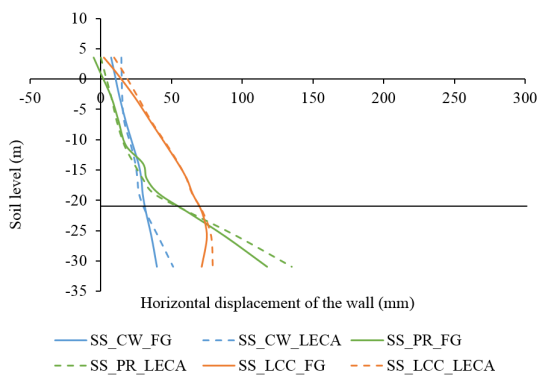


Figure 7.19: Horizontal displacements for left wall obtained with the SS model in the long-term.

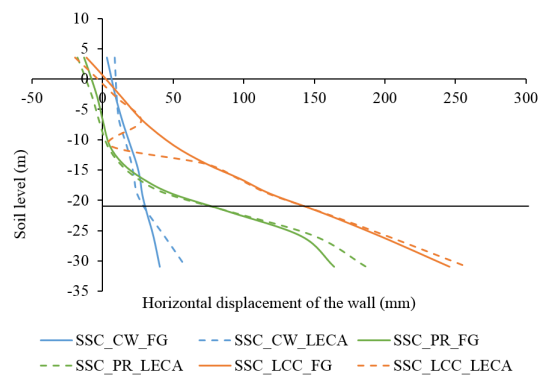


Figure 7.20: Horizontal displacements for left wall obtained with the SSC model in the long-term.

### 7.3.2 Right wall

Horizontal displacements of the right wall in the short-term are presented in Figure 7.21 and 7.22. The behaviour is very similar to the one obtained for the left wall, and the cross-walls alternative is still the one presenting the lowest displacements. With the SSC, the maximum displacement for piled raft is three times larger than the maximum obtained with the SS model. For lime-cement columns, this value is almost four times higher.

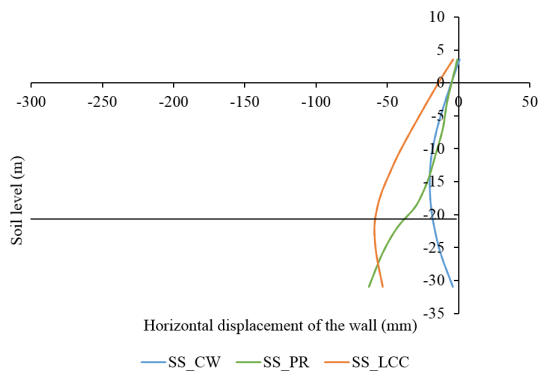


Figure 7.21: Horizontal displacements for right wall obtained with the SS model in the short-term.

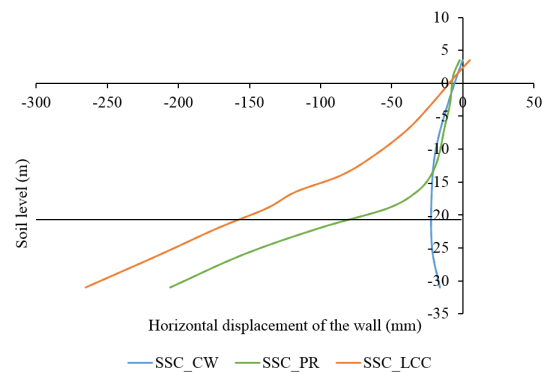


Figure 7.22: Horizontal displacements for right wall obtained with the SSC model in the short-term.

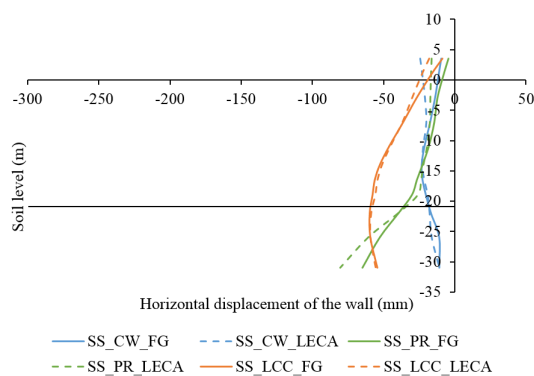


Figure 7.23: Horizontal displacements for right wall obtained with the SS model in long-term.

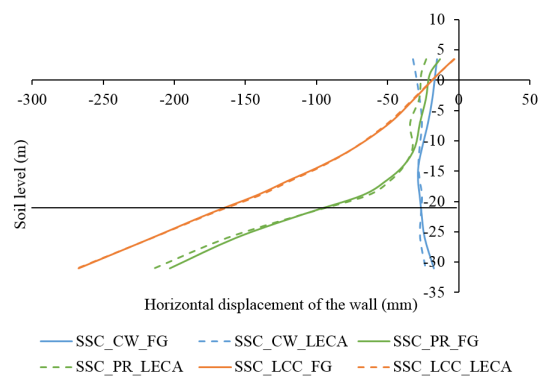


Figure 7.24: Horizontal displacements for right wall obtained with the SSC model in long-term.

The long-term behaviour is presented in Figures 7.23 and 7.23. The displacements obtained with the SS are lower than the ones obtained for the left wall. It is probable that the differences are caused due to the proximity of the bedrock which reduces the pore pressure at this side. The results obtained with the SSC follows a very similar distribution as the ones obtained for the left wall with the same model. This correlates with the graphs for the bottom heave where the large values close to the walls for Alternatives 2 and 3 can be found (see Figure 7.16). All of these indicate that the retaining walls are being pulled to the centre of the pit close to the raft.

## 7.4 Forces

Results of the forces acting on the structural elements are evaluated in this section. Firstly, a revision of the bending moments for both retaining walls is carried out. Secondly, results of the forces on the struts are presented in order to perform a validation of the model with the help of the empirical procedures introduced in Section 3.6.1.

### 7.4.1 Bending moment

Results from bending moments obtained with the SS model for both retaining walls are presented in Figures 7.25 and 7.26, the analysis was performed only for the long-term scenario. The graphs for bending moments resulting from short-term analysis can be seen in Appendix N. As demonstrated, the resulting moments for both walls have a similar distribution, but the values reached in the right wall are slightly lower than the ones on the left wall. These correlate well with the displacement results presented in Section 7.3.

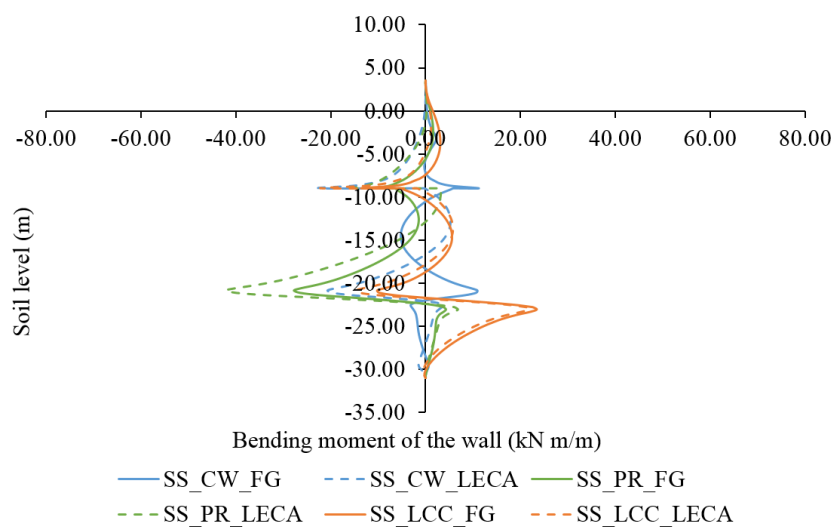


Figure 7.25: Bending moments on left wall obtained with SS model for the long-term.

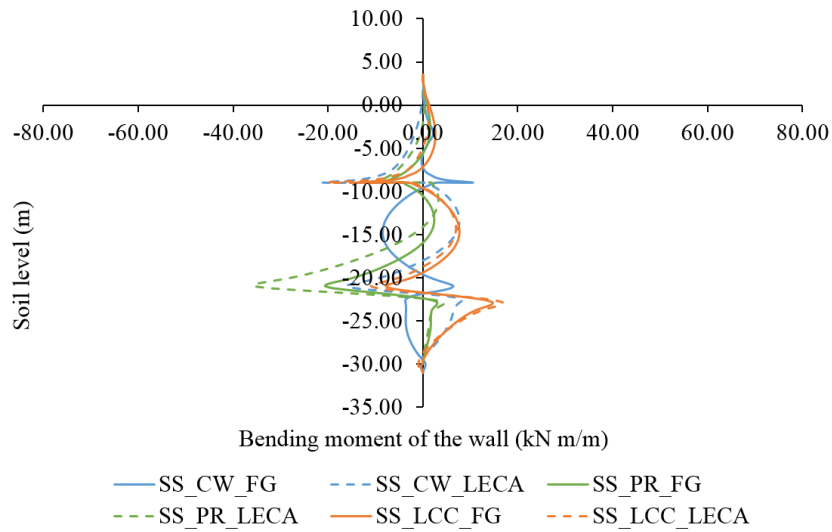


Figure 7.26: Bending moments on right wall obtained with SS model for the long-term.

Figures 7.27 and 7.28 show the values obtained with the SSC model. The magnitude of the bending moments is much higher in the SSC model compared to the SS model. For all the modelled scenarios, the areas where the larger moments are presented correspond to the location of the horizontal structures (raft and roof), and in the tunnel area.

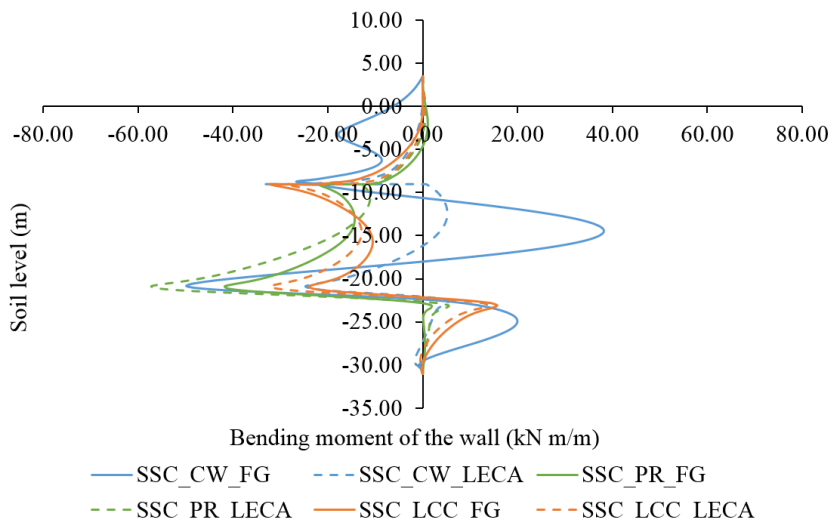


Figure 7.27: Bending moments on left wall obtained with SSC model for the long-term.

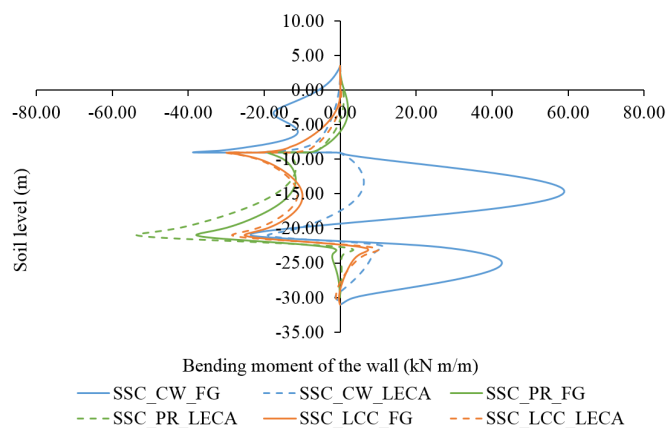


Figure 7.28: Bending moments on right wall obtained with SSC model for the long-term.

## 7.4.2 Strut forces

In Table 7.1, the resultant strut forces are presented. The first three columns refer to the strut loads for each modelled alternative calculated with PLAXIS 2D. The remaining two present the results for the two empirical models explained in Section 3.6.1 from Terzaghi and Peck (T. and P.) and Twine and Roscoe (T. and R.)

The values obtained from the FEM models were retrieved in the short-term behaviour in the stage where the whole excavation was completed and, thus, all the struts were activated. The empirical strut loads were calculated using the mentioned envelopes and the half method procedure (see Ou [116]).

Table 7.1: Strut loads calculated through FEM and empirical methods.

| Strut Force (kN/m) | CW-FEM      | PR-FEM      | LCC-FEM     | T. and P. | T. and R. |
|--------------------|-------------|-------------|-------------|-----------|-----------|
| Strut 1            | 1222        | 721         | <b>1476</b> | 940       | 1530      |
| Strut 2            | 1481        | <b>2298</b> | 1246        | 1012      | 716       |
| Strut 3            | 1494        | 1475        | <b>1724</b> | 1012      | 716       |
| Strut 4            | 1804        | 1197        | <b>2080</b> | 1012      | 716       |
| Strut 5            | 1925        | 1546        | <b>2463</b> | 795       | 563       |
| Strut 6            | 2118        | 1701        | <b>2709</b> | 723       | 511       |
| Strut 7            | <b>2652</b> | 831         | 1571        | 940       | 665       |

Table 7.1 suggests that strut loads from both empirical methods are mostly lower than the values predicted with the FEM models, except for the first strut where the load calculated with Twine and Roscoe envelope is larger than the values from the models. This might be caused by a limited number of parameters taken into account in the theoretical models. Both empirical models take only three parameters into account, which are the depth of excavation, friction angle or undrained shear strength and  $\gamma$ , they simplify the strut behaviour and highly under predict the forces.

## 7.5 Factor of safety

Safety analysis is performed in PLAXIS 2D by implementing an additional stage in the process with safety calculation. This is done with a  $\phi/c$  reduction which means that both the friction angle ( $\phi$ ) and the effective cohesion ( $c'$ ) are reduced in the model until failure is reached. The safety factor value from PLAXIS 2D is obtained as the result of dividing the available strength of the system with the strength at failure. In this way, if the value is more than 1 it means that the system is safe as the total strength of the reference model is enough to prevent failure.

Safety calculation was performed twice to check the safety factor for both short- and long-term conditions. Tables 7.2 and 7.3 presents the obtained values.

Table 7.2: Safety factor for modelled alternatives with Soft Soil model.

| Alternative | Short-term  | Long-term   |
|-------------|-------------|-------------|
| 1: FG       | 2.75        | 2.43        |
| 1: LECA     | 2.75        | 2.93        |
| 2: FG       | <b>2.95</b> | 2.08        |
| 2: LECA     | <b>2.95</b> | 2.28        |
| 3: FG       | 2.92        | 3.29        |
| 3: LECA     | 2.51        | <b>3.22</b> |

Table 7.3: Safety factor for modelled alternatives with Soft Soil Creep model.

| Alternative | Short-term  | Long-term   |
|-------------|-------------|-------------|
| 1: FG       | <b>3.29</b> | 2.60        |
| 1: LECA     | 3.28        | 3.08        |
| 2: FG       | 2.67        | 2.08        |
| 2: LECA     | 2.67        | 2.22        |
| 3: FG       | 2.42        | 2.71        |
| 3: LECA     | 2.55        | <b>3.48</b> |

It can be noticed that the available strength of the system for all the modelled alternatives is on the safe side. Higher factors of safety on the long-term condition are obtained when using LECA as fill material. For Alternatives 1 and 2 the higher safety factors are obtained during the short-term analysis while for Alternative 3 the higher values are reached during the long-term. This is due to the lack of foundation support in the short-term which leads to lower strength in the system.

## 7.6 Sensitivity analysis

As presented through the earlier parts of this thesis, the parameter which leads the design of the excavation is the deformation of the soil. Therefore, a sensitivity analysis was performed taking as a principal criterion the displacement in the areas which showed larger displacements. As presented in Section 7.1, the highest displacements of the soil are presented along the base of the excavation on the raft area. Therefore, the selected location for the sensitivity analysis was the central point between the two retaining walls at the level of the bottom of the excavation. This point was also selected as it represents a critical location for the behaviour of a thick raft as the one being modelled in PLAXIS.

The parameters selected for the sensitivity analysis were  $\kappa^*$ ,  $\mu^*$  and  $R_{inter}$ . The modified swelling index ( $\kappa^*$ ) was chosen first and foremost due to its importance in the calculations of an unloading problem such as excavation, but also because of the high uncertainty of its value as a result of poor soil investigation. The modified creep index ( $\mu^*$ ) was selected as it is the parameter of the highest importance in the creep deformations in the SSC model calculation. Here, similarly, poor quality soil investigation imposed a high uncertainty of the value and consequently reliability of the final results. Finally, the strength reduction factor ( $R_{inter}$ ) was chosen to evaluate its impact on the calculations of the soil deformation. The maximum and minimum values set for the sensitivity analysis were selected as the value of the parameter used in the model +/- 10 % respectively.

Table 7.4, presents the results obtained from the sensitivity analysis for the three alternatives. The sensitivity for each parameter is presented in percentage which represents how much the parameter affects the results for displacements in comparison to the other analysed parameters. In this way, the parameter with the sensitivity closest to 100 would be the most sensitive for the overall results from the model.

Table 7.4: Sensitivity values in % separated by the different alternatives modelled in PLAXIS 2D. The higher the value, the more sensitive the parameter is.

| Parameter                 | Symbol      | Alternative 1 | Alternative 2 | Alternative 3 |
|---------------------------|-------------|---------------|---------------|---------------|
| Modified swelling index   | $\kappa^*$  | <b>59</b>     | <b>88</b>     | <b>81</b>     |
| Modified creep index      | $\mu^*$     | 30            | 4             | 11            |
| Strength reduction factor | $R_{inter}$ | 11            | 8             | 8             |

During the analysis, the layer which had the higher values of sensitivity corresponds to Layer 5 which is located below the bottom of the excavation. As seen from Table 7.4, the parameter which has the highest influence over the calculation of the soil displacements is the modified swelling index, which correlates less with the unloading nature of the problem.

## 7.7 Sustainability assessment

Calculation of the total amount of embodied carbon for the three considered alternatives is evaluated in this section. The three materials considered for the assessment are concrete, steel and cement. Given that the primary retaining system is practically the same for the three options, these elements were not taken into consideration. Therefore, the analysis focuses on the materials employed for the construction of the foundation structures. As a simplification, the reinforcement for the concrete elements is not taken into account as the structural design is not the objective of this thesis.

Table 7.5 presents the values obtained for the considered alternatives. For Alternative 1, the elements taken into consideration were the cross-walls and the base raft. For Alternative 2, both concrete and steel piles were considered as well as the raft and the anchors of the piles. Finally, for Alternative 3, the elements used in the calculation were the volume of the lime-cement columns and the raft.

Table 7.5: Embodied carbon calculated for the three modelled alternatives.

| Alternative\Embodied carbon<br>(ton CO <sub>2</sub> /kg) | Concrete | Steel | Cement | Total        |
|--|----------|-------|--------|--------------|
| Alternative 1  | 17172    | 0     | 0      | 17172        |
| Alternative 2  | 11655    | 3.65  | 0      | <b>11659</b> |
| Alternative 3  | 11448    | 0     | 15330  | 26778        |

Large values of embedded CO<sub>2</sub> are obtained with Alternative 3. This is caused mainly by the high quantities of cement needed for the construction of a thick raft and columns as significant amount of energy is used during its production generating almost 1 kg of CO<sub>2</sub> per kg of produced cement.

## 7.8 General discussion for results obtained with PLAXIS 2D

A concise summary of the principal results is presented in Tables 7.6 and 7.7. Based on these, it can be summarised that Alternative 1 seems to perform the best in various categories. It is also visible that foam glass behaviour is the closest to desired for the fill material. This might be caused by the main feature of the fill as the lack of water presence of the closed foam glass voids.

In the short-term analysis, it is Alternative 1 that delivers on the set parameters, but in the long-term analysis its behaviour is changing and Alternative 2 seems to be reacting better. This is claimed to be caused by the presence of end bearing piles that helps to limit the structure settlements in the long-term. The same piles act in tension during short-term analysis and do not provide such support as the stiff

cross-walls. Similarly, cross-walls in the long-term do not provide support for the settlement but only for the differential movements as they are not embedded in the stiff strata.

Table 7.6: Comparison of the main parameters for Soft Soil model.

| Alternative                | Total settlements<br>$ u $ | Surface settlements | Maximum bottom heave | Maximum bending moment<br>(left wall) | Maximum bending moment<br>(right wall) |
|----------------------------|----------------------------|---------------------|----------------------|---------------------------------------|--|
|                            | m                          | mm                  | mm                   | kNm/m                                 | kNm/m                                  |
| <b>Short-term analysis</b> |                            |                     |                      |                                       |  |
| 1: FG                      | <b>0.0855</b>              | <b>-9.85</b>        | 57.27                | -4.23                                 | <b>-4.27</b>                           |
| 1: LECA                    |                            |                     |                      | <b>4.23</b>                           | <b>4.27</b>                            |
| 2: FG                      | 0.0997                     | -30.22              | <b>43.57</b>         | -7.32                                 | -9.77                                  |
| 2: LECA                    |                            |                     |                      | -7.58                                 | -9.99                                  |
| 3: FG                      | 0.1094                     | -29.35              | 60.73                | 7.64                                  | 7.99                                   |
| 3: LECA                    |                            |                     |                      | 7.62                                  | 7.96                                   |
| <b>Long-term analysis</b>  |                            |                     |                      |                                       |  |
| 1: FG                      | 0.1537                     | <b>14.36</b>        | 118.25               | <b>11.24</b>                          | <b>10.51</b>                           |
| 1: LECA                    | 0.1912                     | -42.08              | 130.76               | -22.29                                | -20.57                                 |
| 2: FG                      | <b>0.1323</b>              | -51.18              | <b>101.96</b>        | -27.78                                | -20.67                                 |
| 2: LECA                    | 0.1719                     | -102.58             | 118.62               | -42.01                                | -35.63                                 |
| 3: FG                      | 0.1397                     | -32.86              | 134.82               | 23.41                                 | 14.72                                  |
| 3: LECA                    | 0.1449                     | -39.42              | 140.37               | -22.02                                | -20.06                                 |

**Note:** In the short-term analysis, the total settlements, surface settlements and the maximum bottom heave are independent from the fill material as in Phase 11 it is still not in place.

From both soil models, the maximum bottom heave in the long-term analysis has been estimated to be 197.39 mm. This value can be managed by the proposed CORDEK plate installation below the raft. As the heave seems to be more problematic in service state, it is advised to validate the 2D analysis with a 3D model to provide a better understanding of the foundation behaviour.

Table 7.7: Comparison of the main parameters for Soft Soil Creep model.

| Alternative                | Total settlements<br>$ u $ | Surface settlements | Maximum bottom heave | Maximum bending moment<br>(left wall) | Maximum bending moment<br>(right wall) |
|----------------------------|----------------------------|---------------------|----------------------|---------------------------------------|--|
|                            | m                          | mm                  | mm                   | kNm/m                                 | kNm/m                                  |
| <b>Short-term analysis</b> |                            |                     |                      |                                       |  |
| 1: FG                      | <b>0.1533</b>              | <b>-13.81</b>       | <b>86.67</b>         | 35.87                                 | 38.65                                  |
| 1: LECA                    |                            |                     |                      | -24.71                                | <b>-20.36</b>                          |
| 2: FG                      | 0.2488                     | -106.36             | 109.05               | -38.85                                | -36.58                                 |
| 2: LECA                    |                            |                     |                      | -38.22                                | -38.10                                 |
| 3: FG                      | 0.2954                     | -124.94             | 173.06               | <b>-18.66</b>                         | -21.80                                 |
| 3: LECA                    |                            |                     |                      | -21.28                                | -20.75                                 |
| <b>Long-term analysis</b>  |                            |                     |                      |                                       |  |
| 1: FG                      | <b>0.1640</b>              | <b>-44.32</b>       | <b>136.72</b>        | -49.81                                | 58.91                                  |
| 1: LECA                    | 0.2028                     | -71.55              | 157.83               | -24.71                                | <b>-20.36</b>                          |
| 2: FG                      | 0.2490                     | -112.68             | 145.01               | -41.69                                | -37.84                                 |
| 2: LECA                    | 0.2876                     | -170.56             | -164.86              | -57.24                                | -53.69                                 |
| 3: FG                      | 0.3347                     | -128.43             | 181.14               | <b>-22.25</b>                         | -29.28                                 |
| 3: LECA                    | 0.3129                     | -135.80             | 197.39               | -32.15                                | -29.61                                 |

**Note:** In the short-term analysis, the total settlements, surface settlements and the maximum bottom heave are independent from the fill material as in Phase 11 it is still not in place.

As seen in both Tables 7.6 and 7.7, the maximum displacement value set for the project of 100 mm is surpassed in the long-term condition for the vertical direction in all the modelled alternatives. Improvements of the performed models can be achieved by implementing the CORDEK plate into the FEM calculation to check if the material can achieve a decrease of the obtained displacements below the allowable values.

The available input parameters were sufficient to set up a model using more advanced soil parameters. It is especially appreciated to have a step-wise oedometer test that allows extraction of parameters necessary to creep analysis with SSC model.

Unfortunately, the quality of the soil investigation seems to be disturbing the final outcomes. Due to lack of similar tests within the same boreholes, it is difficult to cross-validate the obtained parameters. More data would allow the sensitivity analysis to be refined and ensure the transparency of the results. Lastly, the additional tests of the bedrock quality would enable the prediction of its behaviour more ade-

quately, especially allowing the checking of the interface value between concrete and bedrock and validate the lack of fracture zones in the section.

As mentioned previously, it is predicted that the quality of soil investigation disturbed the final results. This was especially visible for the derivation of  $\kappa^*$  value as revealed during the sensitivity study. This is most likely caused by the fact that only one step-wise oedometer test has been performed in the borehole where no tri-axial test was done. Consequently, there was no possibility to validate the  $\kappa^*$  value. Similarly, the lack of numerical value of the test results, but merely reading the parameters from the available graphs, is claimed to be the major disturbance factor. The presence of i.e. Excel sheets would significantly increase reliability of the design.

Availability of z-coordinates of the existing boreholes would allow the validation of the geometry of the model. The uncertainties related to the external loads may be diminished by the close study of the available information about surrounding structures. Based on this, a more precise value may be incorporated in the model.

As noticed during the analysis, the presence of the water canal does not disturb the results. It is claimed that the size of the model might be shrunk both in the vertical and horizontal direction in order to improve the efficiency of the calculations. As the size of the mesh elements is dependent of the total size of the model, a more refined average size of elements could be achieved which might possibly contribute to capturing subtle changes in the soil behaviour.

Similarly, the practical knowledge of the construction sequence has been appreciated during the model set up. No negative influence has been noticed based on the construction sequence and presence of the soil-structure interfaces. The previous work experience allowed modelling of the construction sequence in a more reasonable and realistic way. Moreover, the need for monitoring has been recognised and it is advised to provide data from inclinometers and walls and surrounding buildings' target points to ensure the safety of the construction and validate the model [120].

Lastly, relatively high factors of safety for the long-term analysis have been achieved. This might indicate a conservative design in the service state. Thus, it would be beneficial to consider performing underwater excavation to reduce short-term settlements and optimise the safety factor in the long-term. One must remember that this is the stability of the whole system that drives the excavation design and the safety of the design must be achieved, even at the cost of more conservative design in the service state.



# 8

## Conclusions and recommendations

The above research proves that the numerical analysis in geotechnical engineering can provide valuable information for the design of deep excavations. Nevertheless, programmes like PLAXIS are just tools in engineers' hands and must be employed with care. It is of great importance to ensure engineers' understanding of the problem prior to commencing the numerical analysis as it affects the way the problem is handled and disturbs the final output that is highly dependant on the user expertise.

This thesis presents three feasible solutions for the foundation design of the deep excavation in soft clay. Although different parameters were analysed, the most important are the displacements in the soil due to the setting of the station in the urban environment and possible negative impact on the surrounding. Despite obtaining large values in all models, it is the cross-walls alternative that provides the lowest differential displacements. Their values in short- and long-term are claimed to be manageable by means of heave reduction solutions. It has been provide that the retrieved results are compromised due to the poor soil investigation and, therefore, diversified concepts are recommended to refine the design.

### 8.1 Recommendations

It is recommended to carefully review the proposed station design and its effect on the surrounding structures; especially, the ground movements around Hagakyrgan and the effect of pile shortening of Resenlundsbron and Rosenlundskanalen foundation structures. If the last two are to be supported on the top of the tunnel in the long-term scenario, this must be taken into account when analysing the refined numerical model.

Based on Eurocode 7, it is advised to employ observational methods and provide additional monitoring data to validate, and possibly refine, the design along the construction process. Consequently, it is advised to monitor:

- the construction of the excavation to ensure health and safety standards, but also to look for possible design improvements in i.e. propping system to advise the contractor on elimination/addition of propping levels.
- neighbouring buildings to safeguard that the surrounding settlements are within the acceptable limits and do not impose additional risk to the existing structures. This should be done by controlling the level of target points and ensuring

that previously agreed trigger levels are not exceeded.

- lateral movements in diaphragm walls. The movement of the top of the wall can be assessed based on data collected from inclinometers which are advised to be installed during construction. The retaining wall should be monitored based on the target points set between propping levels and validated against the trigger levels previously agreed with the adequate authorities.

Bearing in mind high factors of safety reached in the long-term analysis, it is recommended to investigate the effect of the underwater excavation on the final results in order to deliver more optimised design. It seems to be reasonable to allow for the last few meters of the excavation to be performed under water in order to stabilise the pit when the foundation structure is still not in place. Once constructed, water can be pumped out and construction can proceed with anticipated thinner raft and lower number of strut supporting levels.

In order to improve the carbon footprint of the structure, the use of piled-raft and cross-walls should be considered as the alternatives with the significantly lower embodied energy. Additionally, structural engineers should analyse employing PFA or FBA as a cement replacement, recycled aggregate for concrete mix and locally sourced lightweight fill material to provide further improvements. High care should be paid to temporary work design so the maximum percentage of temporary structures can be dismantled and reused. Finally, it is advised to source all materials locally to minimise the transportation emissions.

### 8.1.1 Further investigation

This thesis proves the importance of high-quality soil investigation as a primary way of ensuring a reliable modelling output. Without precise soil investigation, even the most sophisticated numerical model is not going to predict the soil and structure behaviour appropriately.

Thus, it is recommended to extend the soil investigation scope and provide additional data based on:

- drained triaxial tests for result comparison with other conceptual models
- further oedometer tests executed in different boreholes along the area to enable the sensitivity analysis of obtained parameters
- sampling of bedrock to accurately determine its strength parameters
- creation of groundwater fluctuation maps to gain a better understanding of the groundwater flow and its impact on the proposed structure.

All of the above improvements would facilitate setting up a 3D numerical model. In this way, a more appropriate definition of 3D elements as LCC and cross-walls can be achieved to capture the behaviour of the soil and structural elements closest to reality.

# Bibliography

- [1] G. Shuvrajit (2014) *Nicoll Highway - Subway Tunnel Collapse* [Online]. Available: <https://goo.gl/EBah48>, accessed: 02.02.2017. The Pennsylvania State University.
- [2] SWECO Civil AB Geoteknik (2015) Västlänken, *Station Haga - Geoteknisk utredning för detaljplan*. Published: 29.08.2014, revision A: 30.09.2015, Stockholm, Sweden.
- [3] Göteborgs Stad, Planhandling (2016) *Detaljplan för Västlänken, station Haga med omgivning inom stadsdelarna Haga, Inom Vallgraven, Pustervik samt Vasastaden i Göteborg. Normalt planförfarande*. Published: 06.2016, Gothenburg, Sweden.
- [4] Göteborgs stadsmuseum (n.d.) *Göteborgs stadsmuseum* [Online]. Available: <https://goo.gl/O2cyzo>, accessed: 11.05.2017.
- [5] OpenStreetMap contributors (n.d.) *Detailed map of Hagakyrkan area* [Online]. Available: <https://osm.org/go/0YSAVxydk->, accessed: 05.03.2017.
- [6] Göteborgs Stadsbyggnadskontors Archive (1790) *Kartor från Jubileumsutställningen 1923* [Online]. Available: <https://goo.gl/qRzJy0>, accessed: 16.02.2017.
- [7] Göteborgs Stadsbyggnadskontors Archive (1860) *Kartor från Jubileumsutställningen 1923* [Online]. Available: <https://goo.gl/qRzJy0>, accessed: 16.02.2017.
- [8] Göteborgs Stadsbyggnadskontors Archive (1872) *Historiska kartor* [Online]. Available: <https://goo.gl/8imBBp>, accessed: 16.02.2017.
- [9] Göteborgs Stadsbyggnadskontors Archive (1921) *Kartor från Jubileumsutställningen 1923* [Online]. Available: <https://goo.gl/qRzJy0>, accessed: 16.02.2017.
- [10] Göteborgs Stadsbyggnadskontors Archive (n.d.) *Kajbyggnad vid Rosenlunds Kanalen*. No exact date included, but similar drawings were made in the period between 1860 and 1870. Information requested in person from the archive: 27.02.2017; Gothenburg, Sweden.
- [11] Göteborgs Stad, Trafikkontoret (1999) *Relationshandling*. Produced for Göteborgs Stad by PKAB Enterprenad Byggproduktion o. Konsult Göteborg AB. Published: 02.09.2016, Gothenburg, Sweden.
- [12] Trafikverket (2016) *Ansökan om tillstånd enligt miljöbalken. Västlänken och Olskroken planskildhet. Göteborgs Stad och Mölndals stad, Västra Götalands län, PM Geoteknik Sättningar, TRV 2016/3151*. Published: 15.01.2016, Gothenburg, Sweden.
- [13] Geological Survey of Sweden (SGU) (n.d.) *Quaternary deposits 1:25,000 - 1:100,000* [Online]. Map automatically generated from SGU's database on 02.02.2017.

- [14] Geological Survey of Sweden (n.d.) (2017) *Depth to bedrock 1:50,000* [Online]. Map automatically generated from SGU's database on 02.02.2017.
- [15] Geological Survey of Sweden (n.d.) (2017) *Bedrock map 1:50,000* [Online]. Map automatically generated from SGU's database on 02.02.2017.
- [16] Geological Survey of Sweden (n.d.) (2017) *Groundwater reservoir J1: Groundwater reservoir in soil layer, scale 1:50,000* [Online]. Map automatically generated from SGU's database on 02.02.2017.
- [17] Trafikverket (2016) *PM Inventering grundvattenberoende grundläggning* [Online]. Available: <https://goo.gl/r2JIUS>, published: 10.02.2016.
- [18] United Nations (n.d.) *Sustainable goals. Goal 7: Environmental Sustainability* [Online]. Available: <https://goo.gl/mVJdAu>, accessed: 13.05.2017.
- [19] Concrete Centre (2006) *Sustainable Solutions using Concrete* [Online and print]. Available: <https://goo.gl/XlyYDq>, accessed: 13.05.2017.
- [20] K. Terzaghi (1943) *Theoretical Soil Mechanics*, John Wiley and Sons, New York.
- [21] K. Terzaghi and R. B. Peck (1967) *Soil Mechanics in Engineering Practice*, 2<sup>nd</sup> ed., John Wiley and Sons, New York.
- [22] R. B. Peck et al. (1977) *Foundation Engineering*, John Wiley Sons, New York.
- [23] *Trenching practice*, Construction Industry Research and Information Association, Report 97, 1992.
- [24] Health and Safety Executive (n.d.) *Health and safety statistics* [Online]. Available: <https://goo.gl/9j4Xd5>, accessed: 30.04.2017.
- [25] M. Puller (2006) *Deep Excavations: a practical manual*, 2<sup>nd</sup> ed., London, the UK, Thomas Telford.
- [26] H. Kempfert and B. Gebreselassie (2006) *Excavations and Foundations in Soft Soils*, 1<sup>st</sup> ed., Berlin, Springer-Verlag.
- [27] Deutsche Gesellschaft für Geotechnik e.V. (1994) *Empfehlungen des Arbeitskreis „Baugruben“ der Deutschen Gesellschaft für Geotechnik*, 3<sup>rd</sup> ed., Berlin, Ernst & Sohn.
- [28] A. M. Puzrin et al. (2010) *Geomechanics of Failures*, 1<sup>st</sup> ed., Springer Netherlands.
- [29] H. F. Schweiger (2002) *Benchmarking in geotechnics. Part 1 and 2. Report no. CGG IR006 2002*, Computational Geotechnical Group, Institute for Soil Mechanics and Foundation Engineering, Graz University of Technology, Graz, Austria.
- [30] J.A. Knappett and R.F. Craig (2012) *Craig's Soil Mechanics*, 8<sup>th</sup> ed., London, the UK, Spon Press.
- [31] D. M. Wood (1990) *Soil behaviour and critical state soil mechanics*, Cambridge, the UK, Cambridge Univ. Press.
- [32] A. Casagrande (1936) *Determination of the preconsolidation load and its practical significance* in *Proceedings of the International Conference on SMFE*, Harvard University, Cambridge, vol. 3, pp. 60-64.
- [33] F. Havel (2004) *Creep in soft soils*, PhD thesis, Department of Civil and Transport Engineering, Norwegian University of Science and Technology, Trondheim, Norway. Available: <https://goo.gl/QTYFA9>.

- [34] M. Olsson (2010) *Calculating long-term settlement in soft clays - with special focus on the Gothenburg region* Chalmers University of Technology, Division of GeoEngineering, Gothenburg, Sweden.
- [35] PLAXIS (2016) *PLAXIS Undrained Soil Behaviour in PLAXIS* [Paper]. PowerPoint presentation obtained during the PLAXIS official training, February 2017, London, the UK.
- [36] Rocscience (n.d.) *Description of Cam-Clay and Modified Cam-Clay critical state strength models* [Online]. Available: <https://goo.gl/RhXRdE>, accessed: 14.03.2017.
- [37] J. Jaky (1948) *Earth pressure in silos* in *Proceedings of the 14<sup>th</sup> International Conference on Soil Mechanics and Foundation Engineering*, vol. 1, pp. 103-107, London, England.
- [38] E. Hoek and E. T. Brown (1980a) *Underground excavations in rock*, London, the UK, Institute of Materials, Minerals & Mining.
- [39] E. Hoek and E. T. Brown (1980b) *Empirical strength criterion for rock masses* in *Journal of Geotechnical and Geoenvironmental Engineering Division ASCE*, vol. 106(GT9), pp. 1013-1035. Available: <https://goo.gl/Qey03J>.
- [40] E. Hoek et al. (2002) *Hoek-Brown failure criterion* in *Mining and tunnelling innovation and opportunity: proceedings of the 5<sup>th</sup> North American Rock Mechanics Symposium and the 17<sup>th</sup> Tunnelling Association of Canada Conference*, Toronto, Ontario, Canada, pp. 267-73.
- [41] E. Hoek (1999) *Putting numbers to geology - an engineer's viewpoint* in *Quarterly Journal of Engineering Geology*, vol. 32(1), pp. 1-9. Available: <https://goo.gl/eE1S2W>.
- [42] E. Hoek (2006) *Practical Rock Engineering* [Online]. Available: <https://goo.gl/A9Sm2g>, accessed: 13.02.2017.
- [43] PLAXIS (2017) *PLAXIS Reference manual* [Online]. Available: <https://goo.gl/2MGUvq>.
- [44] D. M. Wood (2004) *Geotechnical modelling*, London, the UK, Routledge.
- [45] PLAXIS (n.d.) *PLAXIS Material models manual* [Online]. Available: <https://goo.gl/93WRwO>.
- [46] COST C7 (2002) *Guidelines for the use of advanced numerical analysis*, London, the UK, Thomas Telford Publishing.
- [47] D. M. Potts and L. Zdravkovic (1999) *Finite element analysis in geotechnical engineering: [Vol. 1] : Theory*, London, the UK, Thomas Telford.
- [48] D. M. Potts and L. Zdravkovic (2001) *Finite element analysis in geotechnical engineering: [Vol. 2] : Application*, London, the UK, Thomas Telford.
- [49] D. Twine and H. Roscoe (1999) *Prop loads: guidance on design*, London, the UK, CIRIA.
- [50] R. Sarsby (2000) *Environmental Geotechnics*, London, the UK, Thomas Telford.
- [51] G. Barnes (2016) *Soil Mechanics. Principles and practice*, 4<sup>th</sup> ed., London, the UK, Palgrave Macmillan.
- [52] Göteborgs Stadsbyggnadskontors Archive (1899) *Pejlingssektioner i Fat-tighusån, Rosenlundskanalen och Vallgrafven*. Requested in person from the archive: 27.02.2017; Gothenburg, Sweden.

- [53] C. Souder (2015) *Temporary structure design*, New Jersey, John Wiley & Sons, Inc.
- [54] J. B. Burland et al. (2004) *Design and construction of deep basements including cut-and-cover structures*, London, the UK, the Institution of Structural Engineers.
- [55] *Code of practice for earth retaining structures*, British Standard Institution BS8002, 1994.
- [56] R. B. Peck (1969) *Deep excavations and tunneling in soft ground* in *Proceedings of 7<sup>th</sup> International Conference of Soil Mechanics & Foundation Engineering*, pp. 225-290, Mexico.
- [57] Balfour Beatty UK (n.d.) *King post walls* [Online]. Available: <https://goo.gl/cHegug>, accessed: 02.04.2017.
- [58] Balfour Beatty UK (n.d.) *Retaining walls* [Online]. Available: <https://goo.gl/F9VyiQ>, accessed: 02.04.2017.
- [59] Balfour Beatty UK (n.d.) *Diaphragm walls* [Online]. Available: <https://goo.gl/VFAZnU>, accessed: 02.04.2017.
- [60] W. G. K. Fleming et al. (1985) *Piling engineering*. Glasgow and John Wiley, New York, Surrey University Press.
- [61] J. A. Hemsley (2000) *Design application of raft foundations*, London, the UK, Thomas Telford.
- [62] K. Karlsrud et al. (2006) *Diaphragm walls with cross-walls used to prevent bottom heave in soft clay for lot 2 of Lilla Bommen tunnel in Gothenburg* in *Proceedings of 5<sup>th</sup> International Symposium TC28*, pp. 835-844, Amsterdam, the Netherlands.
- [63] S. Rampello and S. Salvatori (2012) *3D finite element analysis of deep excavations with cross-walls* in *Geotechnical aspects of underground construction in Soft Ground*, pp. 505-513, London, the UK, Taylor and Francis Group.
- [64] B. C. B. Hsiung et al. (2001) *The Effectiveness of Jet-Grout Slabs and Cross-walls in Restricting Wall Movements in Deep Excavations* in *Proceedings 14<sup>th</sup> Southeast Asia Geotechnical Engineering Conference*, vol. 1, pp. 339-355, Hong Kong, China. Available: <https://goo.gl/dmsSsU>.
- [65] H. S. Hsieh et al. (2008) *Effects of joint details on the behaviour of cross walls* in *Journal of Geo Engineering*, vol.3 (2), pp. 55-60.
- [66] C. Y. Ou et al. (2011) *Performance of excavations with cross walls* in *Journal of Geotechnical and Geoenvironmental Engineering*, vol. 137(1), pp. 94-104.
- [67] S. H. Wu et al. (2014) *Probabilistic observational method for estimating wall displacements in excavations* in *Canadian Geotechnical Journal*, vol. 51(10) pp. 1111-1122.
- [68] S. H. Wu et al. (2013) *Predicting wall displacements for excavations with cross walls in soft clay* in *Journal of Geotechnical and Geoenvironmental Engineering*, vol. 139(6), pp. 914-927.
- [69] S. J. Abbey et al. (2015) *Understanding the performance of deep mixed column improved soils - A review* in *International Journal of Civil Engineering and Technology*, vol. 6(3), pp. 97-117.
- [70] M. Kitazume and M. Terashi (2013) *Deep mixing method*, the Netherlands, CRC Press/Balkema Publishers.

- [71] M. Terashi and M. Kitasume (2009) *Current practice and future perspective of quality assurance and quality control for deep mixed ground*, in *International Symposium on Deep Mixing and Admixture Stabilization*, pp. 61-99.
- [72] H. Krenn and U. Vogler (n.d.) *Numerical Modelling of Deep Mixed Columns*, PowerPoint Presentation, University of Strathclyde. Available: <http://www.strath.ac.uk>, accessed: 03.05.2017.
- [73] Hayward Baker Inc. (Keller Company) (n.d.) *Jet Grouting* [Online]. Available: <https://goo.gl/2ILDY4>, accessed: 15.04.2017.
- [74] H.-J. Köhler et al. (1999) *Soil and structure deformations due to reconstruction of an old lock built on unsaturated submerged clay* in R. Jamiolkowski et al. (editor) *Pre-failure Deformation Characteristics of Geomaterials - Proceedings of the 2<sup>nd</sup> International Symposium on Pre-failure Deformation Characteristics of Geomaterials*, Torino, Italy, vol. 1, pp. 793-800, Rotterdam, Balkema.
- [75] K. Karlsrud and L. Andresen (2008) *Design and Performance of Deep Excavations in Soft Clays*. Sixth International Conference on Case Histories in Geotechnical Engineering, Missouri University of Science and Technology.
- [76] D. Denman et al. (1987) *Marina Bay station and tunnels. Deep cut and cover construction in soft marina clay* in *Proceedings of the Singapore Mass Rapid Transit Conference*, April 1987.
- [77] J. N. Shirlaw et al. (2009) *Deep Excavations in Singapore marina clay* in *Proceedings of 5<sup>th</sup> International Symposium Geotechnical Aspects of Underground Construction in Soft Ground*, Amsterdam, the Netherlands.
- [78] S. J. Boone and A. M. Crawford (2000) *Braced Excavations: Temperature, Elastic Modulus, and Strut Loads* in *ASCE Journal of Geotechnical and Environmental Engineering*, vol. 126(10), pp. 870-881.
- [79] W. Powrie and M. Batten (2000) *Comparison of measured and calculated temporary-prop loads at Canada Water Station* in *Géotechnique*, vol. 50(2), pp. 127-140.
- [80] Department for Communities and Local Government, the United Kingdom (1996) *Party Wall etc. Act 1996*, London, the UK.
- [81] N. Collins (2011) *Support and sealing at the toe of a retaining wall extending to bedrock: theory and practice*, MSc. thesis, Yhdyskunta- ja ympäristötekniikan laitos, Aalto -yliopisto Insinööritieteiden korkeakoulu, Helsinki, Finland. Available: <https://goo.gl/aP1yEj>.
- [82] *Rakennuskaivanto-ohje RIL 181-1989*, Suomen Rakennusinsinöörin Liitto, 1989.
- [83] ROADEX Network (2014) *ROADEX e-learning platform* [Online]. Available: <http://www.roadex.org/elearning/>, accessed: 08.04.2017.
- [84] Y. Min (2002) *Study on reducing-settlement pile foundation based on controlling settlement principle* in *Chinese Journal of Geotechnical Engineering*, vol. 22(4), pp. 481-486.
- [85] B. El-Garhy et al. (2012) *Behavior of raft on settlement reducing piles: Experimental model study* in *Journal of Rock Mechanics and Geotechnical Engineering*, vol. 5(5), pp. 389-399.

- [86] S. Hansbo (1984) *Foundations on Friction Creep Piles in Soft Clays*. International Conference on Case Histories in Geotechnical Engineering, Missouri University of Science and Technology.
- [87] D. T. Bergado et al. (1999) *Deep soil mixing used to reduce embankment settlement in Ground Improvement*, vol. 3(4), pp. 145-162.
- [88] S. J. Farr et al. (2012) *Jet Grouting for Earth Retention Performed in Low Headroom for Subway Station Expansion in Proceedings of the Fourth International Conference on Grouting and Deep Mixing*, pp. 963-971, New Orleans, Louisiana.
- [89] Hayward Baker Inc. (Keller Company) (n.d.) *Compensation Grouting* [Online]. Available: <https://goo.gl/QMvrmw>, accessed: 22.04.2017.
- [90] VINCI Construction (2014) *Club Travaux Souterrains; Crossrail C510 - Overview* [Online]. Available: <https://goo.gl/EfzYXL>; accessed: 22.04.2017.
- [91] Crossrail Ltd (2017) *Ground settlement - managing effect of tunneling* [Online]. Available: <https://goo.gl/CzjyZ6>, accessed: 17.04.2017.
- [92] The Royal Holloway University of London (2017) *Cellcore installation beneath reinforced concrete floor slabs to protect against the potential effects of ground heave* [Online]. Available: <https://goo.gl/VdriyY>, accessed: 28.03.2017.
- [93] Cordek Ltd (n.d.) *Cellcore installation under the raft* [Online]. Available: <https://goo.gl/0snZiD>, accessed: 28.03.2017.
- [94] S. J. Horvath (1999) *Lessons Learned from Failures Involving Geofoam in Roads and Embankments*. Manhattan College Research Report No. CE/GE-99-1 [Online]. Available: <https://goo.gl/2GmF4j>, accessed: 17.04.2017.
- [95] S. Lee and D. A. Spears (1994) *Potential groundwater contamination from pulverised fuel ash (PFA) in Mineralogical Magazine*, vol. 58A, pp. 515-516, Goldschmidt Conference, Edinburgh, Scotland.
- [96] N. S. Pandian (2004) *Fly ash characterization with reference to geotechnical applications in Journal of the Indian Institute of Science*, vol. 84(6), pp. 189-216.
- [97] geosynthetica.net (n.d.) *PFA with reinforcement mesh used for the road construction on the soft ground* [Online]. Available: <https://goo.gl/THnDik>, accessed: 28.03.2017.
- [98] L. Davies et al. (2014) *Lightweight backfill materials in integral bridge construction in Proceedings of the Institution of Civil Engineers: Bridge Engineering*, vol. 167(1), pp. 3-16.
- [99] LECA Building Material Trading (n.d.) *What is Leca?* [Online]. Available: <http://www.leca.ae/>, accessed: 17.04.2017.
- [100] Geocell Schaumglas GmbH (n.d.) *GEOCELL foam glass gravel* [Online]. Available: <https://goo.gl/ZN7LJk>, accessed: 28.03.2017.
- [101] Techfil Europe Ltd (n.d.) *Cross-section photo of Lightweight Expanded Clay Aggregate* [Online]. Available: <https://goo.gl/4ZOHpn>, accessed: 28.03.2017.
- [102] T. Auvinen et al. (2013) *Covering the Highway E12 in the centre of Hämeenlinna - innovative use of foamed glass as light weight material of approach embankment*. The XXVIII International Baltic Road Conference, Vilnius, Lithuania. Available: <https://goo.gl/eWGykg>.
- [103] Cordek Ltd (n.d.) *Filcor EPS - Structural Fill* [Online]. Available: <https://goo.gl/9Jn27U>, accessed: 17.04.2017.

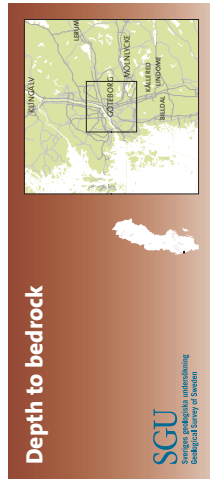
- [104] G. Hudson-Nec (2016) *Work taking place on Cowgate roundabout* [Online]. Available: <https://goo.gl/X5f55T>, accessed: 15.04.2017.
- [105] EPS Industry Alliance (n.d.) *Fire Performance & Safety* [Online]. Available: <https://goo.gl/0hXrjf>, accessed: 17.04.2017.
- [106] B. Ferreira (2016) *Why Is Styrofoam Still a Thing?* [Online]. Available: <https://goo.gl/twy586>; accessed: 17.04.2017.
- [107] Trafikverket (2015) *Tvarsektion km458+990, km459+100 och km459+060* [Online]. Available: <https://goo.gl/mwrJ7z>, accessed: 09.03.2017.
- [108] (2015) *BVS 1586.26 - Banöverbyggnad - Plattformar. Geometriska krav vid ny-och ombyggnad*, TDOK 2014:0686, 2015.
- [109] ABAKO Arkitektkontor AB (n.d.) *Västlänken Station Haga. Underjordisk station i kulturhistorisk miljö* [Online]. Available: <https://goo.gl/oixW1A>, accessed: 29.04.2017.
- [110] P. W. Mayne and F. H. Kulhawy (1982). *K<sub>0</sub>-OCR relationships in soil* in *Journal of Geotechnical Engineering*, vol. 108(GT6), pp. 851-872.
- [111] R. Obrzud and A. Truty (2012) *The hardening soil model - a practical guidebook*, Zace Services.
- [112] Á. Kézdi (1974) *Handbook of Soil Mechanics*, University of Virginia, El Sevier.
- [113] K.-A. Magnusson (1976) *In situ determination of elastic constants in rock, using a hammer seismograph* in *Geologiska Föreningen i Stockholm Förhandlingar*, vol. 98(3), pp. 244-250.
- [114] E. Hoek (2012) *Blast Damage Factor. Technical note for RocNews* [Online]. Available: <https://goo.gl/qa2aoR>, published: 02.02.2012.
- [115] J. G. Potyondy (1961) *Skin friction between various soils and construction materials* in *Géotechnique*, vol. 11(4), pp. 339-353.
- [116] C.Y. Ou (2006) *Stree and deformation analysis: simplified method* In: *Deep Excavation - Theory and Practice*, pp. 209-227, London, the UK, Taylor and Francis Group.
- [117] *Code of practice for dead and imposed loads*, Building Department Hong Kong, 2011.
- [118] M. D. Bolton (1986) *The strenght and dilatancy of sands* in *Géotechnique*, vol. 36(1), pp. 65-78.
- [119] H. S. Aksoy and M. Gör (2016) *A new design chart for estimating friction angle between soil and pile materials* in *Geomechanics and Engineering*, vol. 10(3), pp. 315-224.
- [120] T. Bhatkar et al. (2017) *Prediction of behaviour of a deep excavation in soft soil: a case study* in *International Journal of Geotechnical Engineering*, vol. 11(1), pp. 10-19.
- [121] Trafikverket (2014) *Trafikverkets tekniska krav för geokonstruktioner TK Geo 13* [Online]. Available: <https://goo.gl/LGU060>, published: 01.05.2014.
- [122] Trafikverket (2015) *Tvarsektion km458+890* [Online]. Available: <https://goo.gl/RMXfdf>, accessed: 09.03.2017.
- [123] Trafikverket (2015) *Tvarsektion km459+120 och km459+165* [Online]. Available: <https://goo.gl/zhpKhR>, accessed: 09.03.2017.
- [124] Trafikverket (2015) *Tvarsektion km459+120 och km459+165* [Online]. Available: <https://goo.gl/SgkXZT>, accessed: 09.03.2017.

- [125] Trafikverket (2015) *Tillfälligt markanspråk. Plankarta km458-500 - 459+000* [Online]. Available: <https://goo.gl/vQtJA3>, accessed: 09.03.2017.
- [126] Trafikverket (2015) *Permanent markanspråk. Plankarta km458-500 - 459+000* [Online]. Available: <https://goo.gl/ih3vJr>, accessed: 09.03.2017.
- [127] Trafikverket (2015) *Tillfälligt markanspråk. Plankarta km459-000 - 459+500* [Online]. Available: <https://goo.gl/BJwPKP>, accessed: 09.03.2017.
- [128] Trafikverket (2015) *Permanent markanspråk. Plankarta km459-000 - 459+500* [Online]. Available: <https://goo.gl/5F8Owr>, accessed: 09.03.2017.
- [129] C. Alén (2012) *Pile foundations – Short handbook*, version 1.1, Chalmers University of Technology, Gothenburg, Sweden.

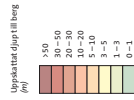
# Appendix A. Quaternary deposits



# Appendix B. Depth to bedrock map



The map presents an overview of the thickness of superficial materials over bedrock. It is based on interpolations of depth values from wells, other drillings, and seismic investigations. The locations of rock outcrops from geological maps have been used to correct the interpolated values. The uncertainty of the calculated depth values increases with distance from drill sites and rock outcrops. For distances exceeding several hundred meters, the uncertainty is considerable. Drill sites are shown only on the map in scales of 1:50 000 and 1:100 000.



• Uppskattat djup

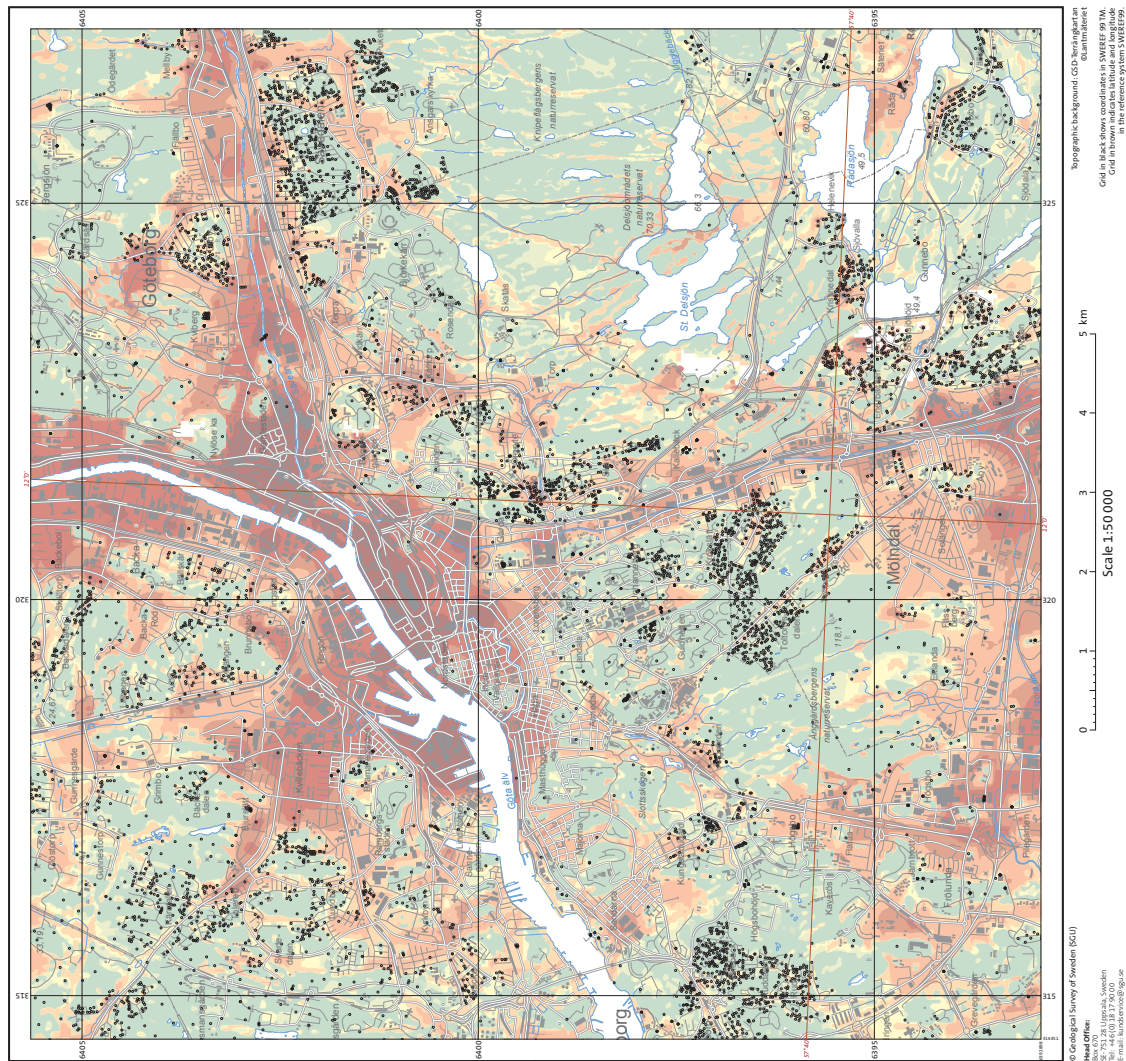


Figure B.1: Map presenting depth of superficial materials over bedrock in Gothenburg in scale 1:50,000 [14].

# Appendix C. Bedrock characterization map



# Appendix D. Groundwater reservoirs



There may be several groundwater reservoirs at different levels, as seen from the ground surface. The upper level is called J1 or S1 and the underlying levels are called J2, J3 and S2, S3. J stands for reservoirs in soil layer (jordlager in Swedish) and S stands for sedimentary bedrock. SGU's data mainly contains information on groundwater in larger reservoirs, along eskers and in sedimentary bedrock, in connection with mapping. Things such as the directions of groundwater flow, groundwater divides, and the groundwater reservoir's size and extraction possibilities are determined.

When mapping on a detailed scale, the reservoir's catchment areas, surface water contacts, etc. is established. The database contains both overall, regional information (scale 1:250,000) and more detailed, local information (1:50,000). Where detailed information is available the overall information has been replaced with the detailed information. The "Mapping Methods" page shows which objects belong to which mapping type. The regional information comes from SGU's county maps published in SGU's Ah series.

- ↑ General direction of groundwater flow
- Fixed groundwater divide
- - - Boundary of catchment area J1
- Delineation of groundwater reservoir J1
- ▨ Soil strata with low permeability covering aquifer J1
- Estimated exploitation potential in the order of
  - <1 l/s
  - 1-5 l/s
  - 5-25 l/s

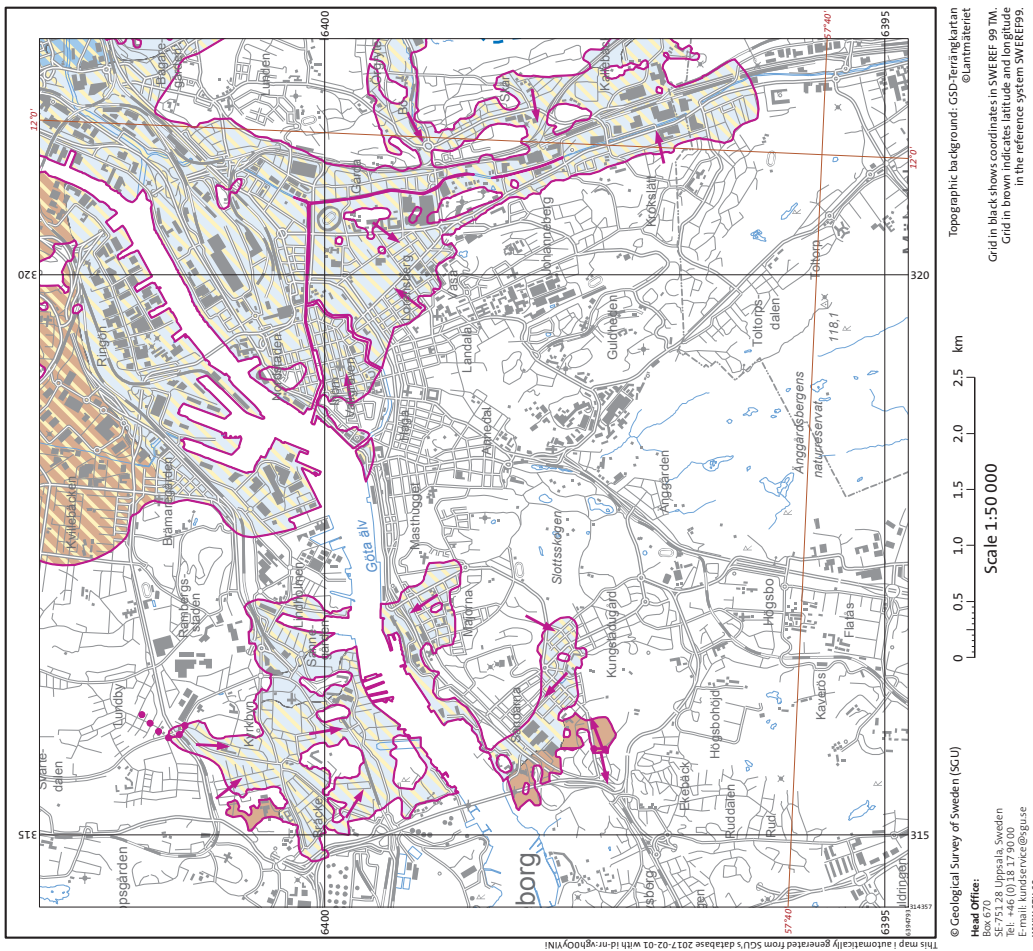


Figure D.1: Map presenting the groundwater reservoirs in Gothenburg in scale 1:50,000 [16].

# Appendix E. Comparison of the soil models and their application in PLAXIS

Considering different types of soils

| Model                   | Concrete | Rock | Gravel | Sand | Silt | OC clay | NC clay | Peat (org) |
|-------------------------|----------|------|--------|------|------|---------|---------|------------|
| Linear Elastic model    | C        | C    |        |      |      |         |         |            |
| Mohr-Coulomb model      | A        | B    | C      | C    | C    | C       | C       | C          |
| Hardening Soil model    |          |      | B      | B    | B    | B       | B       |            |
| HS small model          |          |      | A      | A    | A    | A       | B       |            |
| Soft Soil Creep model   |          |      |        |      |      |         | A*      | A*         |
| Soft Soil model         |          |      |        |      |      |         | A*      | A*         |
| Jointed Rock model      |          | A**  |        |      |      |         |         |            |
| Modified Cam-Clay model |          |      |        |      |      |         | C       | C          |
| NGI-ADP model           |          |      |        |      |      |         | A*      | A*         |
| Hoek-Brown model        |          | A**  |        |      |      |         |         |            |

A : The best standard model in PLAXIS for this application

B : Reasonable modelling

C : First order (crude) approximation

\* : Soft Soil Creep model in case time-dependent behaviour is important; NGI-ADP model for short-term analysis, in case only undrained strength is known

\*\* : Jointed Rock model in case of anisotropy and stratification; Hoek-Brown model for rock in general

Figure E.1: Comparison of the soil models available in PLAXIS and their suitability of the modelling of various soil types [35].

Considering different types of applications (consider also type of soil!)

| Model                   | Foundation | Excavation | Tunnel | Embankment | Slope | Dam | Offshore | Other |
|-------------------------|------------|------------|--------|------------|-------|-----|----------|-------|
| Linear Elastic model    |            |            | C      |            |       |     |          |       |
| Mohr-Coulomb model      | C          | C          | C      | C          | C     | C   | C        | C     |
| Hardening Soil model    | B          | B          | B      | B          | B     | B   | B        | B     |
| HS small model          | A          | A          | A      | A          | A     | A   | A        | A     |
| Soft Soil Creep model   | B          | B          | B      | A          | A     | B   | B        | B     |
| Soft Soil model         | B          | B          | B      | A          | A     | B   | B        | B     |
| Jointed Rock model      | B          | B          | B      | B          | B     | B   | B        | B     |
| Modified Cam-Clay model | C          | C          | C      | C          | C     | C   | C        | C     |
| NGI-ADP model           | B          | B          | B      | A          | A     | B   | A        | B     |
| Hoek-Brown model        | B          | B          | B      | B          | B     | B   | B        | B     |

A : The best standard model in PLAXIS for this application

B : Reasonable modelling

C : First order (crude) approximation

Figure E.2: Comparison of the soil models available in PLAXIS and their suitability of the modelling of various design problems [35].

Considering different types of loading and soils (consider also type of soil!)

| Model                   | Primary compression | Unloading / Reloading | Shear / Deviatoric loading | Undrained loading | Cyclic | Compression + Shear | Extension + Shear |
|-------------------------|---------------------|-----------------------|----------------------------|-------------------|--------|---------------------|-------------------|
| Linear Elastic model    | C                   | C                     |                            |                   |        |                     |                   |
| Mohr-Coulomb model      | C                   | B                     | C                          | C                 |        | C                   | C                 |
| Hardening Soil model    | A                   | B                     | B                          | B                 | C      | A                   | A                 |
| HS small model          | A                   | A                     | A                          | B                 | B      | A                   | A                 |
| Soft Soil Creep model   | A                   | B                     | B                          | B                 | C      | A                   | B                 |
| Soft Soil model         | A                   | B                     | B                          | B                 | C      | A                   | B                 |
| Jointed Rock model      | B                   | B                     | B                          |                   |        | B                   | B                 |
| Modified Cam-Clay model | C                   | C                     | C                          | C                 | C      | C                   | C                 |
| NGI-ADP model           | B                   | B                     | B                          | A                 | C      | B                   | B                 |
| Hoek-Brown model        | B                   | B                     | B                          |                   |        | B                   | B                 |

A : The best standard model in PLAXIS for this application

B : Reasonable modelling

C : First order (crude) approximation

Figure E.3: Comparison of the soil models available in PLAXIS and their suitability of the modelling of various loading types [35].

# Appendix F. Cordek Cellcore HG data sheet

Ground Heave Solutions

Data Sheet

## Cellcore HG Data Sheet



The Cellcore HG range of collapsible products has been designed to protect foundations from the effect of ground heave.

The product consists of a cellular construction of expanded polystyrene combined with a robust polypropylene board, which has been designed and tested to tight tolerances to achieve the specified performance characteristics.

The range of products are available in a variety of depths and grades to suit the most commonly encountered combinations of soil heave potential and concrete depths that exceed the capacity of the standard Cellcore HX range. If a suitable product for your requirements is not listed within this data sheet then please contact our sales support desk for further assistance.

In addition to the Cellcore HG range, the following variations of the product are available:

- Cellcore HX suitable for providing heave protection to lightweight slabs, ground beams and pile caps
- Cellcore HX Plus with EPS insulation incorporated
- Cellform HX with integral formwork for ground beams
- Cellvent which includes protection against VOC's and ground gases

### Key Features

- Reduces the upward force transmitted to the structure
- Wide range of depths and grades to suit most applications
- Meets the NHBC's Technical Standards
- Consistent performance supported by extensive testing

For further information on the full range of Cordek's Ground Heave Solutions, please contact the Cordek technical team on 01403 799600, [techsupport@cordek.com](mailto:techsupport@cordek.com) or consult our website at [www.cordek.com](http://www.cordek.com).

M-D534 Cellcore HG Data Sheet V2 01/16

- Available with integral EPS insulation, permanent formwork for ground beams or voids for gases to vent by request

### Installation

The procedure for installing Cellcore panels is straightforward, but the following points should be adhered to:

- Please ensure that the Cellcore panels are placed upon a suitable firm and level surface. Typically a layer of concrete blinding beneath the panels is recommended.
- The lightweight but durable panels can be easily laid by one person. Where they are required to be cut this can be carried out using a fine tooth saw or hot wire cutter (available for hire from Cordek – please contact our sales team on 01403 799600).
- When installing Cellcore adjacent to piles, we suggest the use of Cordek Claymaster pile collars is considered – please see the Cordek Claymaster data sheet for further information.
- Individual panels should be butted together, with taping of the joints using the Cordek formwork tape to avoid any grout loss between the panels.
- Reinforcement spacers can be positioned directly upon the Cellcore panels. The upper surface of the panels can be reinforced with a layer of concrete blinding to spread the spacer loads if a very heavy reinforcement cage has been specified.



## Storage & Handling

All products are delivered in a polythene wrapping and are clearly labelled. Both packs of Cellcore and individual panels can be manually handled and offloaded upon delivery, taking into account any site specific manual handling regulations.

Due to the relatively light nature of the product, all of the packs of Cellcore should be weighted down or secured should they be stored outside prior to installation. No further storage requirements are needed as the product is unaffected by both UV light and water.

**Table One**

| Results of Soil Analysis | NHBC Category      | Predicted Ground Movement or BRE/NHBC requirement | Depth of Cellcore HG required to achieve 'Equivalent Void' |
|--------------------------|--------------------|---|--|
| Plasticity Index         | Shrinkage Category | Void Dimensions (mm)                              | Product depth (mm)   |
| 10 - 20                  | Low                | 50  | 100  |
| 20 - 40                  | Medium             | 100   | 200  |
| 40 - 60*                 | High               | 150   | 300  |

\* When the analysis exceeds 60 or a deeper void is required, please consult our Technical Services team.

Secondly, the grade of the product is determined by the depth of the concrete to be cast on the Cellcore, as detailed in table two below:

**Table Two**

| Grade* | Safe Load (kN/m <sup>2</sup> ) | Fail Load (kN/m <sup>2</sup> ) | Maximum Depth of Concrete* (mm) |
|--------|--------------------------------|--------------------------------|---------------------------------|
| 30/40  | 30                             | 40                             | 1140                            |
| 40/50  | 40                             | 50                             | 1540                            |
| 50/65  | 50                             | 65                             | 1940                            |

\*Based on the Eurocode and a live load allowance of 1.5 kN/m<sup>2</sup>

For concrete thicknesses between 0 – 900mm please refer to the Cellcore HX data sheet. For concrete thicknesses above 1940mm, please contact the Cordek technical team on 01403 799600.

## Design Notes

- Each Cellcore grade is designed to support a given thickness of concrete plus a live load allowance of 1.5 kN/m<sup>2</sup> with negligible creep compression during a 16 hour curing period: this is known as the **SAFE LOAD**.
- At the pre-determined load the polystyrene legs of the Cellcore panels will buckle and collapse due to the upward movement of the ground beneath; this is known as the **FAILURE LOAD**.
- The slab, beam or pile cap must be designed to accept the difference between its self-weight and the fail load (please see example below).

## Product Sizes

**Standard Panel:** 2400mm x 1200mm

**Beam Widths:** 2400mm x 1200mm to 300mm (in 25mm increments)

## Product specification

Firstly the depth of the Cellcore HG panel should be determined by the heave potential of the soil, as detailed in table one below:

## Design Example

### Reinforced Concrete Ground Beam / Slab (1500mm thick)

- Assume the soil survey showed a plasticity index of 25.
- Table 1 shows that the potential for ground movement is medium.
- BRE/NHBC data recommends a clear void of 100mm.

1. Total deadweight/downward load is:

$$1.5\text{m} \times 25 \text{ kN/m}^2 = 37.5 \text{ kN/m}^2$$

$$\text{Live load allowance} = 1.5 \text{ kN/m}^2$$

$$\text{TOTAL LOAD} = 39.0 \text{ kN/m}^2$$



2. Table 2 indicates the nearest **SAFE LOAD** value is 40.0 kN/m<sup>2</sup> based upon the suggested use of the **Cellcore HG Grade 40/50** (Fail load of 50.0 kN/m<sup>2</sup>)

3. A maximum 100mm ground movement is predicted and Table 1 shows that:

The Cellcore HG depth to accommodate this = 200mm, therefore the full product specification is **Cellcore 200mm HG 40/50**

As stated above, this Cellcore HG grade has a **FAIL LOAD** of 50.0 kN/m<sup>2</sup>

The slab must be suitably designed to accommodate the transmitted load and two possible modes of failure should be considered:

- i) The slab being lifted off the foundation
- ii) Failure of the slab in bending or shear due to the uplift

### Additional Cellcore Products:

#### Cellcore HX

The Cellcore HX range of collapsible products has been designed to protect lightweight (under 900mm in depth) foundations from the effects of ground heave.

This BBA approved product consists of a cellular construction of expanded polystyrene which has been designed, moulded and tested to tight tolerances to achieve the specified performance characteristics.

#### Cellcore HX Plus

In cases where insulation is also required beneath the slab, the Cellcore HX Plus range can be utilised to provide combined ground movement protection and insulation from a single product.

The thermal thickness of the Cellcore HX Plus is based upon the thickness of insulation incorporated within the panels, as outlined in the table below. Please contact the Cordek Technical Team on 01403 799600 for further assistance with determining the most appropriate Cellcore HX specification.

| Thickness (mm) | Thermal Resistance m <sup>2</sup> c/w |
|----------------|---------------------------------------|
| 50 (Standard)  | 1.39                                  |
| 75             | 2.08                                  |
| 100            | 2.78                                  |
| 125            | 3.47                                  |
| 150            | 4.17                                  |

#### Cellform HX

Cellform HX combines the benefits of Cellcore HX with an economical and simple to install permanent formwork system.

Each Cellform HX panel is supplied to the required beam width and depth. The principle is that the hinged side panels are supported off the reinforcement cage by concrete spacers, this then allows the excavation to be backfilled. The backfill then supports the formwork against the concrete pressure whilst the beam is cast and thereby avoids the need for fixing and striking traditional formwork.

#### Cellvent

Cellvent HX protects a building from both ground heave and hazardous ground gases, for use under suitably reinforced concrete floor slabs.

For further details and design examples please refer to the Cellvent HX data sheet which is available for download from [www.cordek.com](http://www.cordek.com).

Issued: 01/2016

DISCLAIMER: Information contained within this 'Technical Data Sheet' is for guidance only, and it is intended for experienced construction industry workers. It contains summaries of aspects of the subject matter and does not provide comprehensive statements of construction industry practice. As conditions of usage and installation are beyond our control we do not warrant performance obtained. Please contact us if you have any doubt as to the suitability of application. The information provided within this document is based on data and knowledge correct at the time of printing.

#### Cordek Ltd

Spring Copse Business Park, Slinfold, West Sussex  
RH13 0SZ, United Kingdom

Telephone (+44) 1403 799600 Fax (+44) 1403 791718  
E-mail [info@cordek.com](mailto:info@cordek.com)

[www.cordek.com](http://www.cordek.com)



M-DS34 Cellcore HG Data Sheet V2 01/16



# Appendix G. Design drawings of Haga station

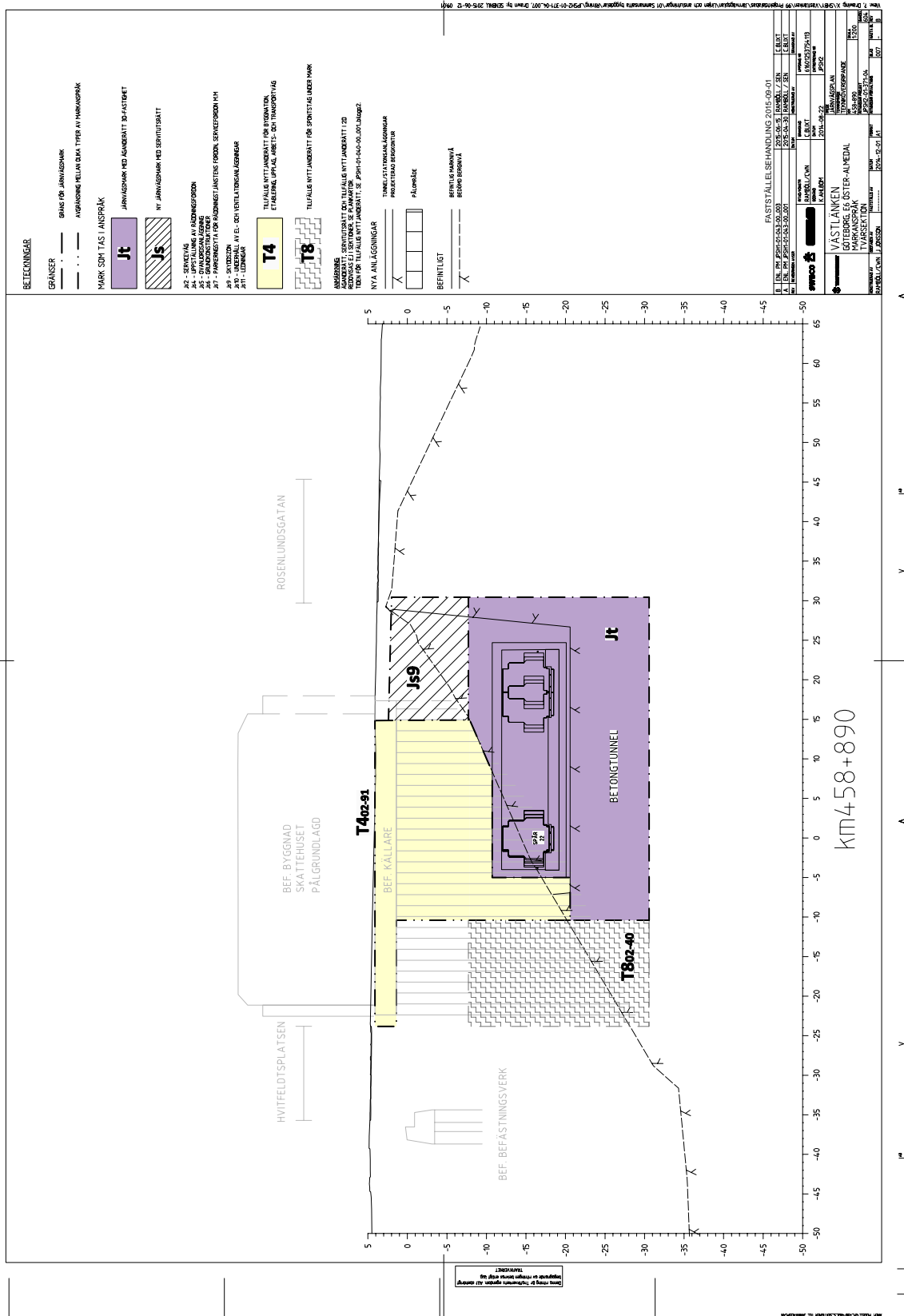


Figure G.1: Cross-section at the km458+890 of Västlänken [122].

















# Appendix H. Soil investigation summary - boreholes

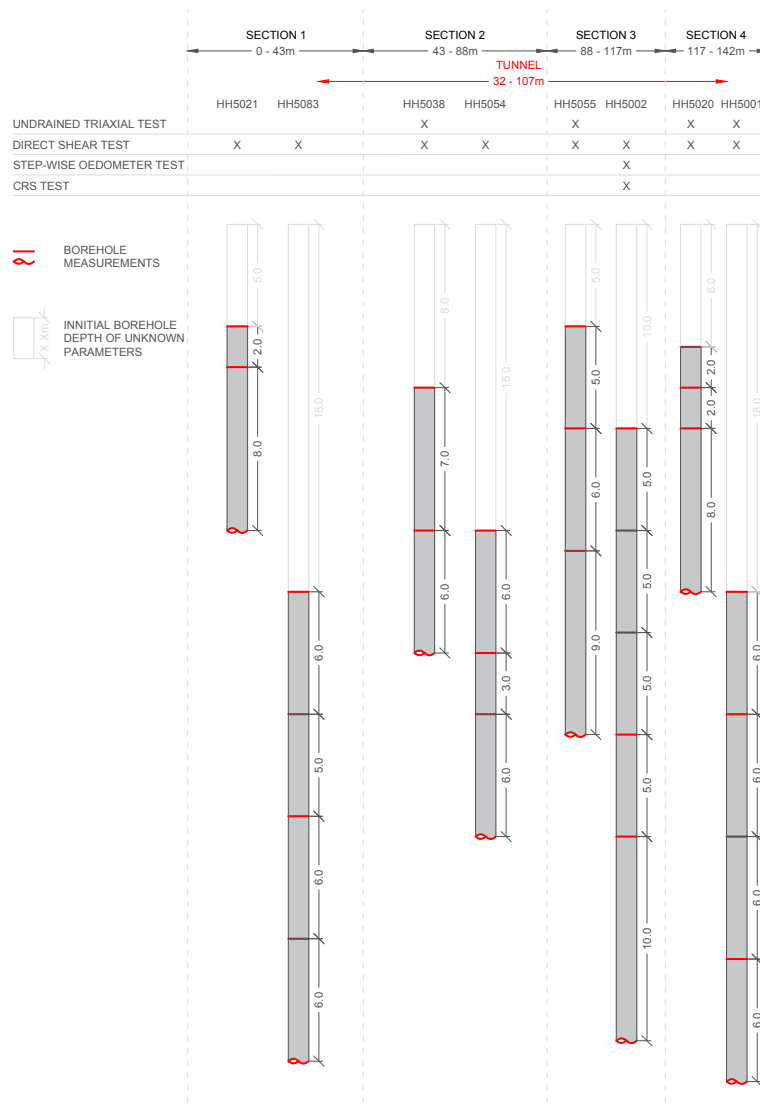


Figure H.1: Figure presents depths of reading from the boreholes presented in SWECO report [2].



# Appendix I. Triaxial test results

Triaxial test were used from available boreholes to analyse the effective strength parameters for the clay layers. The available data from the boreholes did not cover all the layers from the created conceptual model. Therefore, interpolation from the results was made to fill in the missing data where the reliable field data was not available. Presentation of the results for layers Clay 2, Clay 3 and Clay 4 is made in this section.

In Figure I.1, the analysis of the triaxial results for layer Clay 2 is presented. In the graph the plotted deviator and medium stresses correspond to the point of failure in the test. The selected boreholes, depth of the sample and resulting stress for this layer are presented in Table I.1. Due to similarities in soil properties, results from this layer will be extrapolated to layer Clay 1.

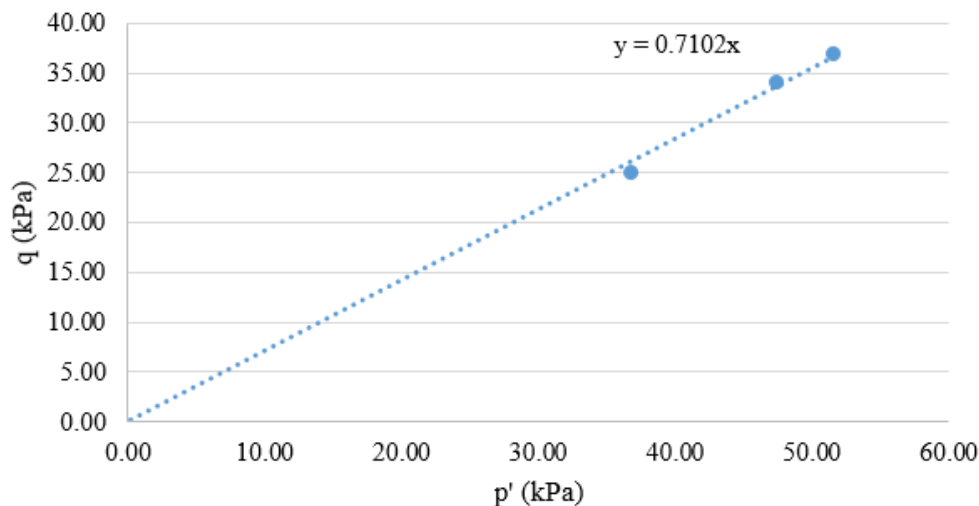


Figure I.1: Triaxial results for Clay 2.

The analysed triaxial results for layer Clay 3 are presented in Figure I.2. For Soil 4 different triaxial tests were available but one of them was excluded from the analysis due to dispersed relation between the sample results and other samples. Additionally, the pictures of the sample showed a high oxidation level along the cross-section. The data related to boreholes selection and resulting stresses for this layer are presented in Table I.2.

| Borehole | Depth (m) | q (kN/m <sup>2</sup> ) | p' (kN/m <sup>2</sup> ) |
|----------|-----------|------------------------|-------------------------|
| HH5055   | 10m       | 25.00                  | 36.73                   |
| HH5038   | 15m       | 37.00                  | 51.50                   |
| HH5001   | 18m       | 34.00                  | 47.33                   |

Table I.1: Retrieved data for analysis of the effective strength parameters for Clay 2.

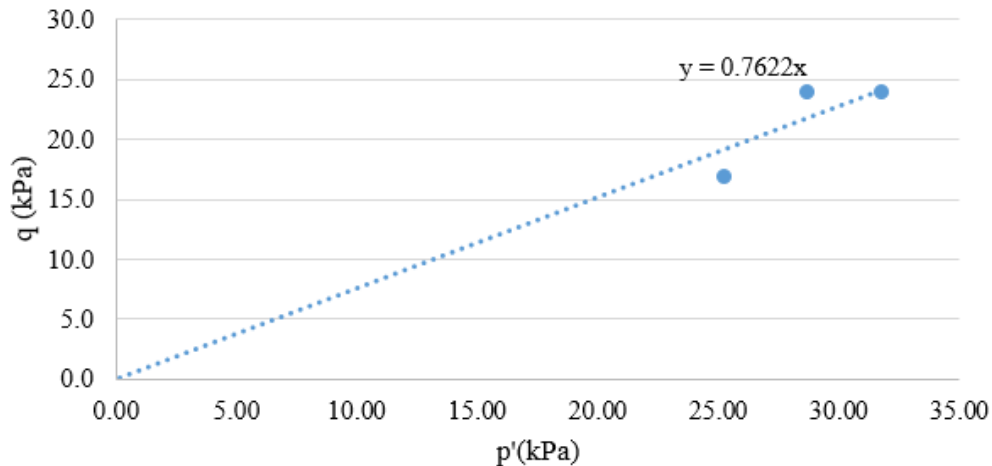


Figure I.2: Triaxial results for Clay 3.

| Borehole | Depth (m) | q (kN/m <sup>2</sup> ) | p' (kN/m <sup>2</sup> ) | Observation     |
|----------|-----------|------------------------|-------------------------|-----------------|
| HH5020   | 6m        | 17.00                  | 25.20                   | -               |
| HH5038   | 8m        | 24.00                  | 29.67                   | -               |
| HH5055   | 5m        | 24.00                  | 31.73                   | -               |
| HH5020   | 8m        | 28.00                  | 42.33                   | Oxidised sample |

Table I.2: Retrieved data for analysis of the effective strength parameters for Clay 3.

Triaxial results for Clay 4 are presented in Figure I.3. For this layer three different triaxial test results were available. As visible in the graph, the inclination of the trendline is much higher than for the previous plots resulting in higher friction angle. This results correlates with other parameters of the soil such as sensitivity and unit weight, which show that the lower layers could correspond to a clay with higher strength than the upper ones. Due to similarities with Clay 5 and 6, results from Clay 4 were extrapolated to the mentioned ones. Description of the borehole selection and resulting stresses for the analysis of this layer are presented in Table I.3

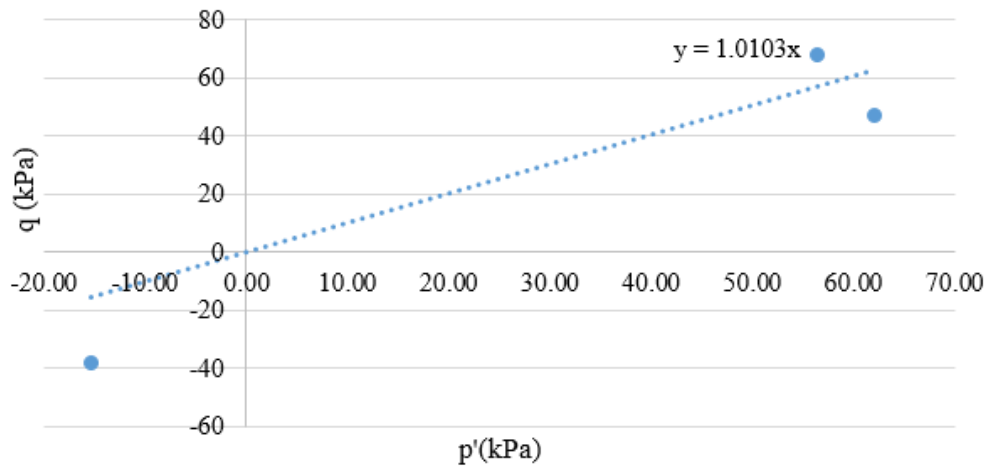


Figure I.3: Triaxial results for Clay 4.

| Borehole | Depth (m) | $q$ (kN/m <sup>2</sup> ) | $p'$ (kN/m <sup>2</sup> ) |
|----------|-----------|--------------------------|---------------------------|
| HH5001   | 24m       | -38.00                   | -15.33                    |
| HH5038   | 21m       | 68.00                    | 56.30                     |
| HH5055   | 21m       | 47.00                    | 62.00                     |

Table I.3: Retrieved data for analysis of the effective strength parameters for Clay 4.



# Appendix J. Oedometer test results

## Incremental oedometer loading test results

Interpretation of oedometer test results is made by means of graphical analysis. In order to retrieve the compressibility parameters of the soil, the results from the oedometer test have to be plotted in a special manner according to the type of parameter which is needed. For the requirements which are applied in this study, the oedometer test results are plotted as natural logarithm of effective stress ( $\ln \sigma'$ ) vs. the volumetric strain ( $\epsilon_v$ ).

The results from the oedometer incremental vertical test are retrieved from one single borehole (HH5002) at different depths. The samples were taken at 10 m, 15 m, 20 m, 30 m and 40 m below the ground level and its results can be observed in Figures J.1 to J.5 respectively. The additional lines drawn on Figures J.1 to J.11 represent the utilised procedure for the determination of the preconsolidation pressure for each test.

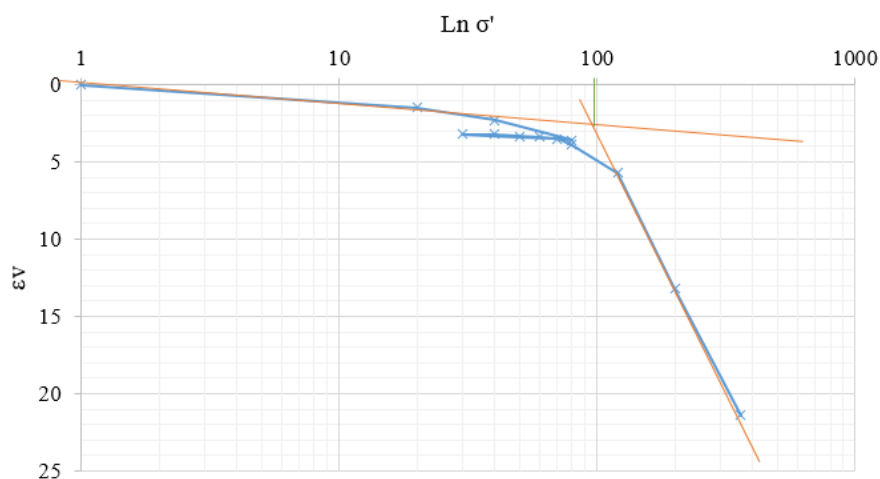


Figure J.1: Oedometer test results at 10 m.

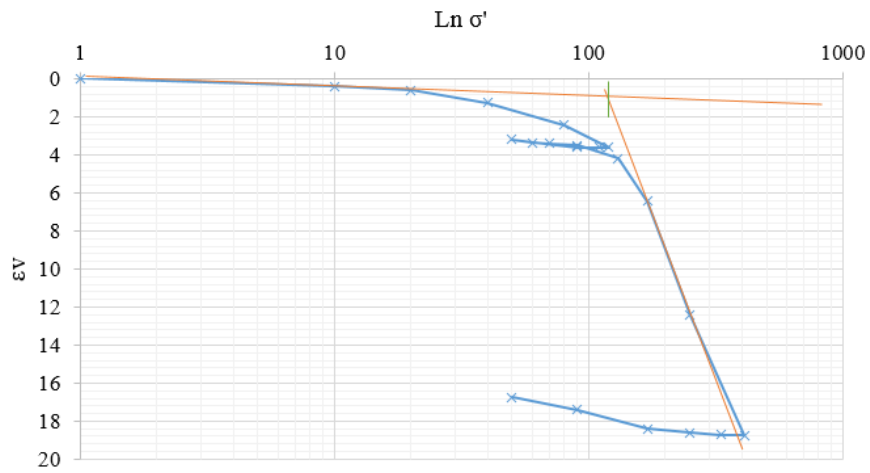


Figure J.2: Oedometer test results at 15 m.

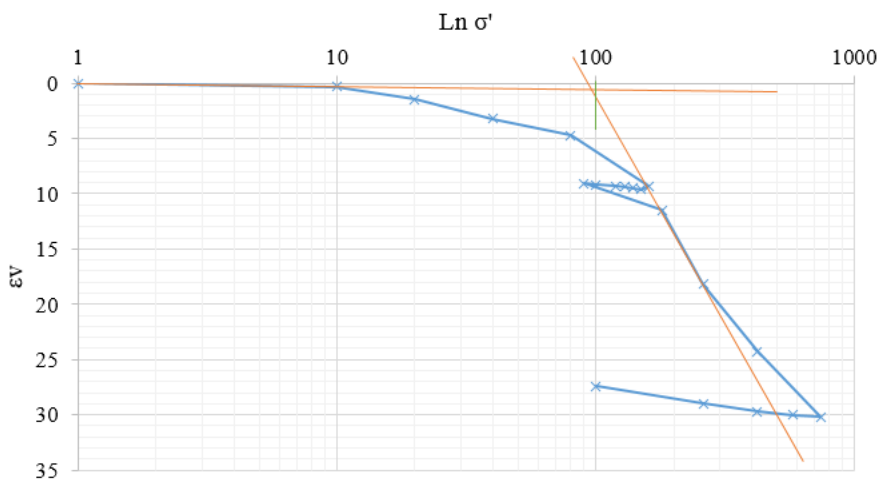


Figure J.3: Oedometer test results at 20 m.

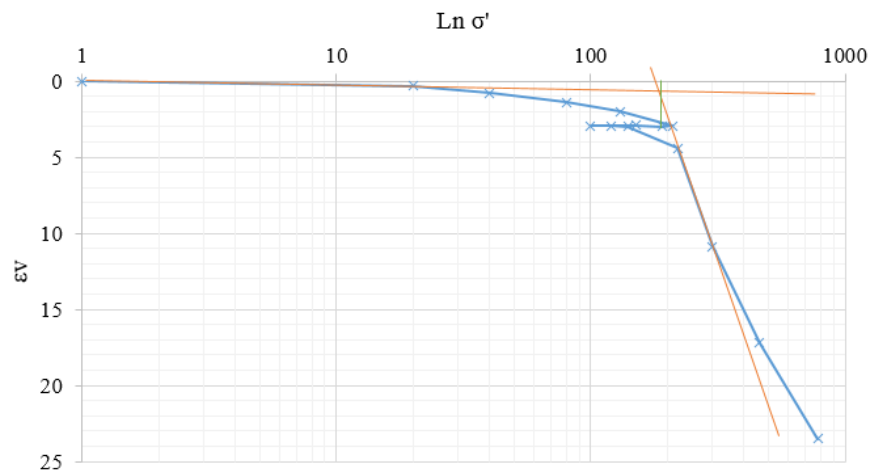


Figure J.4: Oedometer test results at 30 m.

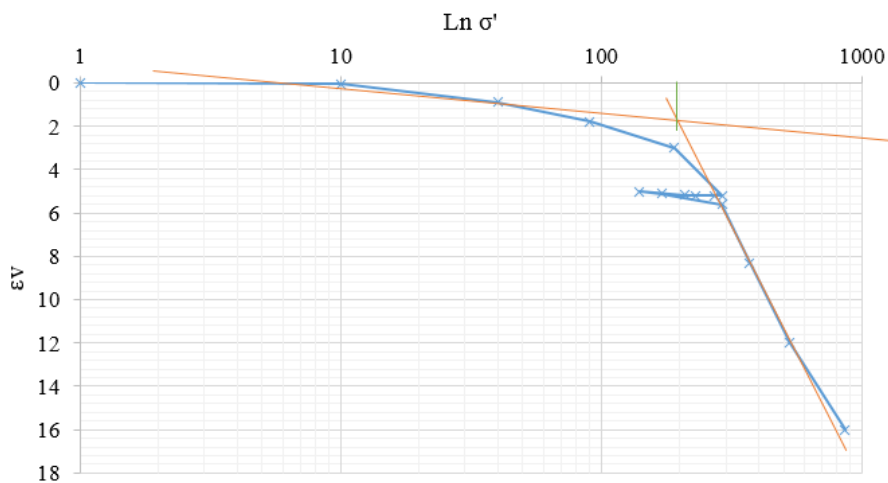


Figure J.5: Oedometer test results at 40 m.

### CRS test results

Samples for the CRS test were also taken from borehole HH5002. The samples were taken at 10 m, 15 m, 20 m, 25 m, 30 m and 40 m below the ground level and its results are presented in Figures J.6 - J.11 respectively. CRS test also provided information of the permeability on site which was used to represent the permeability coefficient value of clay in the model. As seen in Figure J.12, measured permeability remains constant for incremental stress levels at different depths. Therefore, an intermediate value of  $5E(-9)$  m/s for permeability was assumed for the modelled clay layers.

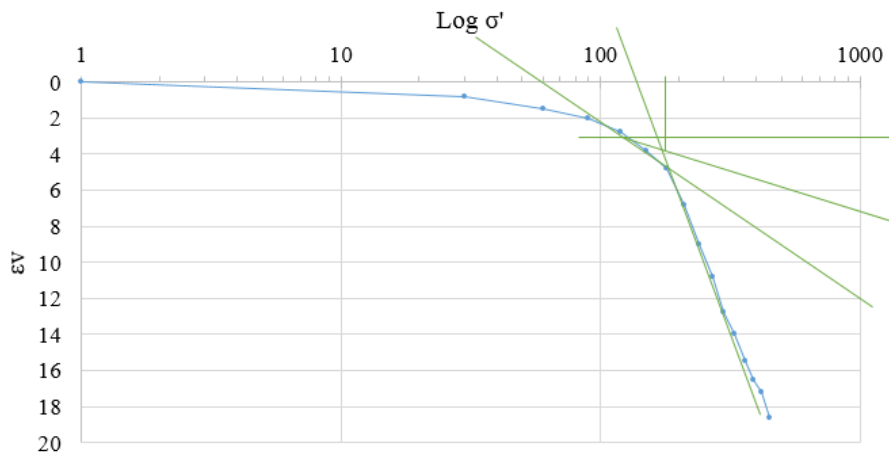


Figure J.6: CRS test results at 10 m.

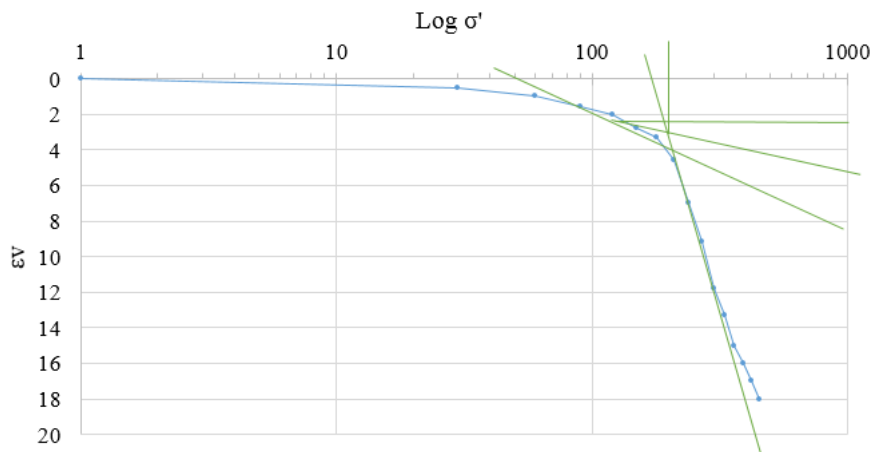


Figure J.7: CRS test results at 15 m.

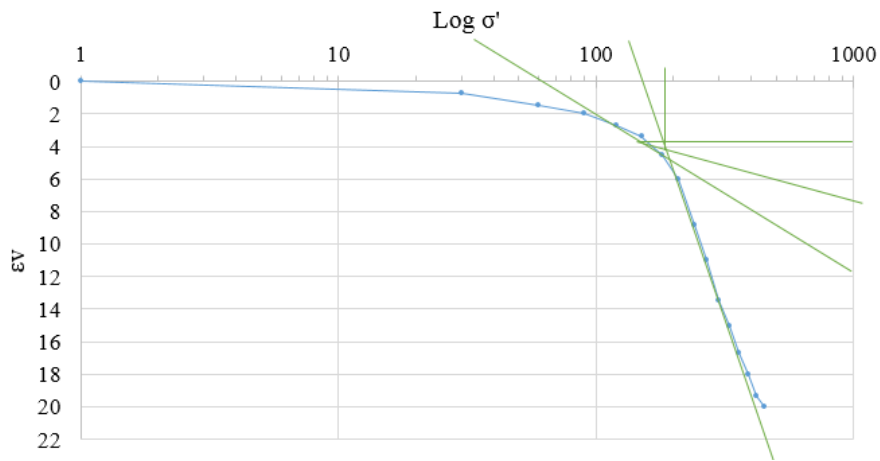


Figure J.8: CRS test results at 20 m.

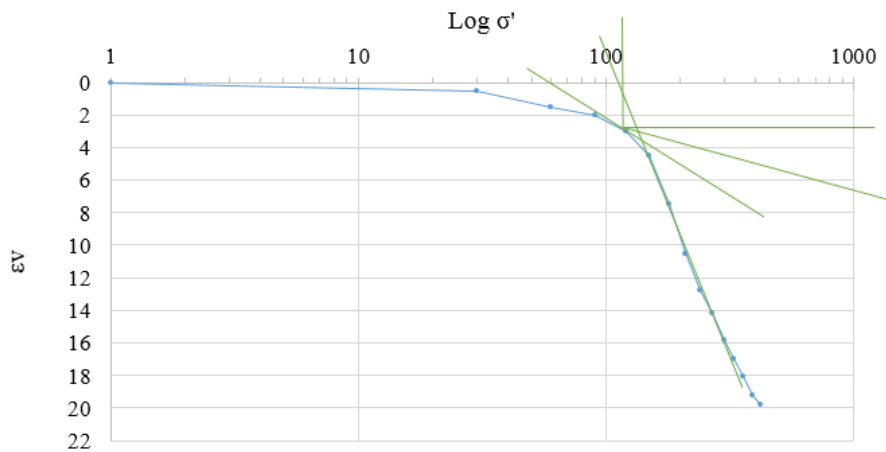


Figure J.9: CRS test results at 25 m.

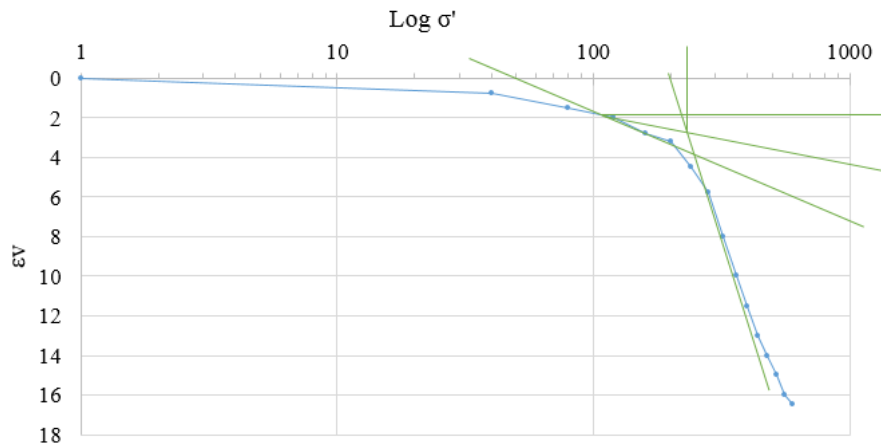


Figure J.10: CRS test results at 30 m.

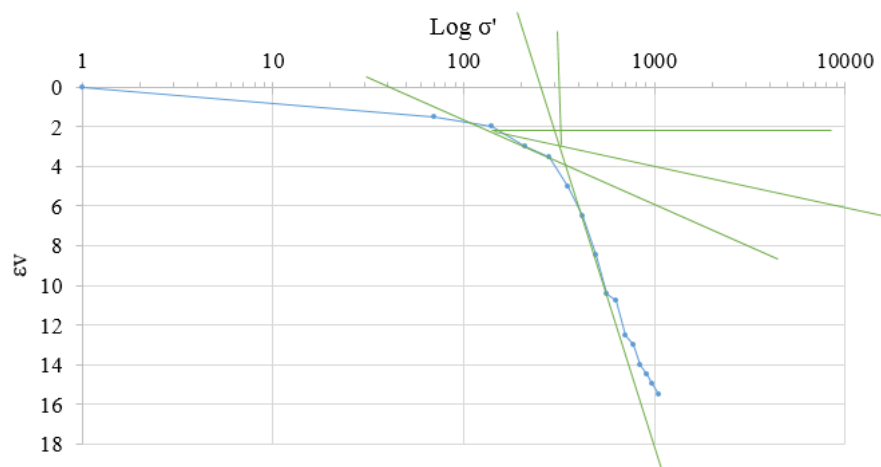


Figure J.11: CRS test results at 40 m.

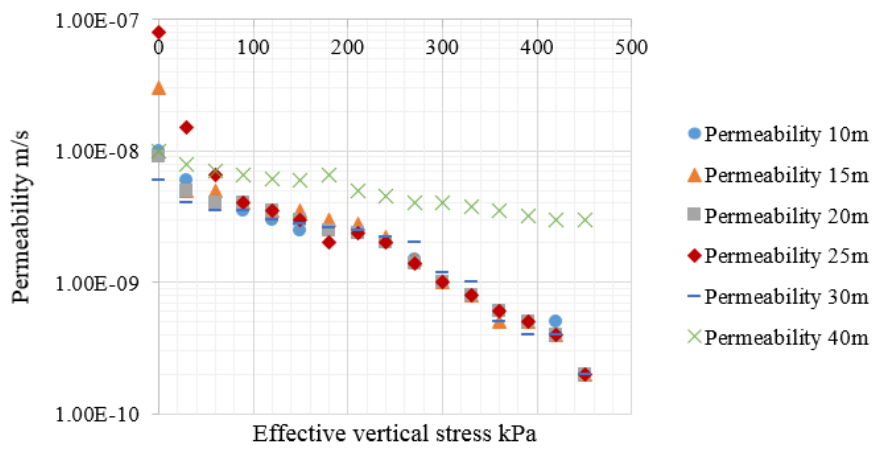


Figure J.12: Average permeability for CRS tests at all depths.



# Appendix K. Parameters of clay

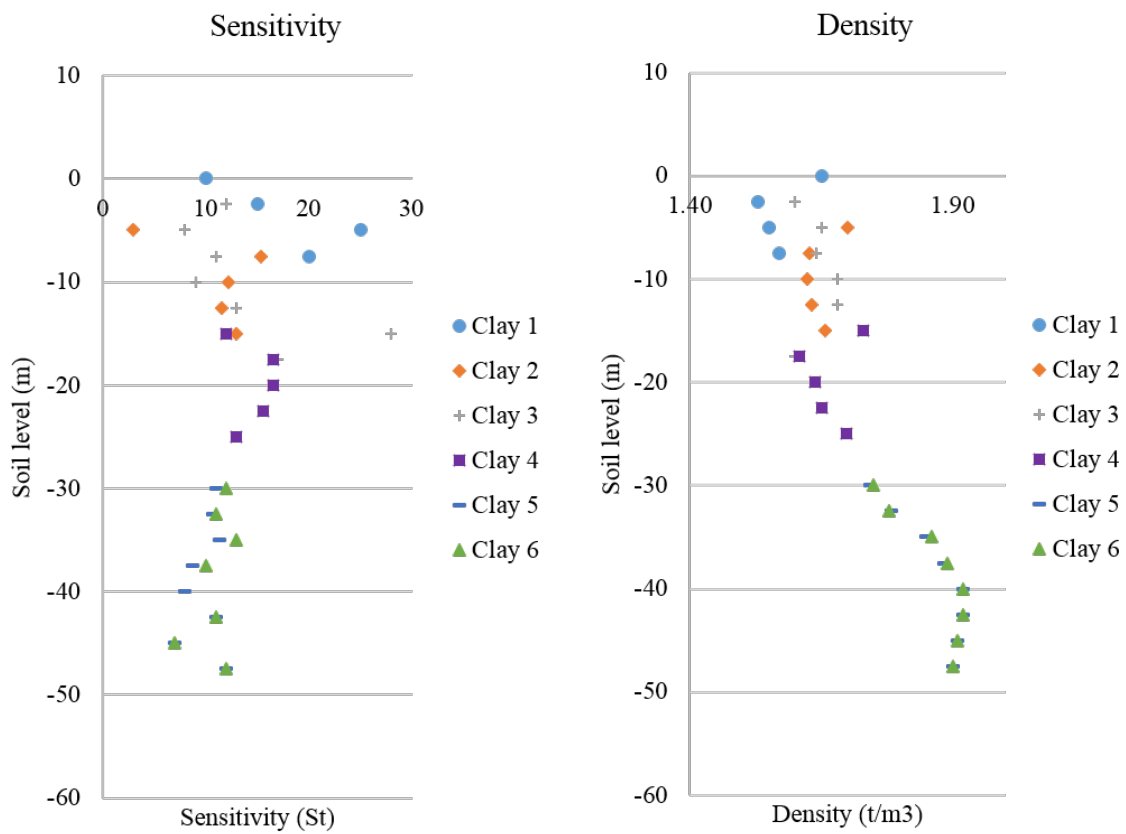


Figure K.1: Sensitivity of clay separated by soil layers.

Figure K.2: Density of clay separated by soil layers.

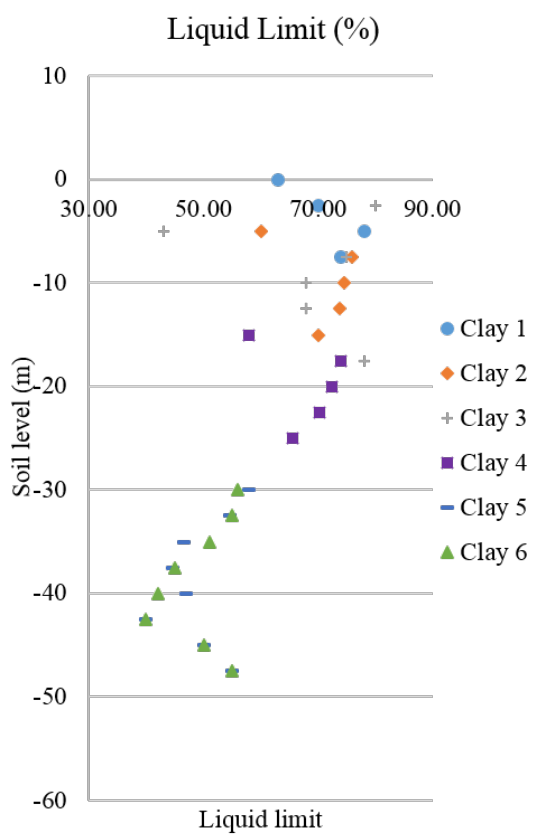


Figure K.3: Liquid limit of clay separated by soil layers.

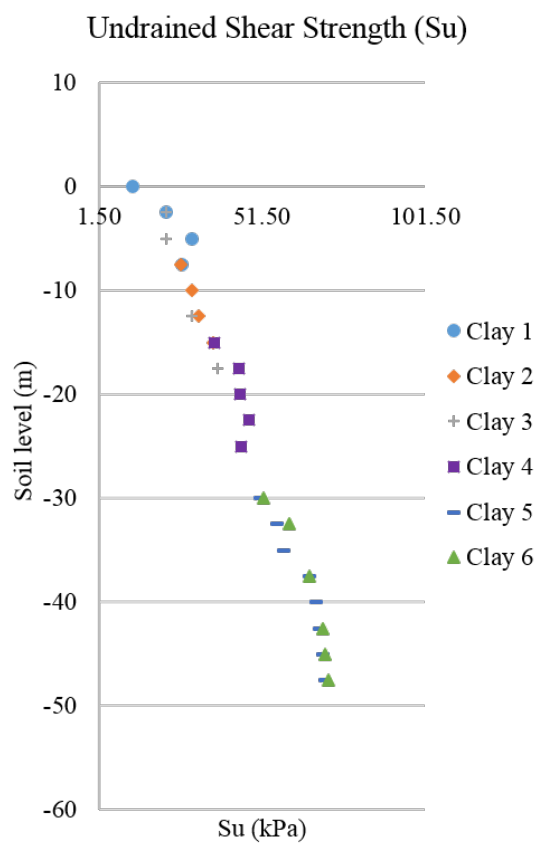


Figure K.4: Undrained shear strength of clay separated by soil layers.

# Appendix L. Design of cross-walls

Below calculations present the design value for the separation of the cross-walls according to the method proposed by Wu et al. [68] and explained in section 3.7.2.

The first step corresponds to the determination of expected settlements with the retaining system of the excavation without foundation. To do this, calculation of the system stiffness with equation 3.10 must be performed. The total system stiffness is a function of  $k_1$ ,  $k_2$  and  $k_3$  which corresponds to axial stiffness of retaining walls, rigidity of retaining walls and axial stiffness of lateral support respectively.

With the initial setup of the model, the parameters used for the calculation consists of: the width of the excavation ( $B=75$  m), length of retaining walls ( $h=31$  m), depth of excavation (24.5 m), length of the out of plane section ( $L=200$ ), thickness of retaining wall ( $t=1.5$  m), Young's modulus of reinforced concrete ( $3.1E7$  kN/m<sup>2</sup>), levels of struts (7). Consequently, the stiffness of the system can be calculated as presented below and results in a total value of  $K$  of  $3.60 \cdot 10^3$  kN:

$$k_1 = \left[ \frac{E \cdot A_{crw}}{B/2} \right]$$
$$k_1 = 3.60 \cdot 10^7 \text{ kN}$$

$$k_2 = \left[ \frac{384 \cdot E/12}{L^3} \right]$$
$$k_2 = 3.60 * 10^3 \text{ kN}$$

$$k_3 = \left[ \frac{E \cdot A_{strut} \cdot L}{B/2} \right]$$
$$k_3 = 8.47 \cdot 10^7 \text{ kN}$$

With this the expected settlement without cross-walls is calculated with equation 3.11. Resulting in a expected settlement of 226 mm. Therefore introduction of the cross-walls is evaluated. Introduction of the parameters of the cross-walls is made where the length of cross-walls  $h_cw=9$  m, and the separation of the cross-walls  $l_cw$  is iterated until the goal settlement of 10 mm is achieved. After iterations a value of 10 m is found to be necessary for the spacing of the cross-walls. The total stiffness of the system with cross-walls has a value of  $8.30 \cdot 10^6$  kN which is much higher than the stiffness without foundation structures.



# Appendix M. Design of cohesion piles for piled raft

Calculations below present the design value of bearing capacity for the cohesion pile based on the Claes Alén pile foundation handbook [129]. No effects related to pile group have been taken into account. The design assumptions are presented below:

- Pile length is 20.0 m below the bottom of the excavation.
- The whole length of pile fits within two clay layers where the mean undrained shear strength is equal to 57 kPa.
- Pile used in the design is Swedish standard SP2 prefabricated reinforced concrete piles of constant cross-section. Thus,  $\alpha = 1.0$ .
- The cross-section area of SP2 pile is equal to 0.27 x 0.27 m.
- In Sweden, partial factor of safety for class SK1 is equal to  $\gamma_n = 1.70$ .
- For safety reasons, the toe resistance is being ignored. Thus,  $f_s = 0$ .
- According to [129], the shaft resistance factors can be reduced by 20% compared to the toe resistance values when a large volume of the soil is being mobilised.
- Partial factor for shaft resistance varies from 1.3 to 1.6. In this example, it has been decided to use  $\gamma_{mm} = 1.35$ . Taking into account the above 20 % reduction,  $\gamma_{mm} = 1.08$ .
- Partial model factor is equal to  $\gamma_{RD} = 1.70$ .

Thus, the shaft adhesion area is equal to:

$$A_{shaft} = 4 \cdot 0.27 \cdot 20 = 21.6 \text{ m}^2$$

and shaft bearing resistance is equal to:

$$f_m = \alpha_u = 1.0 \cdot 57 = 58 \text{ kPa.}$$

Consequently, the characteristic bearing capacity is:

$$R_k = \alpha \cdot \bar{c}_u \cdot A_{shaft} = 1231.2 \text{ kN}$$

and design value of bearing capacity is:

$$R_d = \frac{1}{\gamma_{RD}} \cdot \frac{R_k}{\gamma_m \cdot \gamma_n} = \frac{1}{1.7} \cdot \frac{1231.2}{1.35 \cdot 1.0} = 670.59 \text{ kN}$$



# Appendix N. Bending moment results in short-term

Figures N.1 to N.4 present the bending moments for both retaining walls obtained with the SS and SSC model in PLAXIS 2D in short-term. The magnitude of the moment in short-term is much lower than the results obtained for the long-term due to the large amount of support given by the struts while the excavation pit is open.

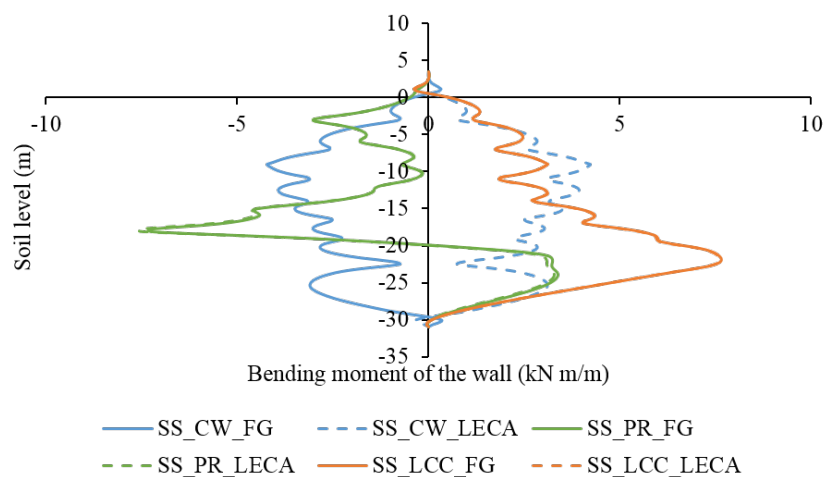


Figure N.1: Bending moment on left wall obtained with SS model for the short-term.

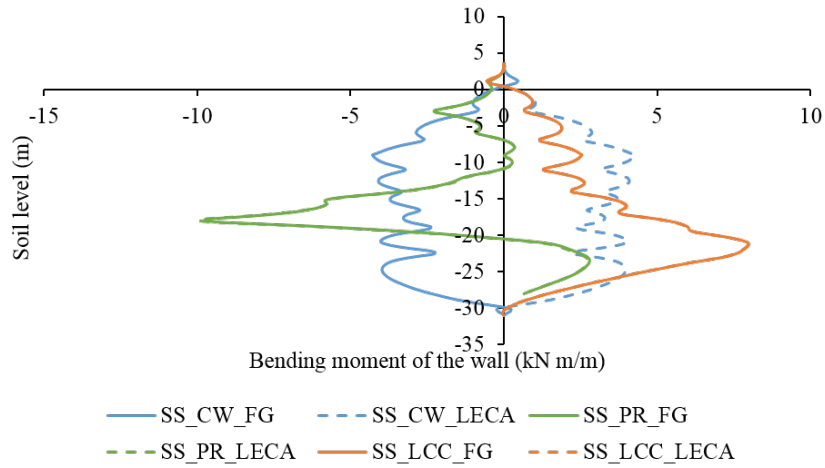


Figure N.2: Bending moment on right wall obtained with SS model for the short-term.

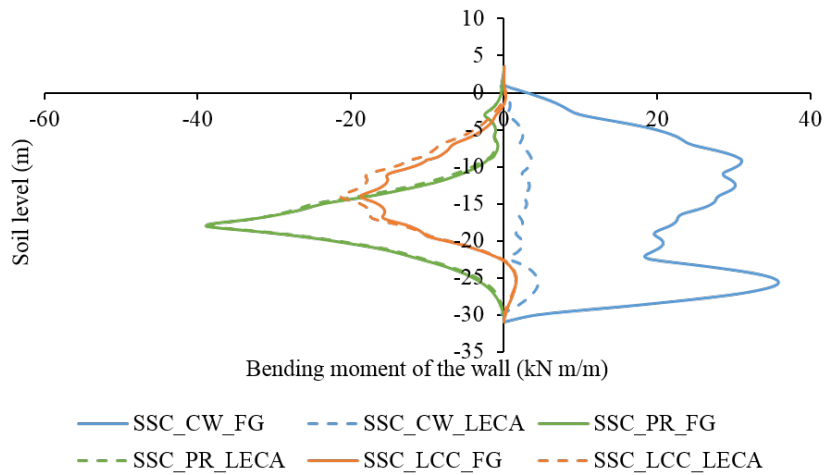


Figure N.3: Bending moment on left wall obtained with SSC model for the short-term.

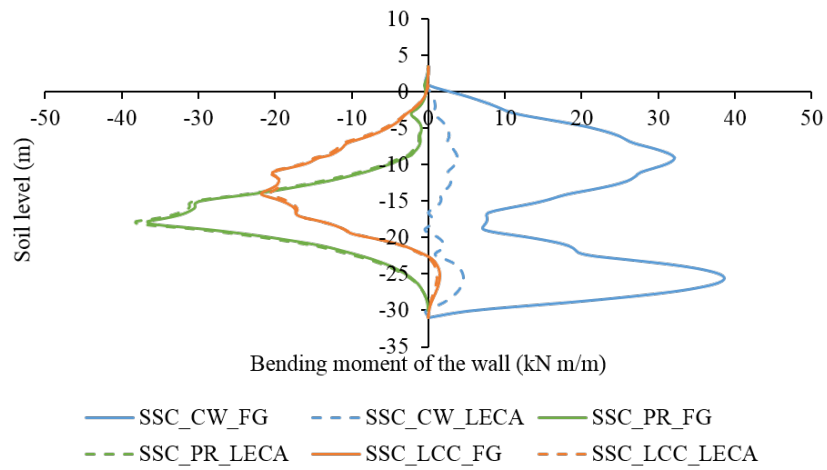


Figure N.4: Bending moment on right wall obtained with SSC model for the short-term.